공학박사 학위논문

Development of genetically encoded fluorescent sensors to study cellular neurophysiology

세포신경생리학 연구를 위한 유전자부호화된 형광센서의 개발

2019년 2월

서울대학교 융합과학기술대학원

융합과학부 나노융합전공

이 성 무

Development of genetically encoded fluorescent sensors to study cellular neurophysiology

지도 교수 : 송 윤 규

이 논문을 공학박사 학위논문으로 제출함

2018년 10월

서울대학교 융합과학기술대학원

융합과학부 나노융합전공

이 성 무

이성무의 공학박사 학위논문을 인준함

2019년 2월

위 원 장 _____ (인)

부위원장 _____ (인)

위 원 _____ (인)

위 원 _____ (인)

위 원 _____ (인)

Abstract

Development of genetically encoded fluorescent sensors to study cellular neurophysiology

Sungmoo Lee
Program in Nano Science and Technology
Graduate School of Convergence Science & Technology
Seoul National University

Optical sensors of cellular neurophysiology have thrived to a level where they can enable probing the voltage change of dendritic spines or neuronal activities from electrophysiologically indistinguishable cell types in a small region. The on-going success of optical recording was achieved by a combination of genetic engineering, optimization of optics for biological imaging, and the development of advanced fluorescent sensors. The emergence of genetically encoded fluorescent bio-sensors facilitated cell-type specific targeting of the optical sensors by

employing the cell of interest's own protein production machinery.

This dissertation will discuss rationally designed strategies to develop genetically encoded voltage indicators, to optimize membrane trafficking of the sensor molecules, and to modify fluorescent proteins' property to confer photoactivatability.

Recording voltage is a direct measurement of neuronal activity. Genetically encoded voltage indicators were first reported in 1997 and had shown considerable improvements in the last seven years. The first part of this thesis paper will introduce the basic concepts and a brief history in genetically encoded voltage indicator development.

One of the main advantages of using a genetically encoded optical sensor is the ability to send the proteins to specific regions, even subcellular. Therefore, means to better locate the sensor proteins were empirically studied and will be discussed in the second part.

Finally, a set of rationally designed mutations to make a sensor protein optically highlightable will be shown. Previous results from the report of the first photoactivatable green fluorescent protein were applied to develop photoactivatable genetically encoded voltage indicators and pH indicators.

Keywords: Optical recording, fluorescent protein, neurophysiology, neuronal activity, voltage indicator, membrane trafficking, photoactivatable fluorescent protein, genetically encoded pH indicator.

Student Number: 2012-22449

Contents

List of figures

List of tables

Chapter 1. Introduction

1.1 Methodologies to study neuronal activity

1.1.1 Electrophysiological recordings

Understanding how the human brain works has been the key question in the history of neuroscience. In the late 1700s, Luigi Galvani discovered that a frog's leg detached from its body could still contract by a touch of a charged electrode [1]. Hodgkin and Huxley first recorded an action potential from a squid giant axon in 1939 (Figure 1.1.A) [2, 3]. The method they used is called intracellular recording where a sharp glass electrode is inserted into the cytoplasm to measure electrical activity (Figure 1.1.B). Intracellular recording records local fluctuation of membrane potential. In modern electrophysiology, this technique is mainly used to study postsynaptic activities such as excitatory postsynaptic potential (EPSP) or inhibitory postsynaptic potential (IPSP). For intracellular recording, a high resistance glass pipette with tip size in the order of tens of nanometers is used to penetrate cell membrane [4]. Although it has been an essential technique, many of its usages were moved to patch clamp technique.

In 1976, Neher and Sakmann devised a technique called patch clamp that enabled recording from a single ion channel (Figure 1.1.B) [5]. Patch clamp has several added benefits to intracellular recording. It does not

have to penetrate through a cell's membrane to reach to the cytoplasm region. Instead, once a tight giga-ohm seal between the membrane and a glass pipette is made, the pipette becomes continuous to the membrane. Then the membrane patch can be removed by applying negative suction. This is called 'whole-cell mode' and it allows the whole-cell level electrical recording and manipulation except for the cells having space clamp issue. The glass pipette for patch clamp recording has tip diameter in micrometer scale instead of the nanometer scale in the intracellular recording. The larger pore size makes lower resistance condition thereby enables whole-cell voltage clamp recording. The voltage clamp experiment allows an experimenter to study the current flow of a neuron while holding its membrane potential at a fixed voltage. Due to neurons' intrinsic electrical property that tries to offset the change in membrane potential, clamping membrane potential of a neuron at a certain holding potential requires immediate correction through a compensatory current injection which could be difficult with the highly resistant intracellular recording electrode [6]. The current-voltage curve (I / V curve) can be obtained with voltage clamp recording. This curve shows a specific channel's conductance over tested voltage values. Figure 1.1.C shows I / V curves of a voltage-dependent (right) and a voltage none-dependent

(left) channels. The none-linearity of the curve on the right means that this channel is voltage-dependent and there is inward current in between – 40 to + 60 mV range. Conventionally, negative current values from an I / V curve means an inward current that can be seen when cations enter or anions leave the cytoplasm [6]. There are other patch clamp recording modes for specific scientific questions such as cell-patch, inside out, outside out and perforated patch.

Extracellular recording measures a brief current sink near a neuron's extracellular region [7]. For instance, when a neuron undergoes a series of action potentials, many sodium ions will enter the cell through voltage-gated sodium channels. This will create a brief deficit of sodium ions in the extracellular side point of view. If an extracellular recording electrode is close enough to the area, it will record spike activity as well. Figure 1.1.D is nicely comparing intracellular and extracellular recordings upon action potential firing. Usually, the extracellular recording does not provide any subthreshold activity of a single neuron.

Local field potential (LFP) is a summed postsynaptic activity from many cells that is measured by a nearby extracellular recording electrode [6]. Practically, LFP is usually recorded from a well-defined brain region such as *Cornu Ammonis* 1 (CA1) of the hippocampus or cortical layers

(Figure 1.1.E) [8]. This is because LFP is unlikely to produce meaningful data when a current source and sink are not clearly defined. For instance, structurally intermingled neuronal processes forming various excitatory and inhibitory synapses will have complicated postsynaptic potentials compared to a well-known structure such as CA1 - CA3 neural circuit.

Multi-electrode array (MEA) and optrode are frequently used in both *in vitro* and *in vivo* recordings of neuronal activity to measure LFP or electroencephalogram (EEG) [9-11]. However, both LFP and EEG recordings are incapable of measuring electrical activity from sparsely located cells. Moreover, recording from electrophysiologically indistinguishable cell types in a deeper brain region is hard to study with conventional methodology [12].

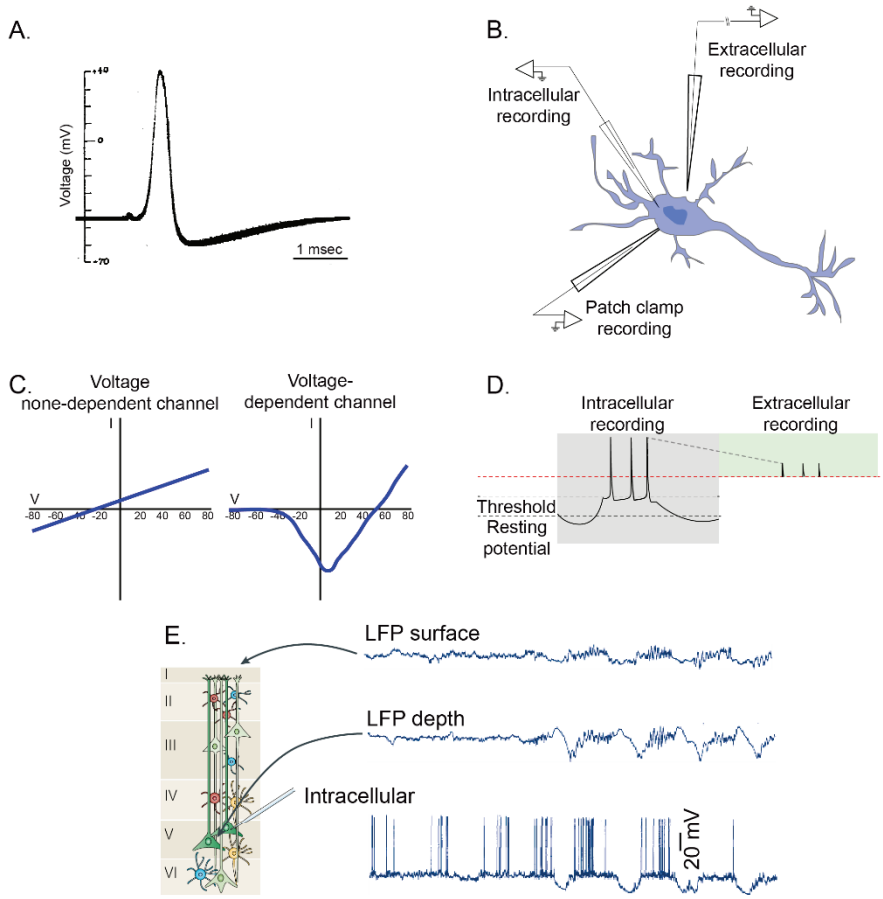

Figure 1. 1 Types of electrophysiological recordings

A. The first action potential recorded from a squid giant axon (intracellular recording) [3]. **B.** Schematics showing three different electrophysiological recordings. **C.** Schematics of I / V curves showing voltage none-dependent and dependent channels measured by voltage clamp recording (patch clamp). **D.** A comparison between intracellular recording and extracellular recording when there are three action potentials fired from a neuron [7]. **E.** Schematics showing

different results from intracellular recording, LFP in depth, and LFP in surface from cortical layer 1-6 [8].

Reprinted by permission from Springer Nature:

A. *Nature*, Action potentials recorded from inside a nerve fibre., Hodgkin A. L. and Huxley A. F. (1939), **D.** *Nature Nanotechnology*, Multi-electrode array technologies for neuroscience and cardiology., Spira M. E. and Hai A., E. (2012), **E.** *Nature reviews neuroscience*, The origin of extracellular fields and currents — EEG, ECoG, LFP and spikes., Buzsaki G., Anastassiou C. A., and Koch C. (2012). COPYRIGHT (1939, 2012, 2012)

1.1.2 Alternatives to electrophysiological techniques

Electrophysiology will still be the principal method to unravel how a complicated neural system works. However, it also has its limitations. Fundamentally, an electrophysiological study is invasive since the electrodes need to have physical contacts on biological tissues or cells. Due to the physical size of the apparatus used, it is prohibitive to simultaneously record from multiple regions especially in the case of *in vivo* patch clamp recording [13]. Although using multi-electrode array (MEA) renders an experimenter to study multiple cells at once, it intrinsically records extracellular signal only. Also, the spatial resolution of electrophysiology has its limits due to the size of the electrode for some small neuronal structures such as dendritic spines [1, 14, 15].

Imaging neural activity by using an optical sensor can complement the fundamental limitations of electrophysiology. It uses light that has spatial resolution determined by the diffraction limit. Multiple regions can be investigated simultaneously depending on the optical setup [16]. Also, optically imaging a biological sample is far less invasive than penetrating an electrode into a tissue [17-19].

The groundbreaking discovery and development of genetic engineering have expanded the potential of optical imaging to studying

a biological tissue [20, 21]. A DNA molecule encodes genetic information for a certain length of a peptide in its codons. The genetic material can be incorporated into a cell of interest, and use the endogenous machinery of the cell to produce a protein [22]. Moreover, using specific promoters allows cell-type specific expression of the proteins. This is depicted in Figure 1.2 where the green fluorescent proteins (GFPs) are expressed in one cell type and the enhanced yellow fluorescent proteins (eYFPs) are in another.

The most successful and effective alternative of electrophysiology technique has been calcium imaging [16, 17, 23, 24]. In neurons, voltage-gated calcium channels conduct calcium ions into cytoplasm upon action potential firing. As a result, measuring the intracellular calcium ion level has proven to be useful and efficient to study out when, where, and how action potential spikes occur. Nevertheless, calcium imaging has fundamental limitations. It is not possible to monitor subthreshold activity. Some researchers use calcium indicators to study hyperpolarization from particular cell types having relatively higher resting membrane potentials, but it is generally considered that a calcium indicator only reports spiking activity [25].

Optical sensors for other ions such as chloride or proton were

developed and used to study neural activity in brain slice as well [26-30]. Detecting these ions gives information about the acidity of the cell. Many cellular neurophysiological mechanisms are dependent on it.

Measuring neurotransmitters can also be an alternative way to study neural activity. There have been many genetically encoded optical sensors detecting neurotransmitters contributing to both ionotropic or metabotropic synaptic transmissions [14, 19, 31]. An electrochemical detection method, cyclic voltammetry has shown to work well in measuring *in vivo* dopamine level as well [32-34].

Unlike all the abovementioned alternatives, a voltage indicator directly measures membrane potential. This optical sensor senses depolarization or hyperpolarization that occurs across the transmembrane region and converts it to change in its optical property. As a result, the optical recording of membrane potential allows neuroscientists to study not only the spiking activity but also subthreshold activity. As long as enough indicator molecules are present, a voltage imaging can be done in tiny cellular structure such as a dendritic spine [35, 36].

To study the electrical activity of multiple cells simultaneously from brain slices or *in vivo* intact brain, LFP or EEG recording can be used.

However, the quality of an LFP recording is inversely proportional to the distance between the current source and the recording electrode [8]. Also, as mentioned earlier, LFP and EEG recordings are unable to selectively investigate sparsely located cells, not to mention that they do not discriminate one cell type to another. On the other hand, a genetically encoded voltage indicator measures the transmembrane potential of individual cells. Therefore, voltage imaging results from a certain type of neurons would be a sum of one type of cells electrical activity. Marshall et al. [12] successfully demonstrated optical recording of neuronal activity from cortical parvalbumin-positive interneurons that known to be sparse. Also, the voltage-sensing system they used optically resolved D1- and D2- receptor expressing striatal medium spiny neurons located in the subcortical region.

Besides all the molecular probe driven methodologies, functional magnetic resonance scanning (fMRI) and functional ultrasound (fUS) imaging can also investigate brain activity. Both techniques measure brain function based on a theory that the blood flow increases when there is more brain activity [37-39].

In the remaining parts of this chapter, different types of genetically encoded voltage indicators and their mechanisms will be discussed. The

importance of optimizing localization of the optical sensors will also be stressed. Lastly, a way to acquire fluorescence from a specific region of interest but not from all the expressed FPs in a specimen will be discussed.

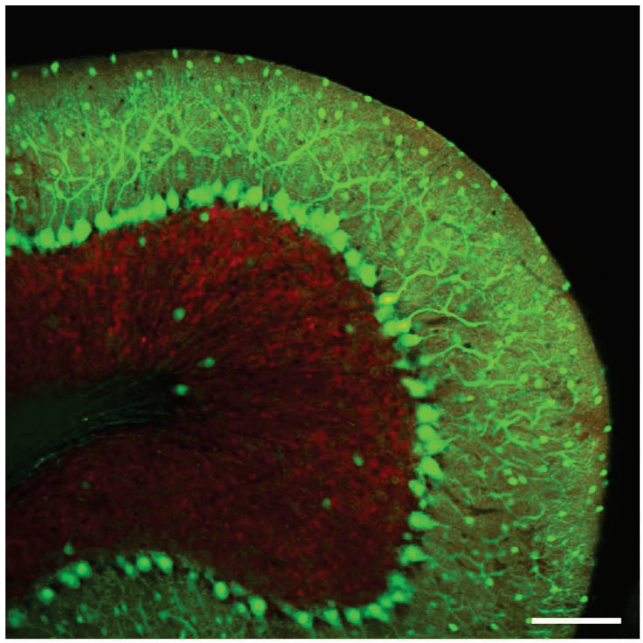

Figure 1. 2. Cell type specific expression of two different fluorescent proteins.

The GFP and eYFP protein sequences were encoded in DNA. The DNAs were preceded by GAD 67 and Kv3.1 promoters that are specific for GABAergic cells and granule cells, respectively. The image is from a cerebellar slice from a transgenic mouse expressing the proteins. GFP in green color and eYFP signal is in red. Scale bar: 100 μm.

This image is from Akemann et al., *Frontiers in Cellular Neuroscience*, 2009 [40]. The reuse permission was not required.

1.2 Genetically encoded voltage indicator

1.2.1 Voltage imaging

Optical properties of a voltage indicator change in responsive to the fluctuation of a cell's membrane potential so that it can measure voltage without using an electrode [41-43]. Figure 1.3 describes an example of voltage imaging either with a single fluorescent protein (FP) based voltage indicator or a fluorescence resonance energy transfer (FRET) based voltage indicator. High speed sensitive scientific camera is necessary to conduct a successful voltage imaging. This is due to the fact that one of the most important neuronal events, action potential, occurs in a millisecond timescale. The minimum frame rate to image action potentials is commonly considered as 500 Hz among voltage indicator developers. Typically, 1000 frames per second or faster speed is used for voltage imaging both in *in vitro* (cells or slices) and *in vivo* (on an animal's brain).

Initially, voltage-sensitive dyes (VSDs) made of synthetic organic chemicals were used to convert voltage into the optical signal. However, since the application of VSDs was incapable of discriminating different cells unless they are injected in a particular cell through a patch pipette, it was not easy to use the synthetic chemicals to optical imaging of a

biological sample that has various cell types closely located to each other [35, 36].

The discovery, development, and application of fluorescent proteins that began to fruit in the 1990s have influenced voltage sensor developers [44-49]. Now the optical reporter part of a voltage indicator could be replaced to fluorescent proteins. As a result, genetically encoded voltage indicators (GEVIs) can be targeted to certain cells and even to subcellular organelles by using the intrinsic function of host cells' protein production machinery [50]. Since its first report in 1997, the versatility of GEVIs improved to a state where a dendritic spine of cultured neurons, and *in vivo* imaging of larval zebrafish, fruit fly and mouse can be conducted [12, 23, 51-54]. In the next few pages, a brief history of the selected GEVIs will be described.

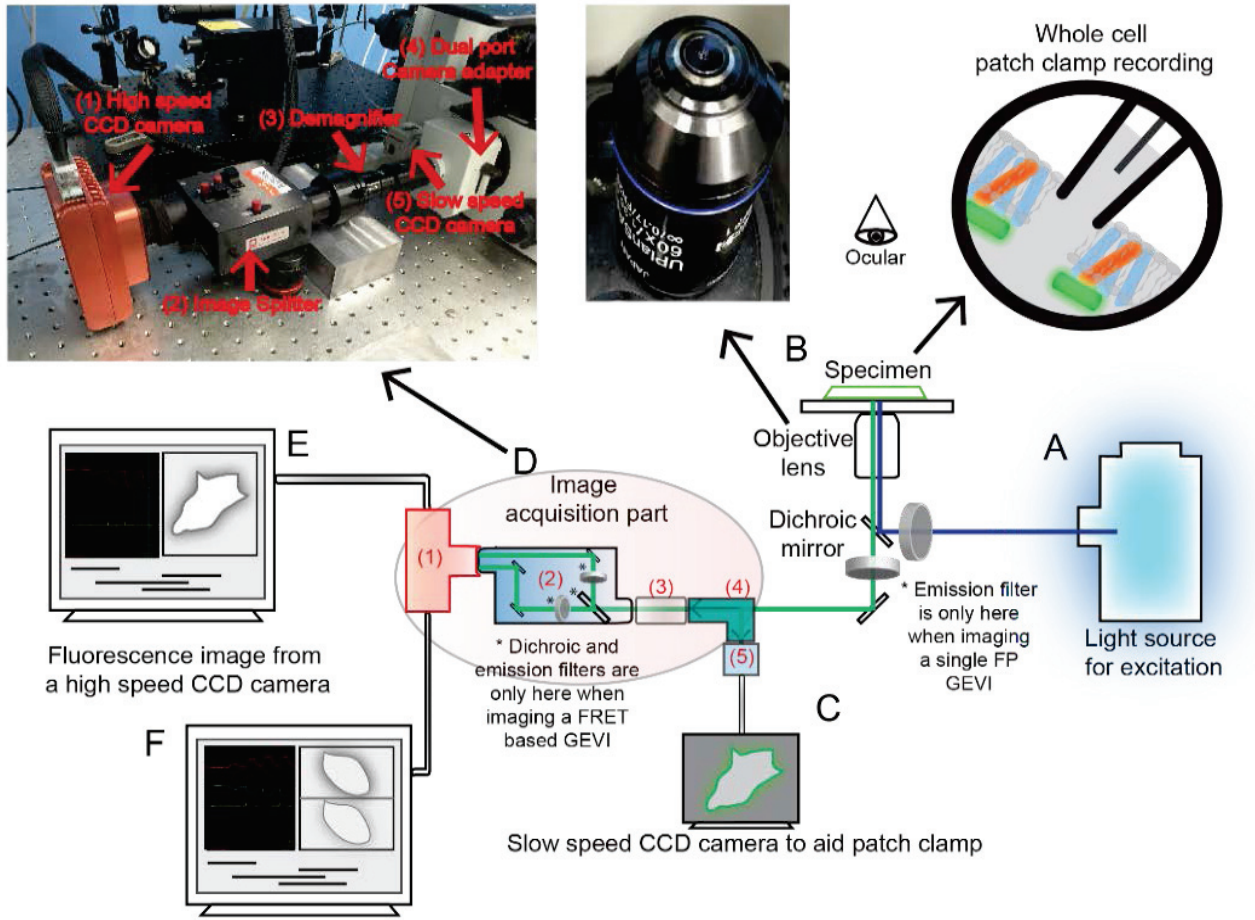
(1) High speed CCD camera
(2) Image Splitter
(3) Demagnifier
(4) Dual port Camera adapter
(5) Slow speed CCD camera
Whole cell patch clamp recording
Ocular
B
Specimen
Objective lens
A
Dichroic mirror
* Emission filter is only here when imaging a single FP GEVI
Light source for excitation
E
D
Image acquisition part
(1)
(2)
(3)
(4)
(5)
* Dichroic and emission filters are only here when imaging a FRET based GEVI
C
Fluorescence image from a high speed CCD camera
F
Slow speed CCD camera to aid patch clamp

Figure 1. 3. An example of the voltage imaging equipment setup for voltage imaging with GEVIs

A. 75W Xenon arc lamp. **B.** A specimen on the stage illumintated by the filtered and reflected excitation light. The inset at the top right corner shows the whole cell patch clamp configuration. **C.** The slow speed CCD camera is used to aid both choice of a cell and patch clamp. **D.** the image acquisition part; (1) the high speed CCD camera, (2) the image splitter for both FRET pair and mono FP GEVIs, (3) the demagnifier to fit the image onto the CCD chip in the high speed CCD camera, (4) the dual port camera adapter to switch the imaging pathway and (5) the slow speed CCD camera with a higher spatial resolution for identification of the cell to patch, **E.** Image acquisition with a single-FP based GEVI and **F.** a FRET-based GEVI. The image is from Lee et al., *Journal of Visualized Experiment*, 2016 [55]. The reuse permission was not required.

1.2.2 Early versions of genetically encoded voltage indicator

The Isacoff group in U.C. Berkeley first reported the GEVI named FlaSh (Fluorescent Shaker) [56]. It was made by a simple fusion of GFP to Shaker potassium channel (Figure 1.4.A). The Shaker potassium channel is sensitive to membrane potential change due to a voltage-sensing domain resides in transmembrane region. Therefore, a change in green fluorescence could be observed in a voltage-dependent manner. This group also developed variants of FlaSh in 2002 [57].

In 2001, VSFP1 (Voltage-Sensitive Fluorescent Protein) was reported by Thomas Knopfel's laboratory in Japan by then (Figure 1.4.B) [58]. This voltage indicator utilized FRET in between a cyan fluorescent protein (CFP) and a yellow fluorescent protein (YFP). The two FPs were located in the S4 region of a truncated potassium channel. The change in FRET efficiency due to the movement of the voltage-sensing S4 domain resolved the membrane potential change.

In 2002, a group led by Vincent Pieribone in Yale University developed SPARC (sodium channel protein-based activity reporting construct). It was generated by a fusion between GFP and the rat skeletal muscle sodium channel [59].

The early versions of GEVI paved the way of an important optical tool

for neuroscience research but they failed to resolve activity from neuronal cells. The main problem was the inability to place themselves in the plasma membrane [60].

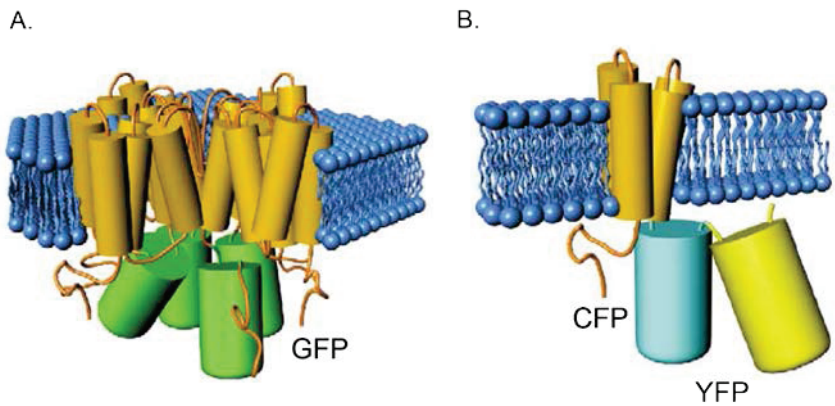

Figure 1. 4. The two early forms of GEVI

A. FlaSh reported by Siegel and Isacoff [56]. A GFP was fused to the Shaker potassium channel. **B.** VSFP1 from Thomas Knopfel's group. VSFP1 uses a potassium channel but it only used S1-S4 domains but S5 and S6. Also, instead of a single type of FP, CFP and YFP were used as a FRET pair [58].

This modified image was reprinted from: Optical probing of neuronal circuit dynamics: genetically encoded versus classical fluorescent sensors., Vol. 29 / No.3, T. Knopfel, J. Diez-Garcia, and W. Akemann, *Trends in Neurosciences*, 160 - 166., Copyright (2006), with permission from Elsevier [61].

1.2.3 GEVIs using voltage-sensing domains from non-conducting voltage-sensitive phosphatase

A breakthrough in the development of GEVIs was due to the identification of a voltage-sensitive phosphatase from *Ciona Intestinalis* in 2005 [62]. This membrane protein is monomeric and has a voltage-sensing domain in the plasma membrane but does not have a pore to conduct ions. This S1-S4 transmembrane segments possessing membrane protein has a cytoplasmic phosphatase connected to the S4 through a linker. Introduction of the monomeric voltage-sensing domain in GEVIs improved their membrane expressions.

Thomas Knopfel's group modified VSFP1 by fusing both FRET donor and acceptor to the voltage-sensing domain from *Ciona Intestinalis* voltage-sensitive phosphatase (Ci-VSD). One of the variants named VSFP 2.3 successfully showed the activity from mouse somatosensory cortex responding to whisker deflections [63].

In 2012, Lawrence Cohen and Vincent Pieribone groups published a paper describing another Ci-VSD containing GEVI, ArcLight [64] (Figure 1.5.A). Interestingly, this GEVI used a single pH-variant of GFP, super ecliptic pHluorin. The FP had a mutation that changed the alanine at 227th position to an aspartic acid. After the A227D mutation, the

response of the GEVI to a 100 mV membrane depolarization was increased for 14 - fold. ArcLight demonstrated resolution of evoked action potentials from cultured mouse neurons in single trial imaging. This GEVI has been successfully applied to *in vivo* studies such as fruit fly odor response and mouse olfactory bulb experiment [23, 53, 54].

Figure 1.5.A also describes a variant of ArcLight, Bongwoori that was developed by Bradley Baker's group [65]. This GEVI also used SE A227D as its fluorescent reporter but it had distinct voltage-sensing domain mutations that made the GEVI exhibit faster kinetics than ArcLight as shown in Figure 1.5.A. The mutations in Ci-VSD also tuned Bongwoori's voltage range to better image action potentials. The possible mechanism of the SE A227D containing GEVIs (ArcLight and Bongwoori) was proposed to be the intermolecular homo-dimerization of the GEVI molecules due to the dimeric nature of the FP used (Figure 1.5.A-right panel). A set of monomeric mutations in SE A227D decreased the amplitudes of voltage-dependent fluorescence responses [66].

A voltage-sensing domain from the voltage-sensitive phosphatase of *Gallus gallus* (chicken) was also used in the development of a circularly permuted GFP (cpGFP) containing GEVI, ASAP-1

(Accelerated Sensor of Action Potentials-1) [67, 68] (Figure 1.5.B). The cpGFP is a circularly permuted version of GFP that the N and C termini are connected to each other through a 6 amino acid long linker (GGTGGS) [69]. In ASAP-1, the cpGFP was placed in between S3 and S4 so that the movement of voltage-sensing S4 region can directly modulate the protonation of the FP's chromophore thereby inducing voltage-dependent fluorescence change [67]. As the acronymized name implies, ASAP-1 showed near 2 msec of time constants per 100 mV depolarization.

A group in Canada also used a red-shifted version of circularly permuted FP to their GEVI, FlicR1 (fluorescent indicator for voltage imaging red) [70] (Figure 1.5.C). Similar to ASAP-1, this GEVI had a red cpFP (cpmApple) fused to S4 of Ci-VSD but in the opposite side. This made the FP stay in the cytoplasm instead of extracellular region. The fused construct was also subject to multiple sets of random mutagenesis followed by high-throughput screening. As a result, FlicR1 was generated and the kinetics of this red GEVI was faster than any Ci-VSD containing GEVIs reported to date. Also, this red-shifted GEVI is one of the few voltage indicators that showed an increase in fluorescence upon membrane depolarization.

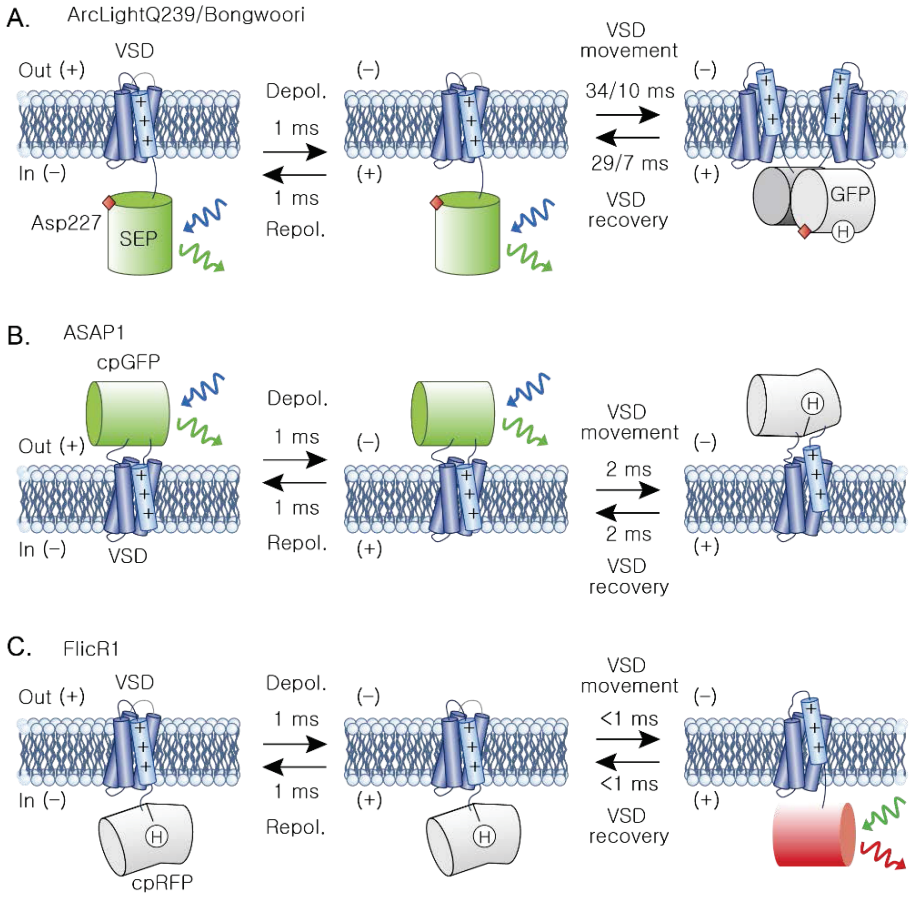
A.
ArcLightQ239/Bongwoori
VSD
Out (+)
In (−)
Asp227
SEP
Depol.
1 ms
1 ms
Repol.
(−)
(+)
VSD
movement
34/10 ms
29/7 ms
VSD
recovery
GFP
H
B.
ASAP1
cpGFP
Out (+)
In (−)
VSD
Depol.
1 ms
1 ms
Repol.
(−)
(+)
VSD
movement
2 ms
2 ms
VSD
recovery
H
C.
FlicR1
VSD
Out (+)
In (−)
H
cpRFP
Depol.
1 ms
1 ms
Repol.
(−)
(+)
VSD
movement
<1 ms
<1 ms
VSD
recovery

Figure 1. 5. The GEVIs using a monomeric voltage-sensing domain

The image is divided in three panels. (Left) Resting state, (Center) Depolarized state, (Right) Actual response of the GEVI(s) for a membrane depolarization. The numbers above and below each arrow indicate the time constants to indicate the kinetics of the optical response.

A. Two GEVIs having a super ecliptic pHluorin A227D as their fluorescent proteins. ArcLight's response is slower than Bongwoori. **B.** ASAP-1 uses a cpGFP that is placed in between S3-S4 loop of its VSD. **C.** FlicR1 is a red-shifted version of GEVI. It also uses a cpGFP but the FP is placed in the cytoplasm side connected to the end of the S4 of the VSD. Please note that this red fluorescent GEVI gets brighter as the cell membrane depolarizes.

1.2.4 GEVIs using microbial rhodopsin

Opsins are light-sensitive membrane proteins that exhibit photocurrent upon illumination with a certain wavelength of light. They have Schiff base inside of their structure that is composed of amino acid residues and a retinal molecule. Optogenetic actuators such as channelrhodopsin-2 or halorhodopsin are opsins and they have been popularly used in broad research areas [71-78].

An opsin from *Halorubrum sodomense* was reported as a voltage indicator in 2011 by a group of researchers in Harvard University [79, 80]. This was called Arch (archaerhodopsin 3) (Figure 1.6.A). The simple voltage-sensing mechanism of this GEVI made it one of the fastest voltage indicators having submillisecond time constants per 100 mV depolarization. This opsin also showed the large fractional fluorescence change upon membrane depolarization. However, since it was an opsin, it had intrinsic photocurrent, namely Arch could change the membrane potential while it was measuring it. Later on, the same group conducted random mutagenesis and generated QuasAr2 that was a variant of Arch but without the light-induced current [81]. The biggest problem of these opsins was the dim brightness of the chromophore. The evolved version still needed 200 W / cm^2 laser illumination for voltage

imaging [82].

In 2013, 2014 and 2015, another type of opsin based GEVIs was reported by Mark Schnitzer's lab in Stanford University [83-85]. They fused a bright FP to one of the opsins and that induced FRET in between the opsin's chromophore and the FP placed in the cytoplasm. In this case, the chromophore in the opsin acts as a FRET acceptor and the FP becomes a FRET donor (Figure 1.6.B). This strategy resulted in a GEVI that is slower than opsin only type but as bright as the voltage-sensing domain containing GEVIs. With these GEVIs, the first demonstration of GEVI in a freely moving mouse was performed in 2016 [12].

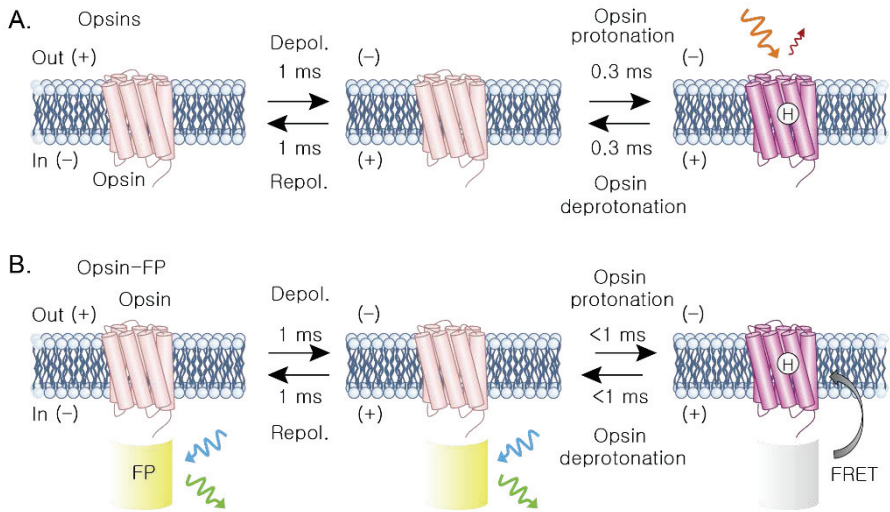

Figure 1. 6. The GEVIs utilizing microbial opsins

(Left) Resting state, (Center) Depolarized state, (Right) Actual response of the GEVI(s) for a membrane depolarization.

A. This type of opsin based GEVIs emit red fluorescence upon depolarization and works in below 1 msec time constant range (the numbers on the image was from QuasAr2) but its quantum yield of below 0.01 produces weak emission.

B. Opsin-fluorescent protein fusion type utilizes FRET to change its FP's fluorescence that gets dimmer upon depolarization. The time constants are for Ace2N-mNeonGreen.

1.3 The importance of membrane trafficking and means to improve it

1.3.1 Consequence of bad membrane expression

In biological systems, the function of a protein is region specific and a failure to place a protein to the specific location often causes malfunction of the system. This aspect is even more crucial for neuronal cells since they have polarized morphology [86]. The synaptic plasticity of axons, dendrites, and dendritic spines is a good example of complicated and elaborate delivery of various molecules to the peripheries. This is also true for optogenetic actuating tools. For instance, the optogenetic actuators such as channelrhodopsin-2 or halorhodopsin must traffick to the plasma membrane to generate photocurrent upon illumination at certain wavelength [50, 75]. The sensors for studying vesicular activity need to situate themselves inside of a vesicle. Also, the part of a voltage indicator sensing the membrane potential change must reside in the membrane since the electric field of the lipid bi-layer dissipates quickly as it travels away [87].

Having an intracellular aggregate of GEVI molecules can damage the imaging of membrane potential. The misplaced fluorescent probe molecules will be distant from the plasma membrane but if the

fluorophore is bright enough at its resting state, it will become a chunk of voltage-insensitive FPs that contribute to the enhanced background fluorescence. The result of having such a bright cytoplasmic spot is described in Figure 1.7. The HEK 293 cell is expressing one of the green fluorescence GEVIs, Bongwoori. From the resting state image (Figure 1.7.A.), a bright but internal spot can be seen. The intracellular aggregate shows a similar level of fluorescence change (ΔF) upon a 100 mV depolarization (Figure 1.7.B.) but due to the background fluorescence, ΔF/F becomes smaller than that of the region 1 where the same GEVI molecules are expressed in the membrane (Figure 1.7.C.). Therefore, optimizing a GEVI's membrane trafficking by reducing the internal expression will improve the voltage imaging ability of the sensor.

This may not be an issue if a high magnification is used for imaging as shown in Figure 1.8. In this configuration, only the pixels responsible for the membrane region can be chosen. However, when a lower magnification objective lens has to be used for population voltage imaging such as in brain slice, a pixel will now get fluorescence from both internal and membrane regions thereby the quality of the optical signal will decrease.

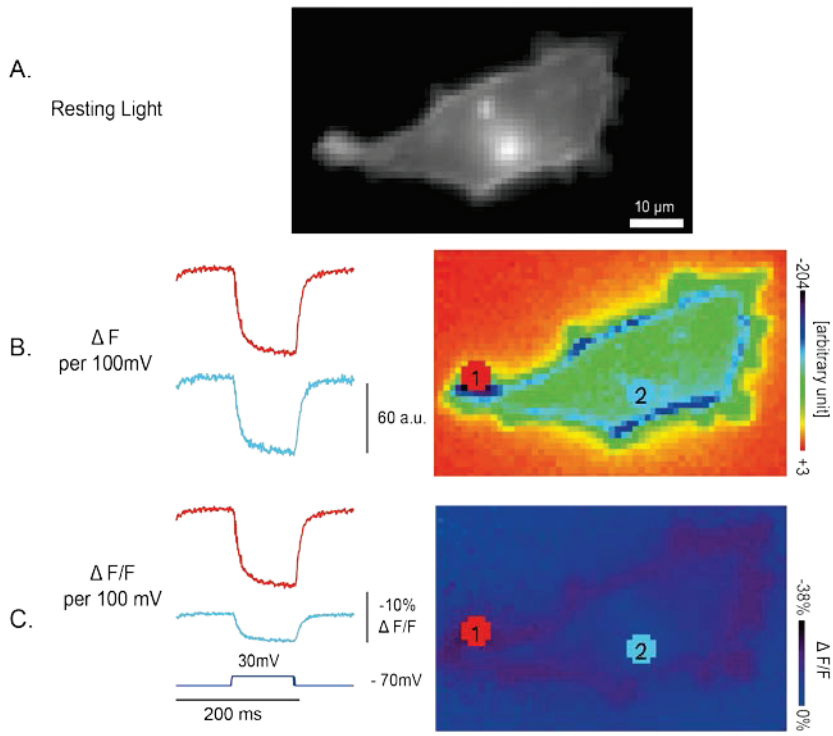

Figure 1. 7. Effect of internal fluorescence on ΔF and ΔF/F

A. An HEK 293 cell expressing a single FP based GEVI, Bongwoori, shown at its resting state. **B.** The fluorescence traces showing kernel averaged ΔF (Fx-F0) values from two different regions, region 1: a membrane region with well localized fluorescence signal and region 2: a cytoplasmic region with bright internal fluorescence. **C.** Traces showing the kernel averaged ΔF/F values from the same regions in B. This image was modified from Lee et al., *Journal of Visualized Experiment*, 2016 [55]. The reuse permission was not required.

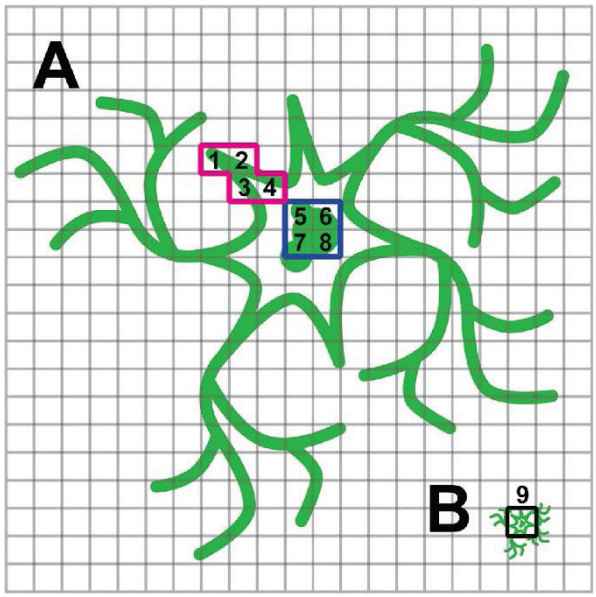

Figure 1. 8. Consequence of internal fluorescence when imaging population of cells

A. A postulated neuron under a high magnification. The grid indicates pixels in a CCD camera. The area for pixel number 5 - 8 shows bright internal fluorescence where in this magnification, an experimenter will choose pixels 1 - 4 to avoid none-responsive fluorescence that decreases ΔF/F. **B.** However, if the magnification is low as in a brain slice voltage imaging, a pixel will receive light coming from both membrane and the intracellular aggregates. This image was modified from Nakajima et al. *Frontiers in synaptic neuroscience*, 2016. The reuse permission was not required.

1.3.2 Optogenetic actuators with optimized membrane expression

One of the microbial opsins, halorhodopsin, that induces a light dependent chloride influx suffered from the same membrane trafficking issue. However, incorporation of membrane trafficking motifs from the inwardly rectifying potassium channel 2.1 (Kir 2.1) improved the membrane trafficking. Kir 2.1 intrinsically have better membrane expression the other members of Kir 2.x. It was shown that an N-terminus and two C-terminus motifs were responsible for the difference [88, 89]. The two C-terminus motifs, namely Golgi to membrane trafficking signal (Golgi TS) and ER export signal (ER ES) were introduced to halorhodopsin and produced eNpHR 3.0. This improved its membrane expression compared to its predecessor as shown in Figure 1.9.

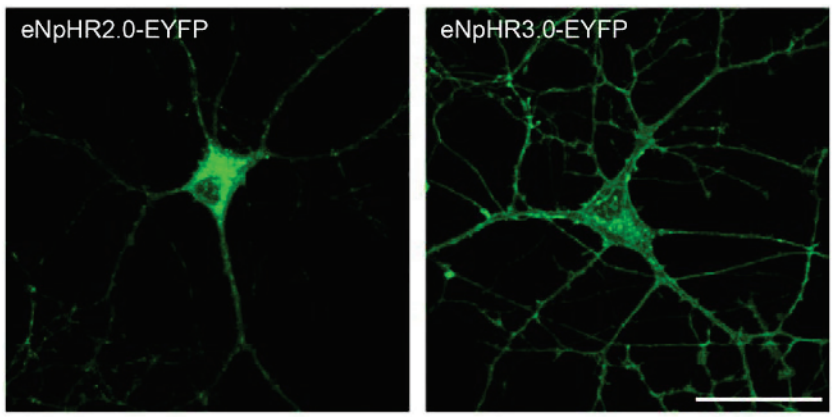

Figure 1. 9. Introducing the two membrane targeting sequences from Kir 2.1 improved membrane expression of eNpHR 3.0

The Golgi to trafficking signal and the ER export signal sequences were introduced to eNpHR3.0. Not only the memrane expression but the photocurrent was also improved. Scale bar = 40 μm.

This modified image was reprinted from: Molecular and cellular approaches for diversifying and extending optogenetics, Vol. 141 / No.1, Gradinaru V. et al., *Cell*, 154 - 165., Copyright (2010), with permission from Elsevier [75].

1.3.3 Voltage indicators with the membrane targeting motifs

Figure 1.10 describes some cases where the three Kir 2.1 originated membrane targeting motifs were used to improve the membrane expression of GEVIs. The locations of the two motifs in eNpHR 3.0 were determined empirically [75] and they were placed in between the opsin and the eYFP for the Golgi TS and after the FP for the ER ES, respectively. VSFP butterfly 1.2 had the Golgi ES in N-terminus of its FRET acceptor, mKate2 [90]. It was interesting that the FRET GEVI showed improved membrane localization with the N-terminus Golgi export signal while the same sequence did not improve the membrane trafficking of the halorhodopsin [75]. The microbial opsin connected to a bright green FP, mNeonGreen, both Golgi TS and ER ES were inserted after the FP to not to disturb the FRET in between the opsin and the FP. Marina is a variant of ArcLight that shows an increase in fluorescence for membrane depolarization. The Golgi TS was inserted at the N-terminus and the ER ES was placed at the C-terminus.

To sum up, while the membrane trafficking motifs were shown to help membrane trafficking but the insertion regions of them were dependent on the composition of each GEVI. These results suggest that the incorporation of the Golgi and/or ER export signal sequences should be

determined for each optical sensor that has a different structure or working mechanism compared to the others.

Kir2.1: Inwardly rectifying potassium channel (1287 bp)

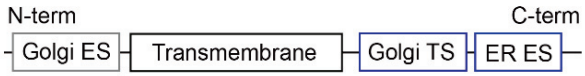

Golgi ES — Golgi export signal (Golgi ES) - RSRFVKKDGHCNVQFINV

Golgi TS — Golgi to membrane trafficking signal (Golgi TS) - KSRITSEGEYIPLDQIDINV

ER ES — ER export signal (ER ES) - FCYENEV

eNpHR 3.0 (1680 bp)

VSFP-Butterfly 1.2 (2038 bp)

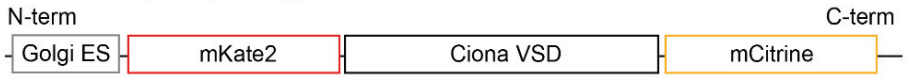

Ace2N-mNeon (1449 bp)

Marina (1464 bp)

Figure 1. 10 Composition of optogenetic tools possessing membrane targeting sequences

Kir2.1 naturally has three signal sequences that help membrane targeting of the ion channel. The inhibitory optogenetic actuactor, eNpHR3.0, used the Golgi to membrane trafficking signal (Golgi TS) and the ER export signal (ER ES) before and after its reporter FP, respectively. For VSFP-Butterfly 1.2, the Golgi export signal (Golgi ES) was located at the N-terminus. Ace2N-mNeon has Golgi TS and ER ES in tandem at the C-terminus to preserve the distance between the rhodopsin and the FP for FRET. The Golgi TS and ER ES were placed at the N-terminus and C-terminus, respectively, for Marina. SE pHluorin : super ecliptic pHluorin.

1.4 Photoactivation and its application in cellular neurophysiology

1.4.1 Photoactivatable fluorescent proteins

The photoactivated localization microscopy can be used to image a biological sample below the diffraction limited spatial resolution by restricting its region of interest to optically highlighted FPs [91-95]. The photoactivatable fluorescent protein enables this advanced imaging technique by activating a few cells using a brief light illumination. The photoactivatable GFP (PAGFP) was first reported in Patterson and Lippincott-Schwartz in 2002 [96].

The wild-type GFP (wtGFP) intrinsically has some degree of photoactivatable property due to its characteristic dual excitation bands at 397 nm and 475 nm. Before photoactivation, its chromophore stays in the protonated (neutral) state. Illumination with 400 nm light is thought to shift the neutral state into the anionic state by deprotonating the chromophore. In this activated state, the excitation band at 470 nm becomes dominant. Figure 1.11.A and B depict this conversion. The PAGFP has T203H mutation that improves the contrast at 488 nm excitation after photoactivation from 3 - fold (wtGFP) to 100 - fold (PAGFP) when experimented on purified protein preparations (Figure

1.11.C). The activated PAGFP also shows a slight shift in its emission spectrum compared to that of wtGFP (Figure 1.11.D) [96].

Various versions of photoactivatable fluorescent protein have been developed. This encompasses variants showing both reversible and irreversible transitions [97-103].

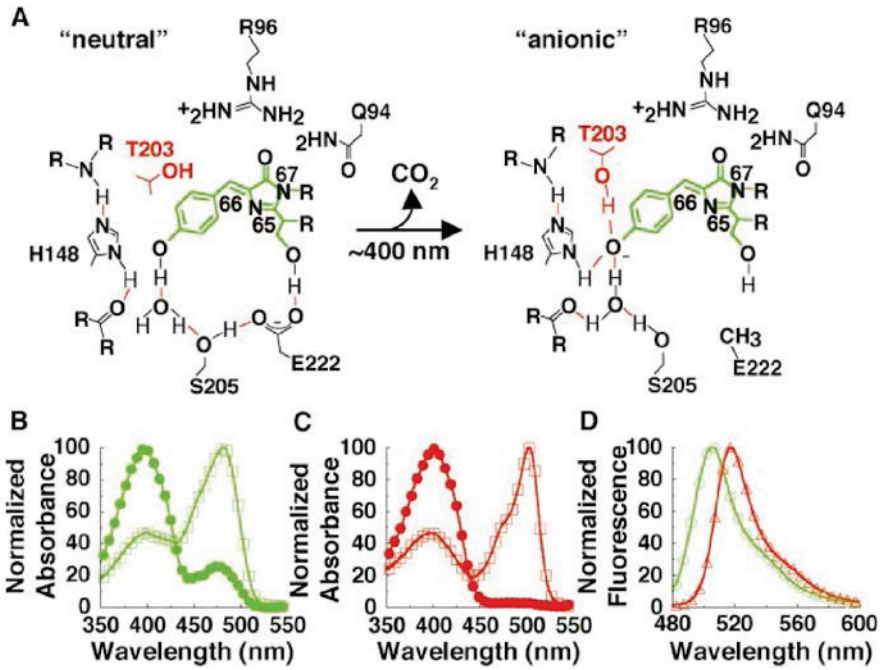

Figure 1. 11 Photoactivatable properties of wtGFP and PAGFP

A. Illumination of wtGFP by an intense 400 nm light shifts the chromophore to the anionic state thereby increase the 470 nm absorbance. **B.** Normalized absorbance of wtGFP before (filled circules) and after (hollow squares) photoactivation. **C.** Normalized absorbance of PAGFP before (filled circles) and after (hollow squares) photoactivation. **D.** Comparison of emission spectra of photoactivated wtGFP (green) and the PAGFP (red) under 475 nm excitation. From Patterson, G.H. and Lippincott-Schwartz J., A photoactivatable GFP for selective photolabeling of proteins and cells. *Science*, 2002. **297**(5588): p. 1873-7. Reprinted with permission from AAAS.

1.4.2 Photoactivatable calcium indicators

Genetically encoded calcium indicators (GECIs) have been the most successful and frequently used optical indicators. The best example of a GECI would be the GCaMP that was first reported in 2001 [104]. The GCaMP family has been developed continuously and showed promising *in vivo* neuronal imaging results including the whole-brain light-sheet microscopy imaging of zebrafish and all-optical stimulation and recording from mouse brain [18, 105].

Coupling the calcium imaging and the photolabeling was demonstrated by Berlin et al. successfully by a rational development that made the photoactivatable GCaMP (PA-GCaMP) [106]. Figure 1.12 shows that a focused 405 nm light on a spot in densely cultured rat neurons can highlight a single neuron expressing the calcium indicator molecules. V115H, L221F, and T222S were the mutations responsible for the photoactivatability of the PA-GCaMP. These mutations correspond to the three photoactivatable mutations in PAGFP (T203H, L64F, and T65S).

While the results and the potential displayed by the PA-GCaMP seem promising, the calcium imaging has fundamental limitations and it is kindly described in Lin and Schnitzer as; “Major limitations of GECI

imaging are that they do not report neurotransmitter receptor activation or AP firing with temporal precision, nor do they report membrane hyperpolarizations or subthreshold voltage changes well" [14].

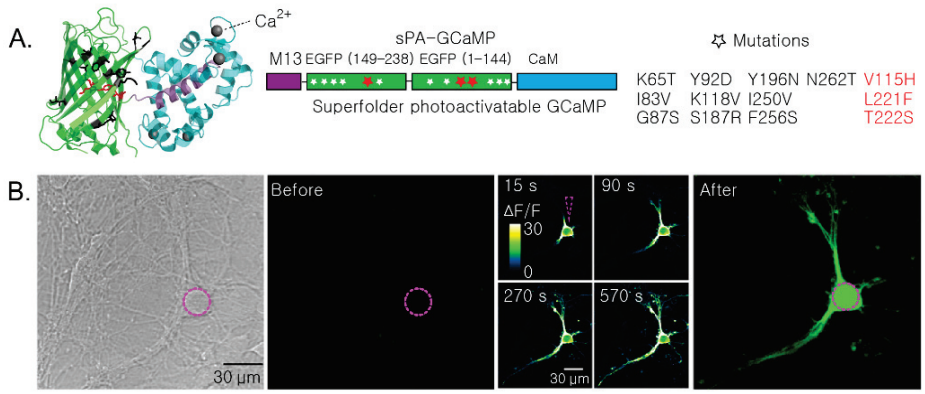

Figure 1. 12 Schematic of the photoactivatable genetically encoded calcium indicator (PA-GCaMP), photoactivatable mutations introduced and a demonstration.

A. Schematic of superfolder photoactivatable GCaMP (sPA-GCaMP) consisting of M13 (purple), cpGFP (green) and calmodulin (CaM, blue) and mutations introduced to confer photoactivatability. The V115H, L221F and T222S mutations were responsible for the photoactivatability. **B.** Densely cultured rat neurons expressing the sPA-GCaMP. (from left to right) transmitted light image, fluorescence image before photoactivation (the purple dashed line circle indicate the illuminated region), time-lapse fluorescence images at 15, 90, 270 and 570 sec after the photoactivation with 405 nm illumination, and the same cell after photoactivation.

Reprinted by permission from Springer Nature: *Nature Methods*, Photoactivatable genetically encoded calcium indicators for targeted neuronal imaging, Berlin et al., COPYRIGHT (2015) [106].

1.4.3 Genetically encoded pH indicators

Measuring pH is also important in studying neuronal activity as the regulation of intracellular proton concentration is involved in synaptic vesicle release and network excitability [14, 26, 29]. During the vesicle release at the presynaptic terminal for a neuron, the pH level in the vesicle lumen is maintained near pH 5.5 and increases to pH 7.3 upon the vesicle release to the synaptic cleft. (Figure 1.13.A). Super ecliptic pHluorin is a pH-sensitive variant of GFP that gets brighter at the basic condition and gets almost completely dark at pH 5.5. Having super ecliptic pHluorin expressed in the synaptic vesicle enables imaging of synaptic vesicle release (Figure 1.13.C).

A genetically encoded pH indicator (GEPI) can also be useful in studying network activity of the brain. Figure 1.14 depicts optical imaging of activity-dependent acidification of hippocampal neurons due to induced epileptiform activity [26]. The other works from Joseph Raimondo also nicely describe how genetically encoded pH sensors can be used to study neuronal activity in brain slices [27, 28].

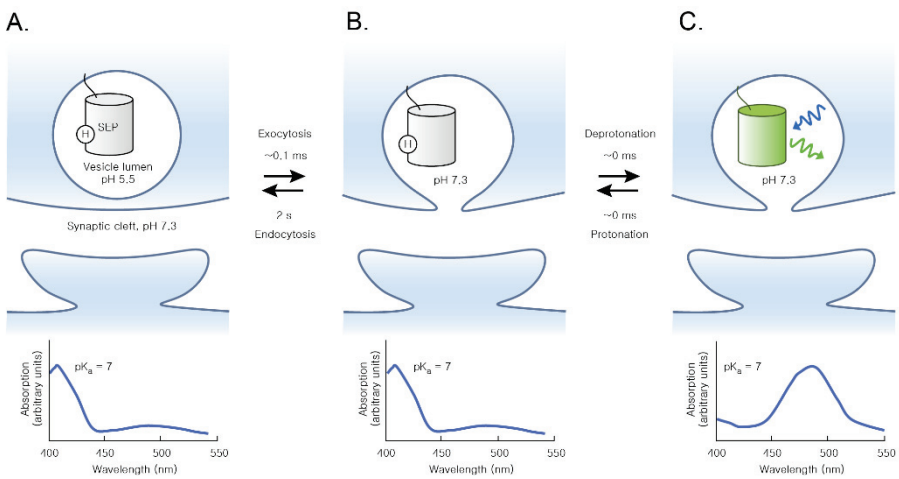

Figure 1. 13 A genetically encoded pH indicator, super ecliptic pHluorin, responding to pH changes during endocytosis or exocytosis

A & B. When a super ecliptic pHluorin (SEP) is expressed inside of a synaptic vesicle. The absorption graph shows that the FP is protonated at pH 5.5 and is unresponsive to a typical GFP excitation wavelength, 488nm. Once the vesicle is released to synaptic cleft (pH 7.3), **C.** the FP's chromophore quickly shifts into the deprotonated state and regain the absorption peak that maximizes near 490 nm. The values shown around the arrow indicate half-rise and half-decay times. Reprinted by permission from Springer Nature: *Nature Neuroscience*, Genetically encoded indicators of neuronal activity, Lin M. Z. and Schnitzer M. J., COPYRIGHT (2016) [14].

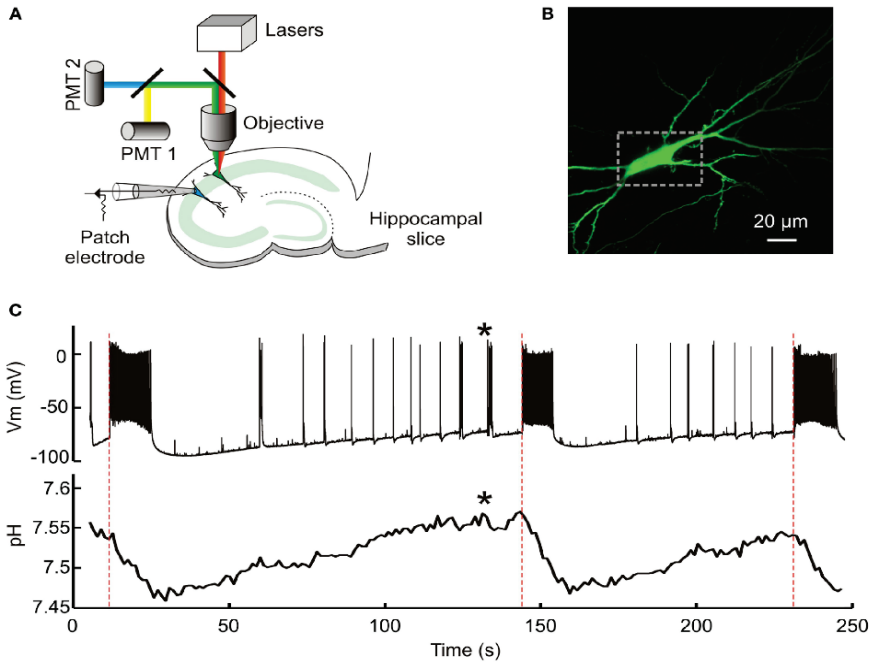

Figure 1. 14 A schematic diagram of representative result of an intracellular pH imaging by using a genetically encoded fluorescent pH indicator during epileptiform activities

A. A cartoon shows a pH indicator transfected neurons prepared as a hippocampal brain slice under an objective lens and a patch clamp electrode recording from an adjacent neuron. **B.** Fluorescence from a pH indicator showing a CA3 neuron expressing a green fluorescent pH indicator. **C.** The simultaneously recorded voltage signal from an adjacent cell and an optical pH trace from the rectangle in B. The epileptiform activity was induced by perfusing 0 Mg^{2+} solution. Note that the decrease in pH signal is associated with the burst of spikes. This image was obtained from Raimondo, J.V., et al., *Front Mol Neurosci*, 2012 [26]. The reuse permission was not required for this journal.

Chapter 2. Rational modification of an interdomain linker region enabled single pixel voltage imaging of action potentials

2.1 Introduction

A genetically encoded voltage indicator (GEVI) converts voltage into fluorescence. The characteristics of a GEVI determine the quality of a voltage imaging experiment. These include a responsive voltage range, amplitude of fluorescence response, the similarity of the optical waveform to the voltage change, the brightness of the fluorescent protein (FP), and the kinetics. Site-directed mutagenesis, directed evolution, or an unintended mutation have contributed in the development of GEVIs with the improved characteristics [52, 63-65, 70, 81, 82, 90, 107-110]. The modifications were spread throughout the GEVI protein molecules but were mainly on the voltage-sensing domain and the FP parts. There has been a limited number of studies that modified the interdomain linker region. Changing the linker length was shown to affect the voltage-dependent fluorescence signal [64, 65, 84, 110, 111]. Jung et al. [110] also reported that the alteration of the linker composition changes the voltage-sensing properties of the zebrafish VSD containing voltage indicator but the alteration was limited to the three amino acid long fusion site only. These results suggest that an interdomain linker is also capable of inducing changes to the voltage-sensing properties.

Based on the previous results, several site-directed mutageneses on a

linker region were conducted to introduce charged amino acid residues and one of the variants showed a ΔF/F of over 50 % at a 200 mV membrane depolarization. Additional mutations in VSD shifted the large response to the physiologically relevant voltage range. This GEVI was named Bongwoori-Pos6. The result from the linker modification was also applied to a previously reported optical sensor, Bongwoori. As a result, Bongwoori-R3 was developed and demonstrated a single trial, single pixel imaging of action potentials.

2.2 Materials and methods

2.2.1 Plasmid DNA construction

As described in Lee et al. [112], gene constructs used in this study were generated by either one-step or two-step polymerase chain reaction (PCR). The CC1 gene construct from a previous project [65] was first used to obtain the VSD of CC1-Neg1. The fluorescent protein part of CC1-Neg1 came from Bongwoori [65]. The first set of linker variants (CC1-Neg2, CC1-Neg3, CC1-Neg4, CC1-Pos5, CC1-Pos6, CC1-Pos7, CC1-Pos8 and CC1-M240) were cloned by two-step overlapping PCRs using CC1-Neg1 as the template. The consecutive single type amino acid linker variants (CC1-9Ds, CC1-9Es, CC1-9Ks, CC1-9Rs, CC1-9Ss, CC1-9Qs and CC1-9As) were generated based on CC1-M240. Then CC1-Pos6 was used to generate D164N-Pos6 and CC1-Pos6-K. Bongwoori-Pos6 was cloned using Bongwoori as a template for the VSD part and CC1-Pos6 for linker and FP parts. Bongwoori linker variants with an arginine at each linker position were mutated from Bongwoori. The pcDNA3.1 / Hygro (+) vector (Thermo Fisher scientific, USA) was used as a backbone vector for all the gene constructs generated. The primers used for gene cloning of individual linker variants are listed in Table 2.1.

Viral vectors to produce adeno-associated virus (AAV) of Bongwoori-R3 and Bongwoori-Pos6 were also generated. To introduce the Bongwoori-R3 insert into an AAV backbone vector with a human synapsin promoter (hSyn), a variant of Bongwoori-R3 that had a BamH1 site at the N-terminus and an EcoR1 site at the C-terminus was synthesized (Integrated DNA Technologies, USA). The pre-existing BamH1 site in the middle of the insert was removed by silently mutating GAT into GAC at 241_{st} amino acid. The gene insert to make the AAV-hSyn-Bongwoori-Pos6 construct was prepared by a simple one-step PCR. SM097A and SM097B primers were used to introduce BamH1 and EcoR1 sites flanking the Bongwoori-Pos6 insert. The synthesized Bongwoori-R3 and the polymerized Bongwoori-Pos6 inserts were then double digested with BamH1 and EcoR1 and ligated into an AAV viral vector.

Primer synthesis and DNA sequencing for construct verification were done commercially (Cosmogenetech and Bionics, both in South Korea).

Primer	Sequence	Construct
NEG1-A	GAATATTTGACTCCCACCAAGAGATGGGGGATCCCATGAG	CC1-Neg1
NEG1-B	GGGATCCCCCATCTCTTGGTGGGAGTCAAATATTCTTGC	
NEG2-A	GAATATTTGATTCCCACGAGGAAATGGGGGATCCCATGAG	CC1-Neg2
NEG2-B	GGGATCCCCCATTTCCTCGTGGGAATCAAATATTCTTGC	
NEG3-A	GAATATTTTATGACCACCAAGAGATGGGGGATCCCATGAG	CC1-Neg3
NEG3-B	GGGATCCCCCATCTCTTGGTGGTCATAAAATATTCTTGC	
NEG-4AA	CAAGAATATTTTATGATCACGAACACGAGGGGGATCCCATGAGTAAAGG	CC1-Neg4
NEG4-BB	CCTTTACTCATGGGATCCCCCTCGTGTTCGTGATCATAAAATATTCTTG	
POS5-A	GAATATTTAGGTCCCACCAAAGAATGGGGAGGCCTATGAG	CC1-Pos5
POS5-B	AGGCCTCCCCATTCTTTGGTGGGACCTAAATATTCTTGC	
POS6-A	GAATATTTAGATCCCACAGAAGGATGGGGAGGCCTATGAG	CC1-Pos6
POS6-B	AGGCCTCCCCATCCTTCTGTGGGATCTAAATATTCTTGC	
POS7-A	GAATATTTTATAGACACCAACGGATGGGGAGGCCTATGAG	CC1-Pos7
POS7-B	AGGCCTCCCCATCCGTTGGTGTCTATAAAATATTCTTGC	
POS8-AA	GCAAGAATATTTTATTCCAGGCAACAAAGGGGCAGGCCTATGAGTAAAGGAGAAG	CC1-Pos8
POS8-BB	CTTCTCCTTTACTCATAGGCCTGCCCCTTTGTTGCCTGGAATAAAATATTCTTGC	
SM014A	GGTTAGCAAGAATATTTTATTCCCACCAACAAATGGGGGATCCCATGAG	CC1-M240
SM014B	CTCATGGGATCCCCCATTTGTTGGTGGGAATAAAATATTCTTGCTAACC	
SM020A	GCTGCGTGTGTGGTTATCTTAGCAAGAATATTTAGATCCCACAGAAGG	Bongwoori-Pos6
SM020B	AAATATTCTTGCTAAGATAACCACACGCAGCAATCTGGCCAACAC	
SM029A	CTTGTTATTTCATGCTGAATTTAGGATTAAGGATATTTGCC	D164N-Pos6
SM029B	GGCAAATATCCTTAATCCTAAATTCAGCATGAAATAACAAG	
SM042A	TTTAAATCCCACAAAAAGATGGGGAAGCCTATGAGTAAAGGAG	CC1-Pos6-Ks
SM042B	GGCTTCCCCATCTTTTTGTGGGATTTAAATATTCTTGCTAACCG	
SM030A	CGCCGGAGAAGGCGGAGAAGGCGCATGAGTAAAGGAGAAGAACTTTTC	CC1-9Rs
SM030B	GCGCCTTCTCCGCCTTCTCCGGCGTCTAAATATTCTTGCTAACCGAACC	
SM048A	GAAAAAGAAGAAAAAGAAAAAGAAGATGAGTAAAGGAGAAGAACTTTTC	CC1-9Ks
SM048B	CTTCTTTTTCTTTTTCTTCTTTTTCTTAAATATTCTTGCTAACCGAACC	
SM049A	GGAAGAAGAGGAAGAGGAGGAAGAAATGAGTAAAGGAGAAGAACTTTTC	CC1-9Es
SM049B	TTCTTCCTCCTCTTCCTCTTCTTCCTCAAATATTCTTGCTAACCGAACC	
SM050A	CTCATCTTCCTCATCCTCTTCCTCAATGAGTAAAGGAGAAGAACTTTTC	CC1-9Ss
SM050B	TGAGGAAGAGGATGAGGAAGATGAGGAAAATATTCTTGCTAACCGAACC	
SM051A	GCAGCAACAGCAGCAACAGCAGCAAATGAGTAAAGGAGAAGAACTTTTC	CC1-9Qs
SM051B	TTGCTGCTGTTGCTGCTGTTGCTGCTGAAATATTCTTGCTAACCGAACC	
SM055A	GATGACGATGATGACGATGATGACATGAGTAAAGGAGAAGAACTTTTC	CC1-9Ds
SM055B	ATCATCGTCATCATCGTCATCATCAAATATTCTTGCTAACCGAACCAC	
SM056A	GCTGCCGCAGCTGCCGCAGCTGCCATGAGTAAAGGAGAAGAACTTTTC	CC1-9As
SM056B	AGCTGCGGCAGCTGCGGCAGCGGCAAATATTCTTGCTAACCGAACCAC	
BR1A	GGTTATCTTAGCAAGAATATTTAGGTCCCACCAACAAGGGG	Bongwoori-R1
BR1B	CCCCTTGTTGGTGGGACCTAAATATTCTTGCTAAGATAACC	
BR2A	CTTAGCAAGAATATTTTATAGGCACCAACAAGGGGATCCC	Bongwoori-R2
BR2B	GGGATCCCCTTGTTGGTGCCTATAAAATATTCTTGCTAAG	
BR3A	GCAAGAATATTTTATTCCAGGCAACAAGGGGATCCCATGAG	Bongwoori-R3
BR3B	CTCATGGGATCCCCTTGTTGCCTGGAATAAAATATTCTTGC	
BR4A	GAATATTTTATTCCCACAGGCAAGGGGATCCCATGAGTAAAGG	Bongwoori-R4
BR4B	CCTTTACTCATGGGATCCCCTTGCCTGTGGGAATAAAATATTC	
BR5A	GAATATTTTATTCCCACCAAAGGGGGGATCCCATGAGTAAAGG	Bongwoori-R5
BR5B	CCTTTACTCATGGGATCCCCCCTTTGGTGGGAATAAAATATTC	
BR6A	GAATATTTTATTCCCACCAACAAAGGGATCCCATGAGTAAAGG	Bongwoori-R6
BR6B	CCTTTACTCATGGGATCCCTTTGTTGGTGGGAATAAAATATTC	
BR7A	GAATATTTTATTCCCACCAACAAGGGAGGCCCATGAGTAAAGGAG	Bongwoori-R7
BR7B	CTCCTTTACTCATGGGCCTCCCTTGTTGGTGGGAATAAAATATTC	
BR8A	CAACAAGGGGATAGGATGAGTAAAGGAGAAGAACTTTTCACTGG	Bongwoori-R8
BR8B	CCTTTACTCATCCTATCCCCTTGTTGGTGGGAATAAAATATTC	

Table 2. 1. Primers used for gene cloning of linker variants.

(This table is from Lee et al., *Scientific Reports*, 2017 [112])

2.2.2 Cell culture and transfection

As described in Lee et al., [112] 10 % fetal bovine serum (Gibco, USA) containing Dulbecco's modified eagle medium (DMEM, Gibco, USA) was supplied to human embryonic kidney 293 cells (HEK 293 cells) cultured in a 5 % CO_2 incubator at 37 °C. Lipofectamine 2000 (Thermo Fisher scientific, USA) was chosen as a transfection reagent. Transient transfection of HEK 293 cells with relevant plasmid DNAs was conducted a day before and incubated for about 20 hours to reach consistent, yet good level of expression for voltage imaging experiment.

Primary neuron culture was prepared by dissecting the hippocampus from embryonic day 17 C57BL/6 mouse (Koatech, South Korea). The dissected hippocampus was subject to mechanical and chemical dissociation steps. Then the dissociated hippocampal neurons were seeded onto a poly-D-lysine (Sigma-Aldrich, USA) coated coverslip at 50,000 cells / mL density. The primary neurons were incubated in a 5 % CO_2 incubator at 37 °C. Animals were handled following an animal protocol approved by the Institutional Animal Care and Use Committee at KIST (animal protocol number 2016-082). At days in vitro (DIV) 5 - 7, primary neurons were transfected with Lipofectamine 2000 (Thermo Fisher scientific, USA) with plasmid DNAs prepared in high

concentration (about 1 μg / μL).

2.2.3 Animals for brain slice voltage imaging

Wild-type C57BL/6 mice (Koatech, South Korea) and Ca^{2+}/calmodulin-dependent protein kinase II (CaMKII) α^{+} - Cre mice (Jackson Laboratory, USA) were used for brain slice voltage imaging. CaMKII α^{+} - Cre mice were bred in a specific pathogen free (SPF) animal facility. Animal experiments were conducted following proper protocols approved by the Institutional Animal Care and Use Committee at Korea Institute of Science and Technology (approval number 2017-031).

2.2.4 Stereotaxic surgery for viral injection in CA1 area

Viral delivery of GEVIs was conducted on at least 6 weeks old male and female mice. Adeno-associated virus (AAV, serotype 2/1) packaged with 'human synapsin1-Bongwoori-R3' or 'human synapsin1-Bongwoori-Pos6' were injected into CA1 area of mouse hippocampus through a glass capillary pipette (0.530 mm inner diameter, World Precision Instruments, USA) connected to a microinjection pump system (Nanoliter injector, World Precision Instruments, USA). The mouse was anesthetized with isoflurane and placed in a stereotaxic device (51730D,

Stoelting, USA). The mouse was immobilized with its front teeth and ears fixed to the device. A small hole was made at coordinate positions 1.7 mm posterior from the bregma and 1.2 mm lateral from the medium line for both hemispheres by using a high speed micro-motor drill (K.1070, Foredom, USA). The virus filled glass capillary tube was then lowered slowly until it reached 1.25 mm ventral position. Four-hundred nanoliter of virus was then injected at a rate of 100 nL / min. Two minutes after the infusion, the glass capillary was removed slowly. The wound was cleaned with phosphate-buffered saline and the scalp was closed with sterile black silk suture. The mouse was then placed back into its own cage and kept at a warm temperature for recovery. Acetaminophen containing water (1.6 mg / mL, Children's Tylenol, Johnson & Johnson, USA) was provided for 3 - 4 days as an analgesic.

2.2.5 Hippocampal brain slice preparation

At least two weeks after the injection, the mouse was euthanized by decapitation for acute brain slice preparation. The scalp and skull were removed with dissecting scissors. The dissected brain was immediately immersed in icy cold, 95 % O_2 / 5% CO_2 gassed high-sucrose artificial cerebrospinal fluid (ACSF). This high sucrose ACSF composed of 87

mM NaCl, 75 mM sucrose, 25 mM $NaHCO_3$, 2.5 mM KCl, 0.5 mM $CaCl_2$, 7 mM $MgCl_2$, 1.25 mM NaH_2PO_4-$2H_2O$, 25 mM $NaHCO_3$, and 25 mM D-glucose at pH 7.4 and was constantly bubbled with 95% O_2 / 5% CO_2 for the whole procedure. Three-hundred micrometer thick hippocampal brain slices were coronally cut using a vibratome (VT-1200, Leica, Germany). Each brain slice was divided into left and right hemispheres before it was placed into 95 % O_2 / 5 % CO_2 bubbled normal ACSF filled mesh chamber that was incubated at 37℃ for at least an hour.

2.2.6 Electrophysiology and fluorescence imaging for HEK 293 cells and primary neurons

The details for cellular electrophysiology protocol is described in Lee et al., [112]. Glass capillary tubes (1B150F-4, World precision instruments, USA) were pulled to pipette resistances of 3-5 MΩ for HEK 293 cells and 3-6 MΩ for cultured primary neurons. Internal solution containing 120 mM K-aspartate, 4 mM NaCl, 4 mM $MgCl_2$, 1 mM $CaCl_2$, 10 mM EGTA, 3 mM Na_2ATP and 5 mM HEPES (pH = 7.2) was filled into the pulled pipettes. The patching chamber was constantly perfused with bath solution containing 150 mM NaCl, 4 mM KCl, 1 mM $MgCl_2$,

2 mM $CaCl_2$, 5 mM D-glucose and 5 mM HEPES (pH = 7.4). Transiently transfected HEK 293 cells or primary neurons grown on a coverslip were then placed in the patching chamber (RC-26G, Warner instruments, USA) that was kept at 34 ºC. A patch clamp amplifier (EPC 10, HEKA, Germany) was used for any electrophysiological recording or stimulation.

Simultaneous fluorescence imaging of transfected HEK 293 cells or cultured neurons was conducted under an inverted microscope (IX71; Olympus, Japan). The light from a Xenon arc lamp (Osram, Germany) was illuminated to the specimen through a 60X oil-immersion objective lens (1.35 numerical aperture, Olympus, Japan). A typical GFP filter set was used (excitation: FF02-472/30, dichroic mirror: FF495-Di03, and emission: FF01-497 / LP, all by Semrock, USA). Emitted light from the fluorescent protein was recorded by a high speed CCD camera (Neuro CCD, RedShirtImaging, USA) at a rate of 1000 frames per second unless otherwise noted. Software from the high speed camera manufacturer (Neuroplex, RedShirtImaging, USA) was used to both control the camera acquisition and initiation of electrophysiological manipulation. For voltage clamp recording, every cell was imaged for 16 trials unless otherwise noted.

2.2.7 Electrophysiology and fluorescence microscopy for brain slice

A 50 μs, single square shaped pulse was modulated by a current stimulator (DS3, Digitimer, UK) and applied to Schaffer collaterals through a bipolar tungsten electrode (30201, FHC, USA).

To observe voltage imaging result from CA1 region, an upright fluorescence microscope (Slicescope, Scientifica, UK) together with a blue, 460 nm LED (YHP-Mic-LED-460, Prizmatix, Israel) was used and it was filtered by a GFP filter set (GFP-3035D-OMF, Semrock, USA). The light intensity was measured to be 3.7 mW / mm^2. Emitted fluorescence was collected by a high-speed CCD camera (Neuro CCD, RedShirtImaging, USA).

Local field potential from CA1 region was simultaneously recorded by an electrode touching the stratum pyramidale area through ACSF (125 mM NaCl, 25 mM $NaHCO_3$, 2.5 mM KCl, 2.5 mM $CaCl_2$, 1 mM $MgCl_2$, 1.25 mM NaH_2PO_4-$2H_2O$, 3 mM Na-pyruvate, 1 mM ascorbic acid, and 25 mM D-glucose and pH 7.4) filled glass pipette (4 - 5 MΩ). A patch clamp amplifier (Multiclamp 700B) and a digitizer (Digidata 1550B, both by Molecular devices, USA) were used to trigger the current stimulator and to record local field potential. The drugs for slice recording were prepared at following concentrations in ACSF: 50 μM

AP5, 40 µM CNQX and 40 µM bicuculline.

2.2.8 Data acquisition and analysis

Fluorescence read-out from voltage imaging experiments was first acquired and analyzed in Neuroplex software (RedShirtImaging, USA). This included calculations of ΔF and ΔF/F from pixels chosen.

$$\Delta F = F_x - F_0$$

$$\Delta F/F = \left(\frac{F_x - F_0}{F_0}\right) * 100$$

Voltage-sensing properties of a voltage indicator and time constants were analyzed by using Microsoft Excel (Microsoft, USA) and Origin Pro 2016 (Origin Lab, USA) as previously described in Piao et al. [65]. Primary neurons expressing a voltage indicator were imaged under whole cell current clamp mode in single trials. Three representative cells showing firing rates of 15 - 25 Hz during a 200 msec current pulse were chosen for each of the five GEVIs shown in this work. Correlation coefficients between the fluorescence signal stored in every pixel versus electrical signal was calculated by using custom codes in MATLAB (Mathworks, USA). All pixels were then sorted by their Pearson's r coefficient values to determine the best pixel. For calculation of signal-to-noise ratio (SNR), first 100 frames (100 msec for 1 kHz recording)

prior to any electrical stimulation was taken and their standard deviation was used as a noise value. This noise value was then used as a denominator of ΔF/F value at a time point of interest.

2.2.9 Photobleaching experiment of HEK 293 cells

The same light source (Xenon arc-lamp) and intensity were used for photobleaching experiment of HEK 293 cells. The light intensity at the specimen was measured to be 1 mW / mm^2. A 40 sec light-on and 20 sec light-off step was repeated to photobleach a cell of interest. The patching chamber was kept at 34 °C with the same bath solution perfused throughout the experiment as described earlier. During the 40 sec light-on period, images were acquired by the high-speed CCD camera (NeuroCCD, RedShirtImaging, USA) at 40 frames per seconds. Fluorescence values from each cell was plotted to fit into an exponential decay function and time constants were determined by using Origin Pro 8.6 (Origin Lab, USA).

2.2.10 Baseline change analysis of neurons

The baseline fluorescence drop of Bongwoori-R3 was analyzed with a total of 14 cells that were patched with either normal or high buffered

internal solution. Drops in ΔF/F values after 200 msec or 800 msec long current pulse were calculated unless a neuron underwent more than 3 mV membrane potential change during the current pulse. Internal solution with high buffering capacity was prepared following Kang and Baker [113] and it contained 100 mM HEPES (pH = 7.2) unlike the normal solution that contained 5 mM HEPES.

2.2.11 Statistics

The sample sizes were similar to those used by others in the field. Normality of data was determined by the Shapiro-Wilk test. Difference between means from two different groups were compared by the two-tailed Student's t-test. Means from more than three different groups were analyzed by one-way analysis of variance (ANOVA) and then the post-hoc Tukey test was performed to find any significance between the averaged values. As some groups did not show normal distribution, the Kruskal-Wallis ANOVA followed by the Dunn's multiple comparisons test was performed. All statistical analyses came from Origin Pro 2016 (Origin Lab, USA) or Prism 7 (GraphPad, USA). Any error bar shown in this work is standard error of the mean (SEM). The shaded area for fluorescence traces also represents SEM.

2.3 Results

2.3.1 Insertion of positively charged amino acid residues in linker regions increased the ΔF/F signal size for depolarization of the plasma membrane, while the negatively charged linkers reduced the size

To test the role of the linker region in resolution of membrane potential change, a voltage-sensing domain derived from the wild-type Ci-VSD (the voltage-sensing domain from *Ciona intestinalis*), CC1 reported in Piao et al. [65], was used.

Eight linker variants of CC1-M240 were generated as shown in Figure 2.1 to further test the hypothesis that an interdomain linker placed in between the VSD and the FP affects the voltage-sensing ability of the indicator. Each of the 8 gene constructs was transfected and tested to examine its voltage sensing properties.

The four negatively charged linkers showed their voltage ranges shifted to more positive membrane potentials compared to the wild-type (Figure 2.2.A). The $V_{1/2}$ values of the positive linkers did not deviate too much from that of CC1-M240 (Table 2.1). In terms of the voltage induced fluorescence signal size, however, the positively charged linkers

appeared to be larger while the negative linkers showed reduced ΔF/F signal size. Representative fluorescence traces versus 5 step voltage pulses are shown in Figure 2.2.C for the lowest (CC1-Neg4) and the highest (CC1-Pos6) change in the fluorescence signals. A substantial increase in the amplitude of fluorescence change could be seen from a CC1-Pos6 expressing HEK 293 cell showing 55 % ΔF/F for a 200 mV voltage pulse.

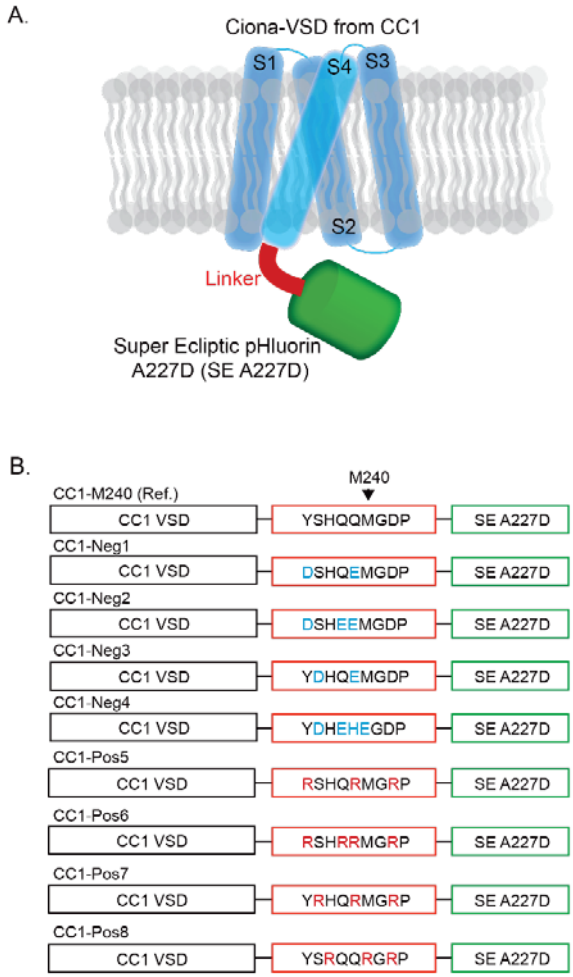

Figure 2. 1. A schematic drawing of the genetically encoded voltage indicator.

A. CC1-M240. **B.** Amino acid compositions of suggested charged linker variants. 'M240' denotes the methionine at 240th amino acid position. * VSD: Voltage-sensing domain, SE A227D: super eclipic pHluorin with A227D mutation. (This figure was modified from Lee et al., *Scientific Reports*, 2017 [112])

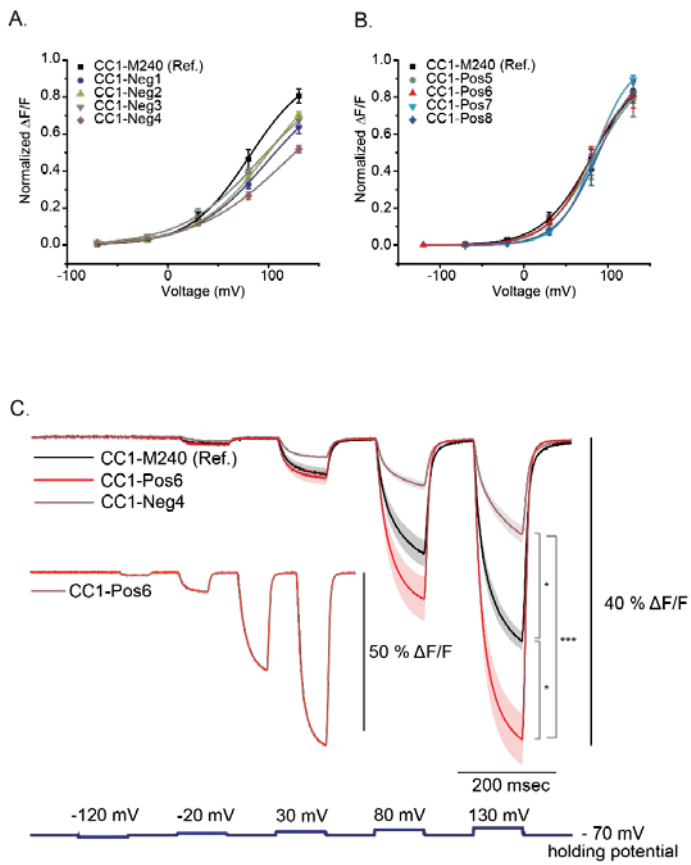

Figure 2. 2. Voltage sensing properties of the 8 linker variants with negative or positive charges.

A. Voltage ranges of the negative linker variants and **B.** positively charged linker variants. **C.** Averaged fluorescence traces of CC1-M240 (reference), CC1-Pos6, and CC1-Neg4. The number of cells analyzed; CC1-M240: 4, CC1-Neg1: 3, CC1-Neg2: 4, CC1-Neg3: 5, CC1- Neg4: 4, CC1-Pos5: 4, CC1-Pos6: 6, CC1-Pos7: 6, CC1-Pos8: 4. Asterisks in C indicate p-value criteria; *$p < 0.05$ and ***$p < 0.001$. (This figure was modified from Lee et al., *Scientific Reports*, 2017 [112])

Constructs	$V_{1/2}$ (mV)
CC1-M240	81 ± 4
CC1-Neg1	98 ± 13
CC1-Neg2	100 ± 7
CC1-Neg3	92 ± 16
CC1-Neg4	116 ± 30
CC1-Pos5	84 ± 1
CC1-Pos6	78 ± 7
CC1-Pos7	85 ± 1
CC1-Pos8	88 ± 1
D164N-Pos6	37 ± 6
Bongwoori-Pos6	-28 ± 3
Bongwoori-R3	-3 ± 1
Bongwoori	6 ± 1

Table 2. 2. $V_{1/2}$ values of linker variants derived from Boltzmann function.

$V_{1/2}$ represents the voltage value a normalized fluorescence trace is at half of its maximum. Standard error of the mean was shown with averaged value. The number of cells for each construct; CC1-M240: 4, CC1-Neg1: 3, CC1-Neg2: 4, CC1-Neg3: 5, CC1-Neg4: 4, CC1-Pos5: 4, CC1-Pos6: 6, CC1-Pos7: 6, CC1-Pos8: 4, D164N-Pos6: 6, Bongwoori-Pos6: 4, Bongwoori-R3: 5, Bongwoori: 4. (This table is from Lee et al., *Scientific Reports*, 2017 [112])

2.3.2 Effects of different charge, size, and polarity of the linker amino acid residues on voltage imaging of membrane potential

The difference between the linker regions of CC1-M240 and CC1-Pos6 was four arginine (R) residues substituted into the latter variant. In order to verify if the positive charge itself caused the increase in the voltage-induced optical signal, another positively charged amino acid, lysine (K) was introduced into the same positions of the arginine residues resulting in the CC1-Pos6-K construct (Figure 2.3). This lysine version of CC1-Pos6 showed very slow kinetics needing longer voltage pulses to test its voltage sensing properties. Also, CC1-Pos6-K's voltage-dependent fluorescence signal was reduced to almost half of its arginine version. This suggests it was not just the positive charge that caused the large magnitude of CC1-Pos6. The difference in the size of lysine and arginine could be another factor and / or relative orientations of the linkers to the VSD and to the FP might have been modified due to the amino acid substitution.

Next, the entire 9 amino acids of the linker region were replaced with only one type of residue. Nine arginines or 9 lysines were inserted in the linker region and they showed indistinguishable fluorescence traces from CC1-M240's. Single type linker variants with negatively charged amino

acids showed even more interesting results. Regardless of whether glutamic acid or aspartic acid was used to make a negative charge only variant, there was very small voltage-induced fluorescence change (Figure 2.4). The figure inset included next to the traces show the good expression in the HEK 293 cell with the CC1-9Ds. Three more single amino acid only constructs consisting of either alanines (none-polar), serines (polar), or glutamines (polar) were also tested. This was to see if none-charged but polar residues exhibit any difference from the charged amino acids. However, the alanine only construct showed the largest $\Delta F/F$ signal size among them meaning the polarity of amino acid residues did not matter.

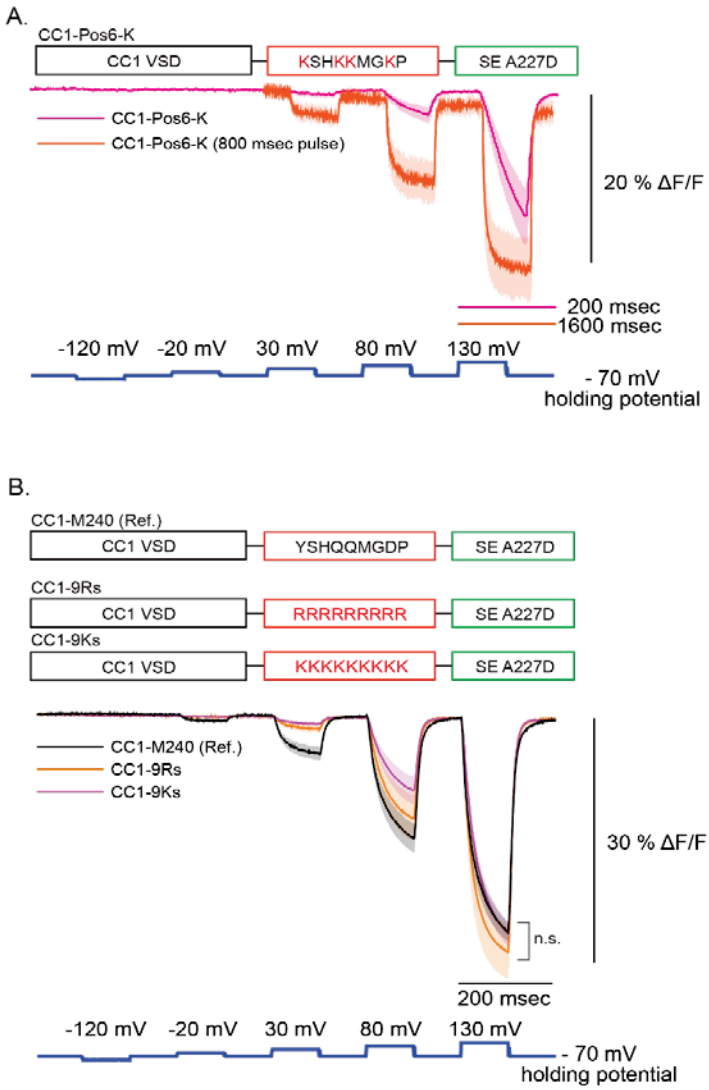

Figure 2. 3. The type and number positive charges in the linker region.

A. CC1-Pos6 with its arginines substiuted to lysines. **B.** Linkers consisted of a single type positive charges. CC1-M240: 4, CC1-Pos6-K: 4, CC1-Pos6-K (800 msec pulse): 4, CC1-9Rs: 4, CC1-9Ks: 4. * n.s. : not significant. (From Lee et al., *Scientific Reports*, 2017 [112])

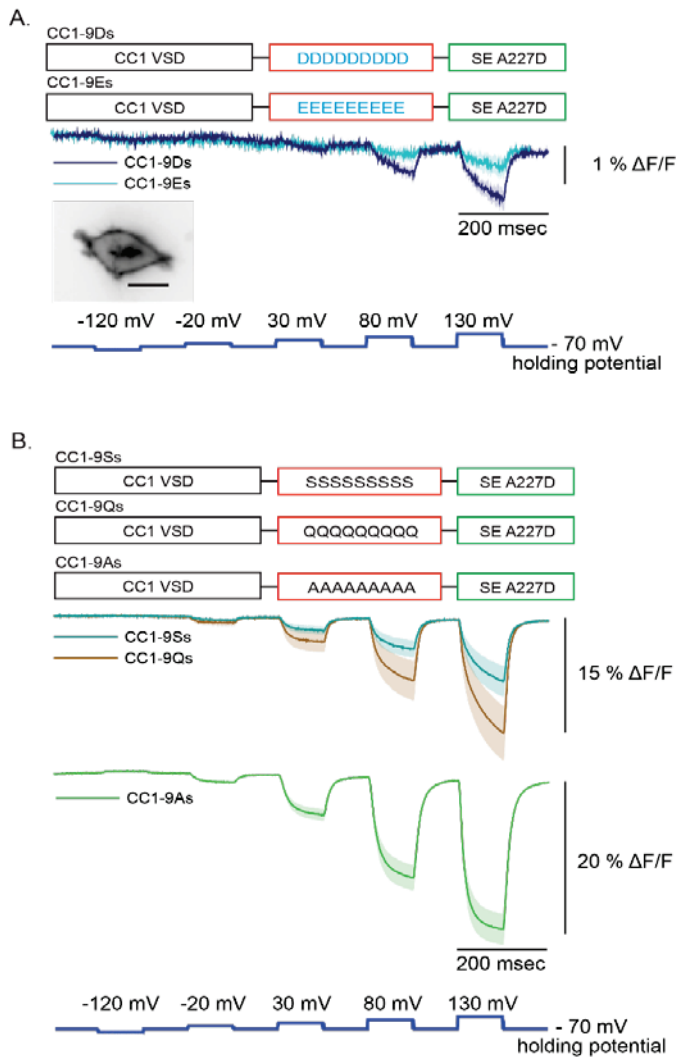

Figure 2. 4. Linker variants with negative or none-charged amino acids.

A. Variants with 9 glutamic acids (E) or 9 aspartic acids. The inset shows a CC1-9Ds expressing HEK 293 cell (D). **B.** Polar amino acids (serine or glutamine) or a none-polar amino acid, alanine linker variants. CC1-9Ds: 3, CC1-9Es: 3, CC1-9Ss: 4, CC1-9Qs: 4, CC1-9As: 5. Scale = 20 µm. (From Lee et al., *Scientific Reports*, 2017 [112])

2.3.3 Introducing voltage-sensing domain mutations to CC1-Pos6 indicated that the positively charged linker shifted the voltage range to more negative membrane potentials

Although CC1-Pos6 showed a large optical response to a 200 mV voltage pulse, the voltage sensitivity is out of physiological range. The on-response was very slow (Figure 2.2.C and Table 2.3). Therefore, a palette of voltage-sensing domain mutations demonstrated by Piao et al. [65] was applied to make the CC1-Pos6's large fluorescence response beneficial to optical imaging for physiologically relevant voltage ranges.

Among many mutations from this previous work, D164N and the triple mutations (A154N, R217Q and R229I) shifted the voltage sensitivity to more negative potentials (Figure 2.5). The D164N shifted $V_{1/2}$ of CC1-Pos6 to 37 ± 6 mV but delayed the off time constant more than 2 - fold (Table 2.3). The left shifted voltage range increased ΔF/F per 100 mV to about 20 % but the slow kinetics caused by D164N mutation was undesirable. The triple mutations to the voltage-sensing domain shifted the responsive voltage range and improved its speed. This novel construct was named Bongwoori-Pos6. The voltage range of CC1-Pos6 was centered at 78 ± 7 mV but now it was left shifted to - 28 ± 3 mV (Figure 2.6). Analyzing the on and off time constants for the 100 mV

voltage pulse suggested that Bongwoori-Pos6 showed similar but slightly faster response than the original Bongwoori (Table 2.3). However, Bongwoori-Pos6's $V_{1/2}$ value was -30 mV more negative than that of Bongwoori. Either the 4 arginines in Bongwoori-Pos6, or the 1 amino acid difference in the linker length, or a combination of the two between the variant and the original Bongwoori might have caused these differences.

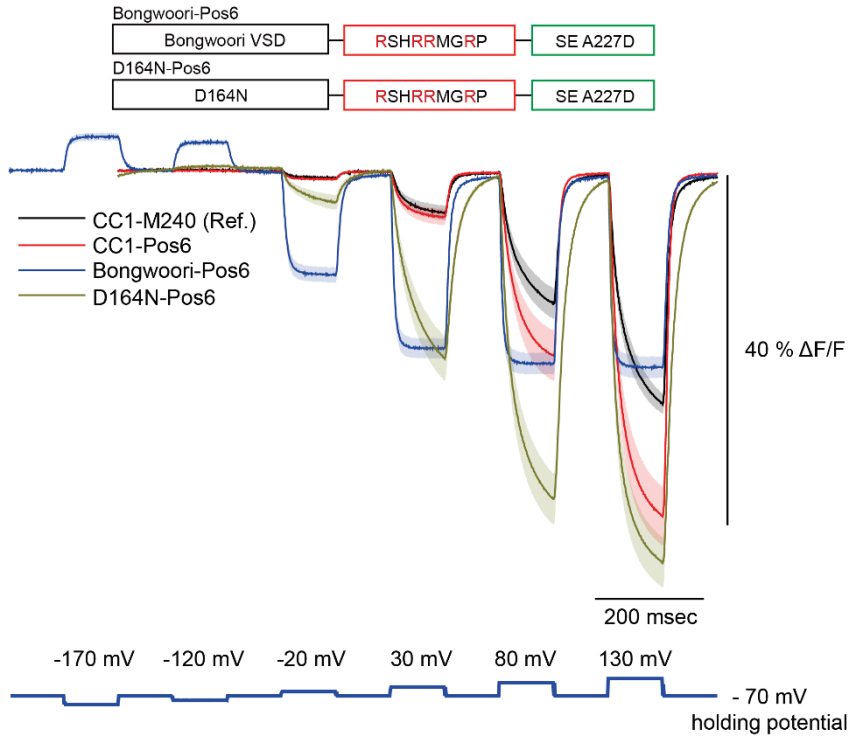

Figure 2. 5. Voltage-sensing domain mutations introduced in CC1-Pos6.

Bongwoori-Pos6 has three voltage-sensing domain mutations (A154D, R217Q and R229I) compared to CC1-Pos6. D164N-Pos6 only has D164N. Twelve trials were averaged for each Bongwoori-Pos6 expressing HEK 293 cell. The number of cells for each construct; CC1-M240: 4, CC1- Pos6: 6, Bongwoori-Pos6: 4 and D164N-Pos6: 6. (This figure is from Lee et al., *Scientific Reports*, 2017 [112])

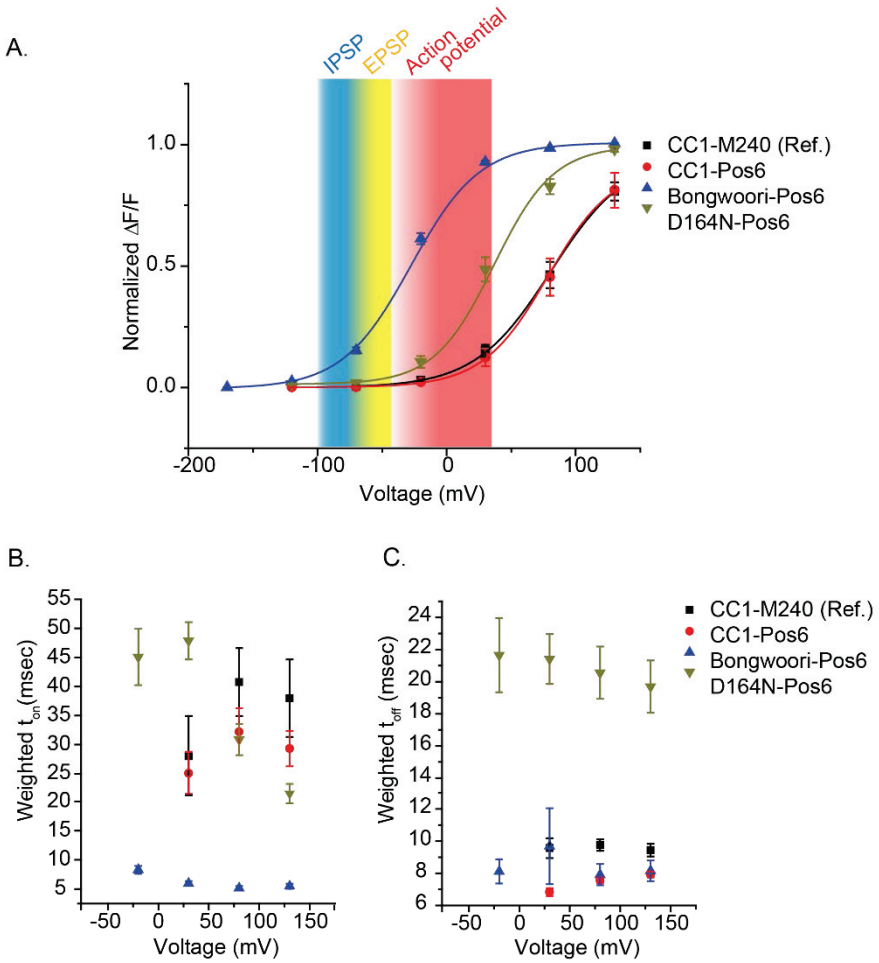

Figure 2. 6. Adjusted voltage sensing properties of CC1-Pos6 variants.

A. Averaged data for each voltage pulse were plotted and fitted to Boltzmann function to assess different voltage ranges. **B.** Weighted time constants for onset of voltage pulses tested. **C.** Weighted time constants for off response. The number of cells; CC1-M240: 4, CC1- Pos6: 6, Bongwoori-Pos6: 4 and D164N-Pos6: 6. IPSP: inhibitory postsynaptic potential, EPSP: excitatory postsynaptic potential. (This figure is from Lee et al., *Scientific Reports*, 2017 [112])

Constructs	State	Weighted τ (msec)	Fast τ (msec)	Slow τ (msec)	% fast
CC1-M240 (Ref.)	On	28 ± 7	15 ± 3	56 ± 16	72 ± 16
	Off	10 ± 1	8 ± 1	24 ± 1	83 ± 7
CC1-Pos6	On	25 ± 4	12 ± 2	60 ± 6	73 ± 8
	Off	7 ± 1	7 ± 1	-	100
D164N-Pos6	On	48 ± 3	17 ± 8	54 ± 2	32 ± 14
	Off	21 ± 2	21 ± 2	-	100
Bongwoori-Pos6	On	6 ± 1	6 ± 1	-	100
	Off	7 ± 1	7 ± 1	-	100
Bongwoori-R3	On	11 ± 1	7 ± 1	45 ± 1	90 ± 1
	Off	10 ± 2	6 ± 1	46 ± 6	91 ± 1
Bongwoori	On	17 ± 1	9 ± 1	40 ± 4	76 ± 2
	Off	14 ± 1	8 ± 1	52 ± 9	86 ± 1

Table 2. 3. Time constants calculated for selected linker variants.

Each time constant came from either double or single exponential decay function. Values are shown as the mean ± SEM (standard error of the mean). The number of cells analyzed; CC1-M240: 4, CC1-Pos6: 6, D164N-Pos6: 6, Bongwoori-Pos6: 4, Bongwoori-R3: 5, Bongwoori: 4. (This table is from Lee et al., *Scientific Reports*, 2017 [112])

2.3.4 A single arginine residue inserted at the third position of Bongwoori's linker region improved the signal size and maintained the voltage range for an efficient measurement of action potentials

Bongwoori-Pos6 exhibited a promising result but its $V_{1/2}$ near - 30 mV hindered the fast kinetics from being fully utilized. An action potential from a neuron is modulated at the millisecond time scale. The voltage range that an action potential spike arises in such a fast phase is usually from - 40 mV to 30 mV. Therefore, having a $V_{1/2}$ near 0 mV will render a voltage indicator fully capable of imaging this fast excitatory neuronal event.

According to the above-mentioned results, a few charges or an amino acid difference in the linker length can affect voltage-sensing properties of Bongwoori even when the same voltage-sensing domain is used. Since Bongwoori was a good voltage indicator for action potential imaging, an arginine was inserted into each position of Bongwoori's linker region as a direct attempt to improve the fluorescence signal strength. Figure 2.7 shows that having an arginine at a linker region was sufficient in making a significant increase in $\Delta F/F$ signal size of Bongwoori especially in the voltage range of membrane depolarization. This position was the third position where an arginine replaced a histidine. Therefore, this new

variant was named Bongwoori-R3. The $V_{1/2}$ value of this novel voltage indicator was optimized to measure action potentials spikes (- 3 ± 1 mV, Table 2.2).

The comparison of Bongwoori to the two linker variants, Bongwoori-Pos6 and Bongwoori-R3 revealed that the new ones both showed improved fluorescence signals for a 100 mV voltage change in HEK 293 cells (Figure 2.8A). The differences in the optical signal sizes of 50 mV (at - 20 mV membrane potential) and 100 mV (at 30 mV membrane potential) depolarization pulses for Bongwoori-Pos6 and Bongwoori-R3 suggest that the latter will likely to show steeper fluorescence increase near the active voltage range of an action potential. The graphic inserted in Figure 2.8B helps understand how the differences in responsive voltage range may affect the voltage imaging experiment of distinct neuronal events.

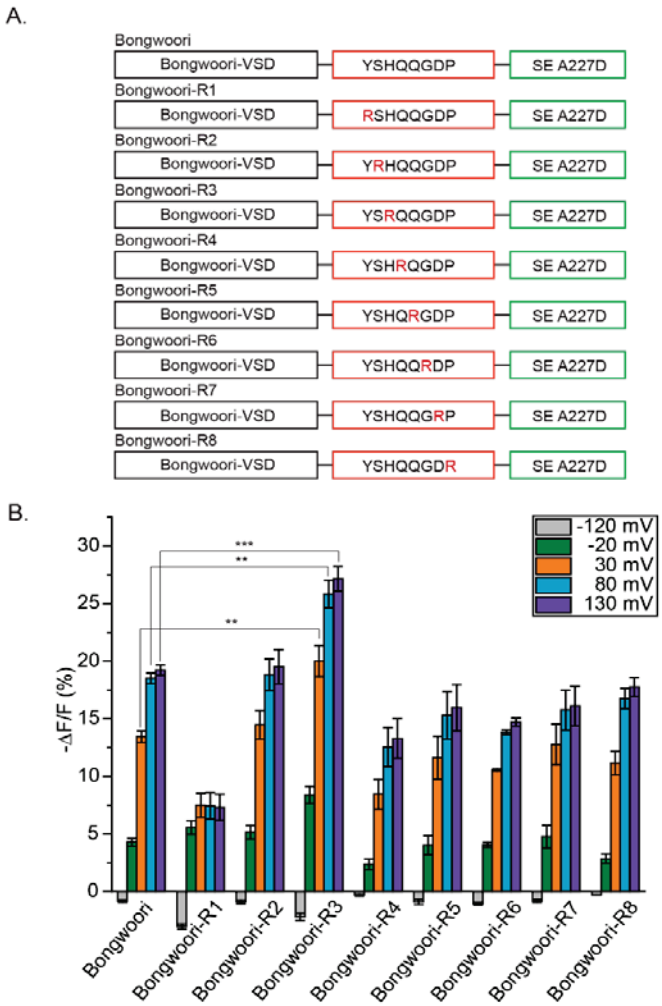

Figure 2. 7. Bongwoori arginine scanning results.

A. Schematic showing variants generated for arginine scanning. **B.** Resulted voltage imaging data of the variants. Bongwoori-R3 showed improved signal size. The number of cell tested; Bongwoori: 4, Bongwoori-R1: 4, Bongwoori-R2: 5, Bongwoori-R3: 5, Bongwoori-R4: 4, Bongwoori-R5: 4, Bongwoori-R6: 4, Bongwoori-R7: 4, Bongwoori-R8: 4 and Bongwoori- Pos6: 4. (This figure is from Lee et al., *Scientific Reports*, 2017 [112])

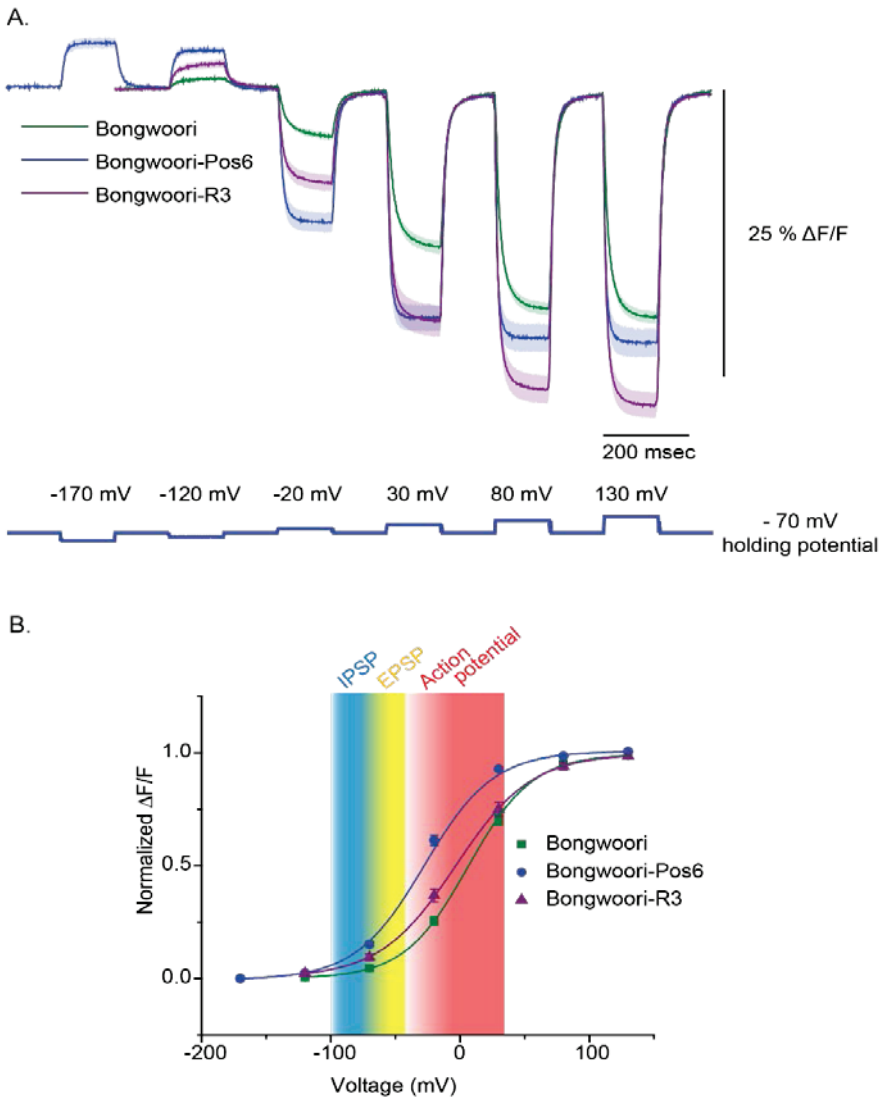

Figure 2. 8. Comparison of Bongwoori and two linker variants.

A. Fluorescence traces of Bongwoori, Bongwoori-Pos6 and Bongwoori-R3. **B.** Normalized ΔF/F values fitted to the Boltzmann function showing responsive voltage ranges. Bongwoori: 4 cells, Bongwoori-R3: 5 cells and Bongwoori-Pos6: 4. (From Lee et al., *Scientific Reports*, 2017 [112])

2.3.5 The improved fluorescence response and the near zero millivolt $V_{1/2}$ of Bongwoori-R3 resolved action potentials with better contrast

The voltage imaging results of Bongwoori-R3 and Bongwoori-Pos6 from HEK 293 cells were compelling enough to expect they may perform better in resolving action potentials than their predecessor, Bongwoori, in neurons. Three previously reported voltage indicators including ArcLight A242 [64], ASAP-1 [67] and Bongwoori [65] were also tested together with the linker variants for comparison (Figure 2.9). Both ArcLight A242 and ASAP-1 also use GFP variants and consisted of a voltage-sensing domain from voltage-sensitive phosphatases. Figure 2.9 shows fluorescence traces averaged from pixels representing either the soma (red) or two separate processes (blue and yellow). All constructs resolved action potentials from each region of interest (ROI) but traces of Bongwoori-R3 most clearly distinguished an action potential spike from subthreshold activity.

Arclight A242's fluorescence signal amplitude responding to an action potential was the largest (Table 2.4) but most of the signal was from subthreshold activity instead of the actual spike. Bongwoori-R3 resolved action potentials with smaller fluorescence amplitude than ArcLight A242 but showed better contrast for the spikes (Figure 2.10.B). The

larger optical signal size of Bongwoori-R3 for the voltage range of action potentials contributed to a signal to noise ratio (SNR) that was comparable to that of ArcLight A242 and twice that of ASAP-1's (Figure 2.10.A and Table 2.3). ASAP-1 clearly visualized each action potential with excellent temporal resolution due to its fast time constants of near 2 msec [67]. However, the total ΔF/F size of ASAP-1 for an action potential was almost one third of ArcLight A242's response. Bongwoori-R3 is neither the fastest GEVI nor does it have the largest ΔF/F, but this GEVI could still manage to visualize evoked action potentials better than the two most popular voltage indicators, ArcLight A242 and ASAP-1. Besides, Bongwoori-R3 was able to resolve spikes firing at a rate of 65 Hz (Figure 2.10.C). Both Bongwoori and Bongwoori-Pos6 resulted similar optical responses except for brightness and SNR which was caused by the variation of expression levels.

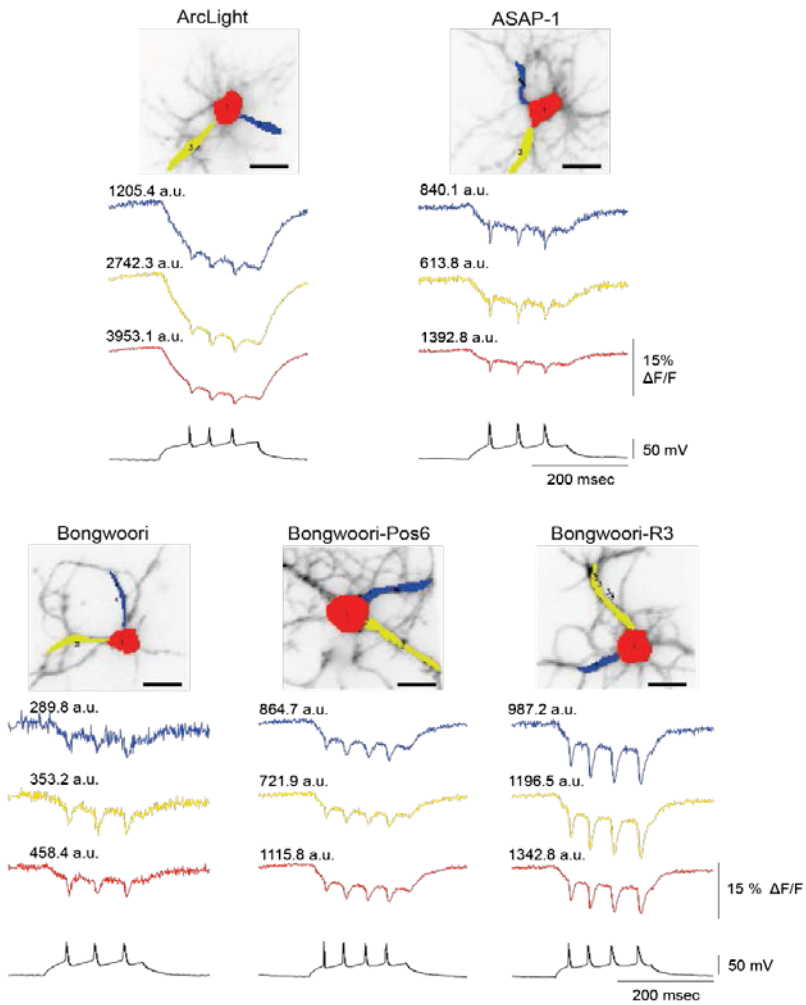

Figure 2. 9. Voltage imaging of evoked action potentials from primary neurons.

Fluorescence traces averaged from selected pixels. Soma is in red, two separates processes are in blue and yellow. The abitrary unit (a.u.) values written above each trace is the averaged brightness of each region of interest. Scale bar = 20 μm. (This figure is from Lee et al., *Scientific Reports*, 2017 [112])

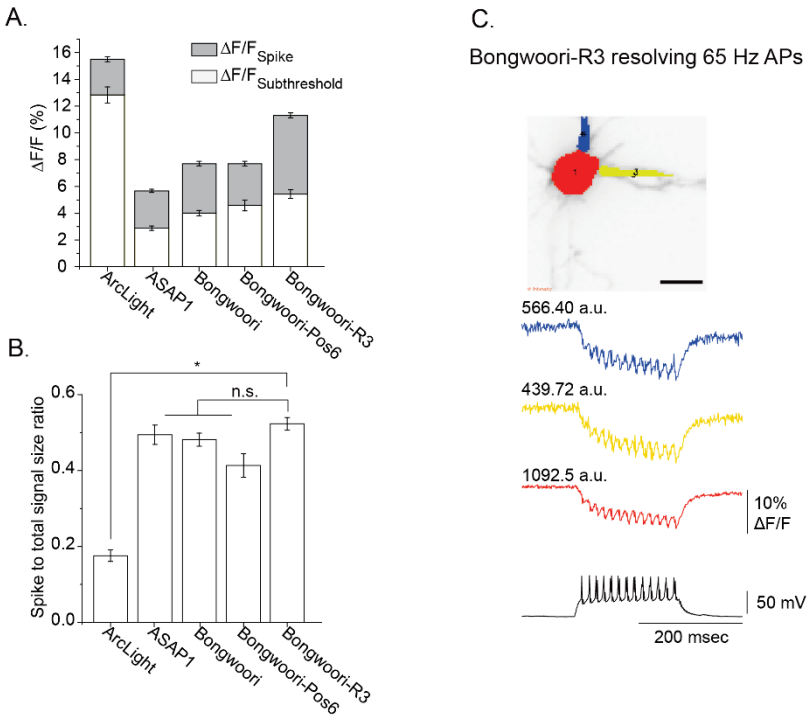

Figure 2. 10. Data analyzed from the spatially averaged traces in Figure 2.9.

A. The gray colored part was averaged from the fluorescence signal responsible from threshold potential to the action potential peak, and the white area shows ΔF/F signal resolving subthreshold voltage range. **B.** The ratio between ΔF/F spike versus ΔF/F subthreshold calculated for each GEVI tested. **C.** A Bongwoori-R3 expressing neuron firing action potentials at 65 Hz. The number of action potentials averaged per cell for each construct; 3, 5 and 4 for ArcLight, 5, 3 and 4 for ASAP-1, 3, 3 and 5 for Bongwoori, 4, 4 and 3 for Bongwoori-Pos6 and 4, 4 and 4 for Bongwoori-R3. The asterisk in B indicates *$p < 0.05$. Scale bar = 20 µm. (This figure is from Lee et al., *Scientific Reports*, 2017 [112])

Soma (Spatially averaged)	ArcLight A242	ASAP1	Bongwoori	Bongwoori-Pos6	Bongwoori-R3
Brightness (a.u.)	1923 ± 350	1162 ± 57	558 ± 41	1034 ± 74	1055 ± 91
ΔF/F - total (%)	15.5 ± 0.5	5.7 ± 0.1	7.7 ± 0.3	7.7 ± 0.4	11.3 ± 0.4
ΔF/F - spike (%)	2.7 ± 0.2	2.8 ± 0.1	3.7 ± 0.2	3.1 ± 0.2	5.9 ± 0.2
Spike to total signal size ratio	0.18 ± 0.02	0.49 ± 0.03	0.48 ± 0.02	0.41 ± 0.03	0.52 ± 0.02
SNR	68 ± 7	26 ± 1	19 ± 1	33 ± 3	52 ± 4
Action potential amplitude (mV)	86 ± 1	85 ± 3	96 ± 2	85 ± 4	80 ± 2

Table 2. 4. Characteristics of the five GEVIs analyzed from the spatially averaged traces responding to induced action potentials.

Values were shown as mean ± SEM. The number of action potentials analyzed were; ArcLight: 12, ASAP1: 12, Bongwoori: 11, Bongwoori-Pos6: 11 and Bongwoori-R3: 12 all from the three best cells per GEVI. (This table is from Lee et al., *Scientific Reports*, 2017 [112])

2.3.6 Single pixel resolution of action potentials with Bongwoori-R3

The true advantage of voltage imaging would be turning every pixel of a CCD sensor into an alternative electrode. The best pixel of the neuronal recordings from previous section may accomplish this goal.

Pearson's correlation coefficients between every pixel and the electrophysiologically recorded voltage signal was calculated for each voltage imaging trial. Then the best pixel for individual recording of ASAP-1, ArcLight A242, Bongwoori-Pos6 and Bongwoori-R3 was determined. Figure 2.11 shows the fluorescence trace of those pixels for each GEVI. Surprisingly, the unfiltered single pixel trace of Bongwoori-R3 successfully visualized all individual action potentials. It was interesting that the brightest pixel from the ArcLight A242 (4879.1 a.u.) recording appeared to have the lowest noise level but still failed to resolve the third action potential spike. The trace from the best correlated ASAP-1 pixel did not robustly show individual action potentials. Since, however, the ASAP-1 pixel's brightness was below 1000 a.u. unlike the others', a dimmer (lower SNR level) pixel from Bongwoori-R3 was also plotted in dark blue color and it still showed all individual action potentials clearly.

Averaging the top 5 % correlated pixels resulted in a trace with better

SNR for each GEVI. The root-mean square deviation analysis (RMSD) of the normalized top 5 % traces versus relevant the voltage signal provided a way to quantify how well each GEVI resembles the shape of the electrophysiologically recorded membrane potential (Figure 2.12.A). Arclight A242 previously showed the highest SNR values from both the spatially averaged traces (Table 2.4) and the single best pixels (Table 2.5) but the RMSD analysis shows that ArcLight A242 differs most among the GEVIs tested. Due to the shifted $V_{1/2}$ towards negative potentials, Bongwoori-Pos6's top 5 % traces deviated more than that of Bongwoori-R3. Bongwoori-R3 and ASAP-1 traces showed similar deviations smaller than the other two GEVIs.

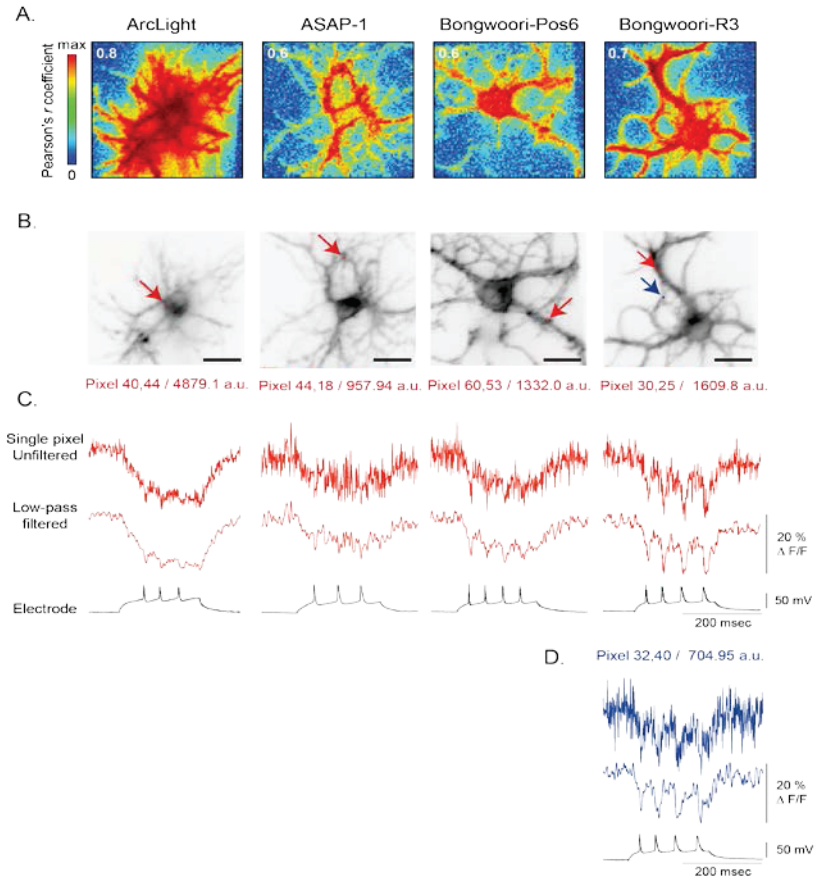

Figure 2. 11. The fluorescence traces from the highest correlated pixels.

A. Heat maps showing correlation coefficient of optical signal from each pixel versus the electrically recorded voltage signal. **B.** The best correlated pixels were indicated with the red arrows. Fluorescence intensities were indicated in arbitrary unit (a.u.). **C.** Fluorescence traces of the highest correlated pixels from B. **D.** A fluorescence trace from the dimmer pixel indicated by a blue arrow in B. for Bongwoori-R3. Scale bars: 20 μm. (This figure is from Lee et al., *Scientific Reports*, 2017 [112])

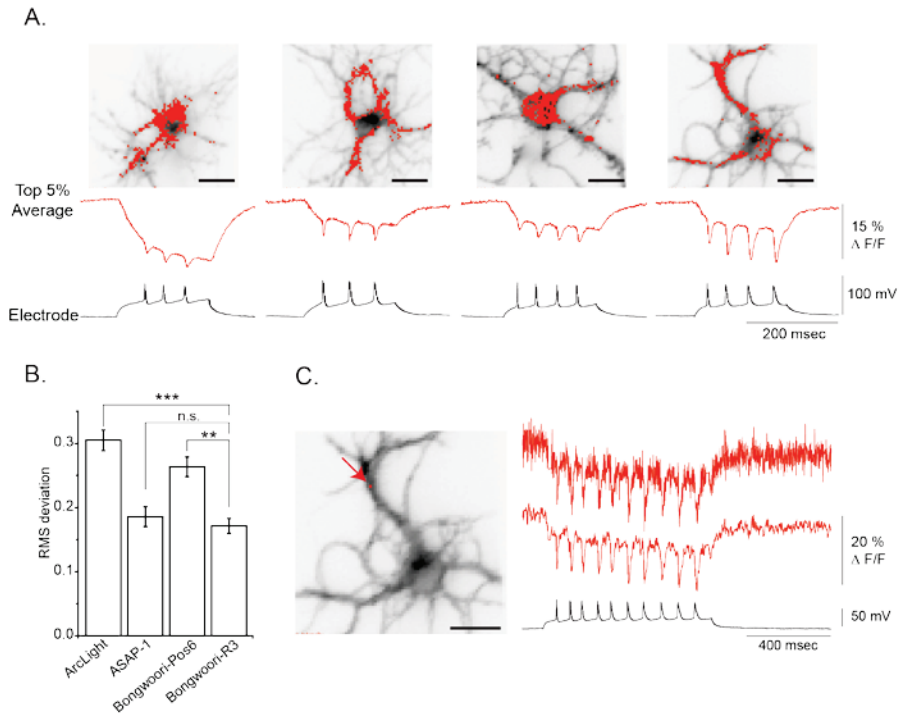

Figure 2. 12. The correlogram based analyses of voltage imaging in neurons.

A. The pixels exhibited top 5 % correlation coefficients were averaged and corresponding fluorescence traces were shown. **B.** Root-mean square deviation of traces averaged from top 5 % pixels versus the electrically recorded voltage signal was calculated for each GEVI. **C.** The highest correlated pixel of Bongwoori-R3 in neuron resolving action potentials evoked by a 800 msec current pulse. The red trace at the bottom was low pass filtered with cut-off frequency of 100 Hz. Error bars are SEM. Asterisks in B. indicate *$p < 0.05$, **$p < 0.01$, ***$p < 0.001$ and n.s.: not significant. (This figure is from Lee et al., *Scientific Reports*, 2017 [112])

Single pixels	ArcLight A242	ASAP1	Bongwoori -Pos6	Bongwoori -R3	Bongwoori-R3 (Two pixels with different brightness)	
					(30,25)	(32,40)
Brightness (a.u.)	2685 ± 390	1044 ± 31	1154 ± 46	1257 ± 130	1609.8	704.95
ΔF/F (%)	-19.7 ± 0.5	-10.8 ± 0.7	-10.7 ± 0.1	-15.4 ± 0.0	-17.1 ± 0.1	-15.0 ± 0.0
SNR	22.2 ± 1.6	7.3 ± 0.6	6.7 ± 1.1	9.6 ± 0.8	9.5 ± 0.6	8.3 ± 0.4
* ΔF/F and SNR were analyzed from low-pass filtered traces						

Table 2. 5. Characteristics of GEVIs analyzed from the highest correlated pixels.

Two individual pixel data shown on the right panel are from the red and blue traces of Bongwoori-R3 in Figure 2.11. All data were acquired from low-pass filtered traces. Values were shown as mean ± SEM. The number of action potentials analyzed were; ArcLight: 12, ASAP1: 12, Bongwoori: 11, Bongwoori-Pos6: 11 and Bongwoori-R3: 12 all from the three best cells per GEVI. (This table is from Lee et al., *Scientific Reports*, 2017 [112])

2.3.7 The baseline fluorescence change of Bongwoori and Bongwoori variants is due to the intracellular pH change

Super ecliptic pHluorin is a pH sensitive variant of GFP that it gets dimmer at acidic conditions and brighter in basic environments [29, 114]. Both Bongwoori-Pos6 and Bongwoori-R3 showed gradual decrease in the baseline fluorescence level during action potential firing (Figures 2.9, 2.11 and 2.12). This was also the case in the previous GEVI, Bongwoori [65]. Since this aspect could complicate optical resolution of action potentials, the exact nature of this event needed to be verified. To distinguish the pH dependent fluorescence change of super ecliptic pHluorin A227D used in the Bongwoori constructs, a farnesylated super ecliptic A227D [113] was transfected in cultured hippocampal neurons. This construct anchors itself at plasma membrane by using the farnesylation motif but is not sensitive to voltage change due to the lack of a voltage-sensing domain. As expected, this construct did not resolve individual action potentials but still showed fluorescence drift before and after the 800 msec long current pulse that induced action potentials (Figure 2.13). On the other hand, Bongwoori-R3 and Arclight, both which consist of a voltage-sensing domain and a super ecliptic pHluorin A227D successfully resolved action potentials while showing decrease

in the baseline fluorescence as well.

Analyzing the correlation between the resting state fluorescence and the degree of activity suggested that the degree of acidification is larger as the cell fires more action potentials. Both high buffering and low buffering capacity internal solutions were used to patch Bongwoori-R3 expressing neurons which showed that using the high buffer may decrease the amplitude of the baseline fluorescence drift but did not completely remove it (Figure 2.14).

It is well known that neurons undergo intracellular acidification upon the firing of action potentials [26, 115]. Interestingly, ROIs of the processes showed a larger decrease in $\Delta F/F$. Since a cell's pH change is a function of the proton influx and intracellular buffering capacity [115], the pronounced drift in the baseline fluorescence may mean that neuronal processes experience larger proton influx versus its buffering capacity than the soma.

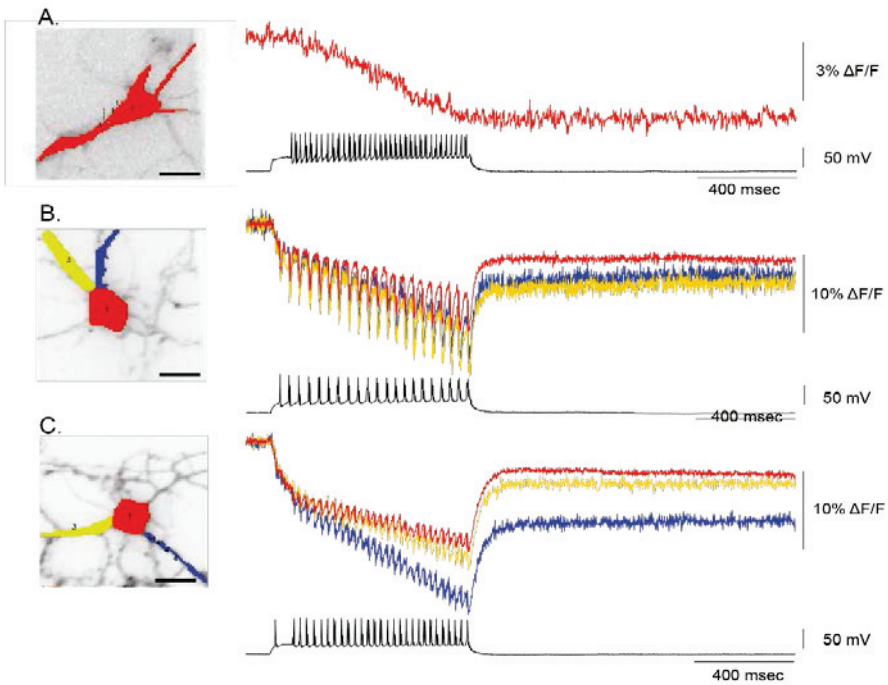

Figure 2. 13 Super ecliptic pHluorin A227D containing optical probes showing the baseline drift caused by the activity dependent acidification of neurons.

A. The membrane targeted but voltage insensitive optical probe, farnesylated SE A227D shows a gradual decrease in its baseline fluorescence during a 800 msec long current injection that induced multiple action potentials. **B.** Bongwoori-R3 resolves both voltage and pH changes of a hippocampal neuron. **C.** ArcLight A242 also responded to evoked action potentials but with smaller amplitudes for individual action potential spikes. Red trace is from the soma. Blue and yellow traces are from two different processes. Scale bar = 20 μm. (This figure is from Lee et al. [112])

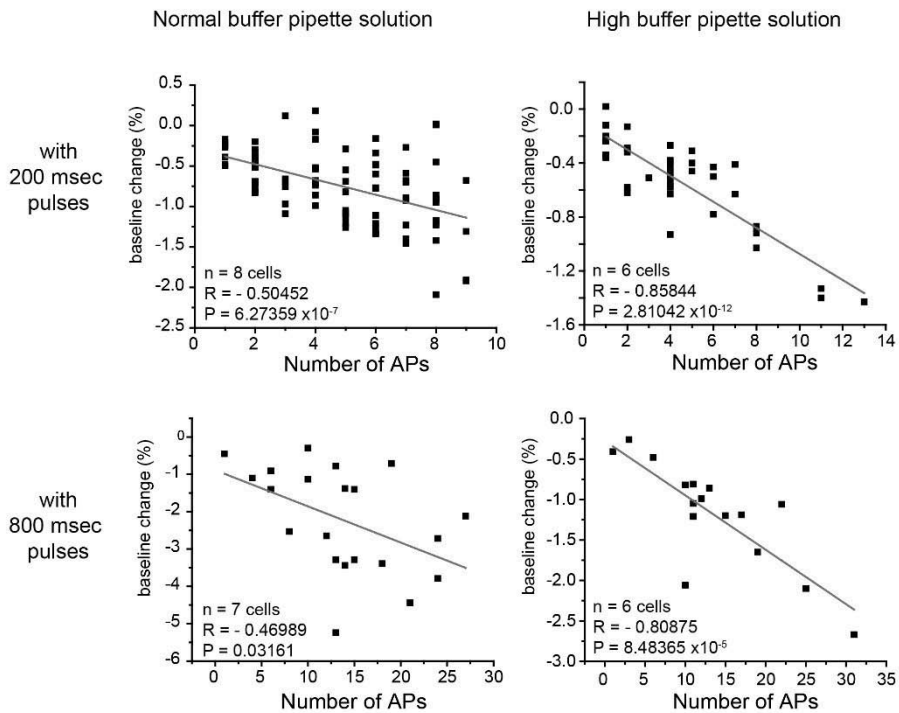

Figure 2. 14 Correlation between the number of action potentials and the baseline drift in ΔF/F measured with Bongwoori-R3 regardless of the durations of injected current pulse.

Either normal buffering capacity (5 mM HEPES) or high buffering capacity (100 mM HEPES) internal solution was used. were used and plotted separately. (This figure is from Lee et al. [112])

2.3.8 Slice recording

The real advantage of using a genetically encoded optical sensor would be utilization of the genetic technique that can specifically target a single cell type in a dense brain tissue. Therefore, a floxed AAV of Bongwoori-R3 was injected into the CA1 area of a mouse hippocampus expressing Cre recombinase only in CaMK2α^{+} neurons to enable voltage imaging of CA1 excitatory neurons responding to synaptic inputs from CA3 (Figure 2.15). To induce synaptic transmission between CA3 and CA1, the Schaffer collaterals were stimulated by a bipolar tungsten electrode. Figure 2.16 shows how Bongwoori-R3 resolves a population spike of the CA1 CamK2α^{+} neurons receiving synaptic inputs from the stimulated Schaffer collaterals. The baseline fluorescence drift was also seen in the brain slice. A $GABA_A$ receptor (Gamma-aminobutyric acid A receptor) antagonist, Bicuculline was applied to block chloride ion influx so that the slice became more excitable for population spikes [116]. The postsynaptic excitatory signal was then blocked by applying a AMPA/kainite receptor antagonist (6-cyano-7-nitroquinoxaline-2,3-dione (CNQX)) and a NMDA receptor antagonist ((2R)-amino-6-phosphonovaleric acid, AP5). Optical signals from Bongwoori-R3 for the no drug, Bicuculline only, and Bicuculline, CNQX and AP5

altogether conditions indicate that the GEVI's fluorescence responded to the neuronal activity.

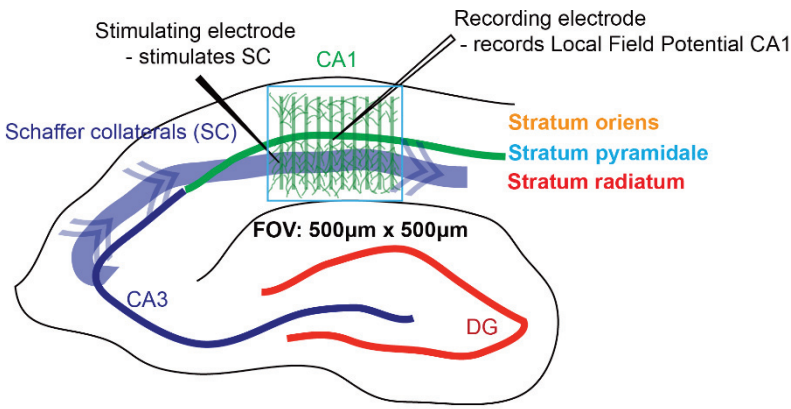

Figure 2. 15 Experimental scheme of voltage imaging in mouse hippocampus slice.

Schaffer collaterals were stimulated with a stimulating electrode to induce synaptic transmission from CA3 to CA1. Simultaneous voltage imaging and local field potential recording were conducted. FOV: field of view. CA: *Cornu Ammonis*, DG: Dentate gyrus.

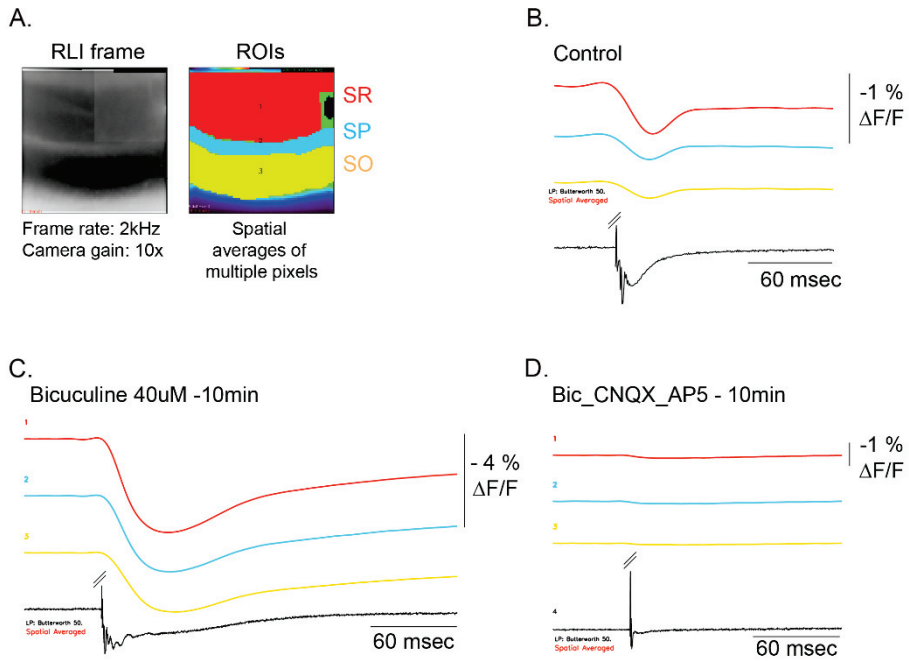

Figure 2. 16 Voltage imaging result with Bongwoori-R3 expressed in CaMK2α^{+} neurons in CA1 area receiving CA3 input.

A. The image at top left corner show an image at resting light intensity (RLI). The next image to the right shows regions of interest (ROIs) selected to represent stratum radiatum (SR), stratum pyramidale (SP) and stratum oriens (SO) regions. **B.** Bongwoori-R3 resolving CA1 neurons that are exhibiting a single upward signal indicating a population spike. **C.** The increased ΔF/F of Bongwoori-R3 responding to $GABA_A$ receptor antagonist (Bicuculline) induced hyperexcitability. **D.** $GABA_A$ receptor, AMPA/kainate receptors and NMDA receptor antoagonists reduced synaptic transmission. The stimulus artefact in voltage signal was cut in the middle. Bic: Bicuculline.

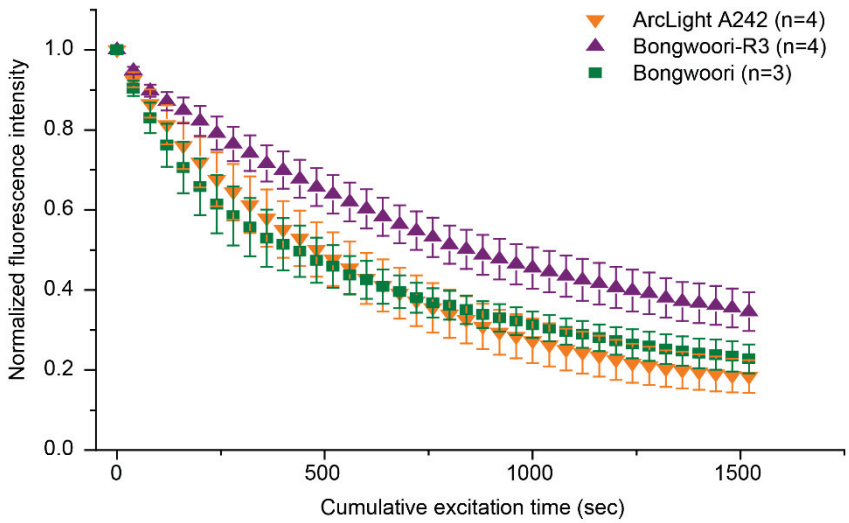

Figure 2. 17. Photobleaching rates of three super ecliptic pHluorin containing GEVIs to show that the mutations introduced in Bongwoori-R3 did not affected the photostability of the FP.

ArcLight A242, Bongwoori or Bongwoori-R3 expressing HEK 293 cells were illuminated with a Xenon arc lamp at intensity of 1mW / mm^2. Each trial was composed of a 40 sec of excitation and a 20 sec of light-off period. Resulted fluorescence signal from each trial was fitted to an exponential decay function. Time constants for the three GEVIs were longer than 450 sec. (This figure is from Lee et al. [112])

2.4 Conclusion

This chapter described a set of rationally designed experiments to develop improved GEVIs. As a result, Bongwoori-Pos6 and Bongwoori-R3 were generated and they exhibited increased ΔF/F for membrane depolarizations. Bongwoori-R3 demonstrated better than the previously reported version, Bongwoori, in the resolution of evoked action potentials from cultured mouse neurons. Specifically, it contrasted the action potential spikes from subthreshold activities. These aspects of the new voltage sensor helped display the action potentials with the fluorescence signal stored in a single pixel from a single trial recording. The difference in the waveforms of the two linker variants analyzed from the root mean square deviation in Figure 2.12.B once again emphasized the importance of having an optimized voltage range. The fact that Bongwoori-Pos6 has just three more arginines and is 1 amino acid longer than Bongwoori-R3 is even more surprising. While the modified linker in Bongwoori-R3 affected the voltage imaging ability it did not seem to alter the FP's intrinsic photostability (Figure 2.17).

Modifications of the linker in between the Ci-VSD and SE A227D throughout this work gave us a glimpse at the possible role and function of the cytoplasmic region. Introducing arginines improved ΔF/F signal

size while the same positively charged lysines did not. The two variants with negatively charged amino acids only abolished the optical signal. This suggests that a voltage indicator developer should be careful when designing linker composition.

The viral injection of the doubled-floxed Bongwoori-R3 gave strong expression in CA1 hippocampus area. This new GEVI successfully showed CA1 population spikes responding to the synaptic transmission from the induced Schaffer collaterals. One drawback of having strongly expressed brain slice was that the resolution of single cell's membrane potentials change was almost impossible due to the background fluorescence. Sparse labeling of a brain region or localization of a region of interest through photolabeling may help alleviate the problem [106, 117].

The intrinsic pH-sensitivity of the SE A227D was also examined in this chapter. The baseline drift in the baseline fluorescence from Bongwoori-R3 was well correlated with the number of induced action potentials. This result strongly suggests that the drift was due to the activity-dependent acidification that was seen in other work as well [26].

Although Bongwoori-R3 showed promising results in cultured neurons and from the population imaging in a brain slice, additional

optimizations such as improved membrane trafficking, better kinetics, and larger ΔF/F will help its performance will enhance its applicability.

Chapter 3. Deciphering consequences of introducing membrane targeting motifs into genetically encoded voltage indicators

3.1 Introduction

The main currency of the cells having excitable membrane is voltage and it only occurs across the plasma membrane. Since the lipid bilayer is situated in between aqueous environments filled with charged and none-charged ions and macromolecules, the electric field dissipates exponentially as it gets far from the membrane where it becomes unmeasurable from 1 nm distance [87]. Therefore, unlike the optical imaging of intracellular chemical substances such as calcium or proton, measurements of membrane potential can only be done with a probe resides in the membrane. This was the reason why GEVI development had leaped to a new phase when a pore deficient, monomeric voltage-sensing domain from the *Ciona Intestinalis* voltage-sensitive phosphatase (Ci-VSP) was identified in 2005 [62, 66, 118]. Although the VSD improved membrane expression, it still needed improvement. GEVIs using a VSD from Ci-VSP often reported intracellular aggregates especially when they are expressed in mouse or rat neurons [70, 90]. Also, Figure 2.12.A of this thesis paper showed that the VSD containing GEVIs exhibited some degree of strong fluorescence from cytoplasm regions.

As described earlier in Chapter 1, the Golgi trafficking signal and the

ER export signals from inwardly rectifying potassium channels (Kir channels) have been extensively used in both optogenetic actuators and optical reporters [50, 75, 83, 109] but they were placed in different regions for different optogenetic tools.

In this chapter, the Golgi and the ER export sequences were incorporated into the previously developed linker variants, Bongwoori-Pos6 and Bonwoori-R3. To find the best insertion locations, the two targeting motifs were introduced either separately or together in several regions. As a result, Bongwoori-R3 with both motifs showed improved fluorescence response. Interestingly, the voltage-sensing properties such as kinetics and a voltage range were affected as well which suggest possible interruptions by the export motifs to the fluorescence mechanism of the voltage probe. Means to address this issue have also been employed and resulted in a Bongwoori-R3 variant with 20 % increased $\Delta F/F$ value at a 100 mV depolarization while maintaining the kinetics.

3.2 Materials and methods

3.2.1 Plasmid DNA construction

Golgi to membrane trafficking signal (Golgi TS) and ER export sequences from Platisa et al. [109] were adopted for this study. Accordingly, the Golgi to membrane trafficking signal sequence was located before the beginning of S1 region (from 71st to 90th amino acid, KSRITSEGEYIPLDQIDINV). A 457 base-pair long gene fragment having a Nhe1 site, Golgi TS, and a Cla1 site was commercially synthesized (Integrated DNA Technologies, USA). The synthesized fragment was then digested and ligated into Bongwoori-Pos6 and Bongwoori-R3 by using the Nhe1 and Cla1 sites. The ER export signal (FCYENEV) was located at the end of Bongwoori-R3 and Bongwoori-Pos6 just before the stop codon. BK27 primer that was designed to have ER export sequence and a Xho1 site was used to add the ER sequence, thereby Bongwoori-Pos6_ER and Bongwoori-R3_ER were created. Then the two Golgi TS sequence carrying constructs were digested with Nhe1 & Cla1 and then ligated into the ER export signal only variants resulting in Bongwoori-Pos6_Golgi & ER and Bongwoori-R3_Golgi & ER.

Bongwoori-R3_Golgi & ER_N-term tandem, Bongwoori-R3_Golgi

& ER_S2-S3, Bongwoori-R3_Golgi & ER_Linker 1, Bongwoori-R3_Golgi & ER_Linker 2, Bongwoori-R3_Golgi & ER_LP spacer, and Bongwoori-R3_Golgi & ER_6aa spacer (aa: amino acid) were cloned based on Bongwoori-R3_Golgi & ER by using primers listed in Table 3.1. Bongwoori-R3_Golgi & ER_C-term tandem construct was generated by using a commercially synthesized 821 base-pair long gene fragment. Both Bongwoori-R3_Golgi & ER_12aa spacer and Bongwoori-R3_Golgi & ER_18aa spacer were prepared by conducting PCR on their 6 amino acid long spacer version as a template.

Primers were synthesized by Cosmogenetech (South Korea) and generated DNA constructs were analyzed by Bionics (South Korea) to verify their gene sequences.

Primer	Sequence	Construct
SM109A	TTCTGCTACGAGAACGAGGTGCCTACTACTGGTGTAGGTCGCGTCCAG	Bongwoori-R3_Golgi & ER_N-term tandem
SM109B	AGGCACCTCGTTCTCGTAGCAGAACACGTTGATGTCGATCTGGTCCAG	
SM110A	GGGTTCTGCTACGAGAACGAGGTGCCTTGGGAGGTGGCTGATGGTTTG	Bongwoori-R3_Golgi & ER_S2-S3
SM110B	AAGGCACCTCGTTCTCGTAGCAGAACCCGTAGGCAAATATCCTTAATC	
SM111A	ATATTTTGCTACGAGAACGAGGTGTATTCCaggCAACAAGGGGATCCC	Bongwoori-R3_Golgi & ER_Linker 1
SM111B	CACCTCGTTCTCGTAGCAAAATATTCTTGCTAAGATAACCACACGCAGC	
SM112A	TTTTTCTGCTACGAGAACGAGGTGGGGGATCCCATGAGTAAAGGAGAAG	Bongwoori-R3_Golgi & ER_Linker 2
SM112B	CACCTCGTTCTCGTAGCAGAAAAATATTCTTGCTAAGATAACCACACGC	
SM113	AGACTCGAGTCACACCTCGTTCTCGTAGCAGAACGGCAGTTTGTATAGTTCATCCATGCCATGTGTAATC	Bongwoori-R3_Golgi & ER_LP stuffer
SM114	GACTCGAGTCACACCTCGTTCTCGTAGCAGAAGCTGCCGCCGGTGCCGCCTTTGTATAGTTCATCCATGCCATGTG	Bongwoori-R3_Golgi & ER_6aa stuffer
SM118	CTAGACTCGAGTCACACCTCGTTCTCGTAGCAGAAgctccctccggttccccGCTGCCGCCGGTGCCGCCTTTG	Bongwoori-R3_Golgi & ER_12aa stuffer
SM119	GACTCGAGTCACACCTCGTTCTCGTAGCAGAAactgcctcctgtcccgccgctccctccggttccccGCTGCCGCCGGTGCCGCCTTTG	Bongwoori-R3_Golgi & ER_18aa stuffer
BK27	GACTCGAGTCACACCTCGTTCTCGTAGCAGAACTTATACAGCTCGTCCAT	Bongwoori-R3_ER and Bongwoori-Pos6_ER

Table 3. 1. Primers used to generate targeting motif variants studied in this section.

3.2.2 Cell culture and transfection

HEK 293 cells and mouse primary neurons were cultured and transfected following Lee et al. [112] and section 2.2.2 of this thesis paper.

3.2.3 Electrophysiology and voltage imaging

Simultaneous electrophysiology and voltage imaging experiments of HEK 293 cells and mouse primary neurons were conducted following the protocol described in Lee et al. [112] and section 2.2.6 of this thesis paper.

3.2.4 Data acquisition and analyses

The initial acquisition of voltage imaging data followed section 2.2.8. The Boltzmann fit analysis to determine the voltage range of a GEVI was done by using Origin 9.0 (OriginLab, USA) and Microsoft Excel (Microsoft, USA). Time constants analysis was also conducted in Origin 9.0 (OriginLab, USA). Statistical significance of the means was determined by using Origin 9.0 (OriginLab, USA) as well.

3.3 Results

3.3.1 Determining the location of Golgi to membrane trafficking signal and/or ER export signal sequences in Bongwoori linker variants

Platisa et al. [109] introduced Golgi to membrane trafficking signal (Golgi TS) and ER export signal sequences in their recently published voltage indicator, Marina, to improve its membrane trafficking efficiency. Marina is a variant of ArcLight [64] that uses the Ci-VSD and a super ecliptic pHluorin A227D (SE A227D). Considering the fact that both Marina and Bongwoori linker variants share the same VSD and FP, the positions of the two membrane trafficking motifs used in Marina were adopted for Bongwoori-Pos6 and Bongwoori-R3. Therefore, the 20 amino acid Golgi TS sequence was substituted in at the cytoplasmic loop region before the S1. The 7 amino acid long ER export signal was then added in between the end of SE A227D and the stop codon.

3.3.2 Bongwoori-Pos6 with Golgi TS and / or ER export signal did not improve fluorescence signal for membrane depolarization

First, Golgi TS and ER export motifs were introduced in Bongwoori-Pos6 separately to distinguish their contributions to membrane targeting.

Bongwoori-Pos6_Golgi and Bongwoori-Pos6_ER were prepared and transfected in HEK 293 cells for a simultaneous patch clamp and voltage imaging experiments (Figure 3.1). As membrane potential change of a mammalian cell is present only at the lipid bilayer only, voltage indicator molecules that are internally expressed in the cytoplasm will not be responsive to the voltage change. This will lead to a higher background fluorescence level that results in a decreased ΔF/F value.

Both Bongwoori-Pos6_Golgi and Bongwoori-Pos6 ER did not improve ΔF/F of Bongwoori-Pos6 at a 100 mV voltage pulse (Table 3.2). The Golgi TS only version showed a general decrease in fluorescent response throughout the tested voltage range (from - 120 to 130 mV). Interestingly, Bongwoori-Pos6_ER showed a 2 - fold increase when hyperpolarized compared to the original version. However, there is a drawback to this variant. A longer voltage pulse (200 msec per pulse) had to be used due to the slow response speed of this variant. The increased ΔF/F during hyperpolarization seemed to result from either better membrane trafficking, or an altered voltage range, or both. A construct consisting of both Golgi and ER was also generated and tested (Figure 3.2). This probe replicated the characteristics of the ER only version. The seemingly larger fluorescence response at 100 mV voltage pulse was not

statistically different from that of Bongwoori-Pos6. Moreover, the Golgi and ER version still had a slower response than that seen in the Bongwoori-Pos6_ER version. Due to the unimpressive amplitude and kinetics of the fluorescence response described above, Bongwoori-Pos6 was not developed further.

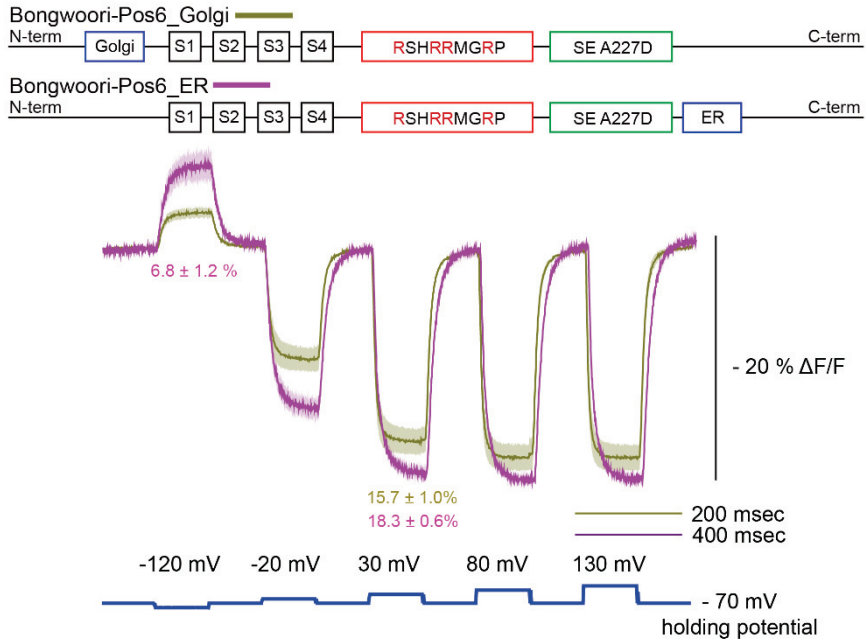

Figure 3. 1. Bongwoori-Pos6 variants with either the Golgi TS or ER export signal sequences.

The values indicated under voltage pulses are averaged ΔF/F. Note that 200 msec voltage pulse was used for Bongwoor-Pos6_ER. The shaded area denotes standard error of the mean. The number of cells analyzed; Bongwoori-Pos6_Golgi: 3, Bongwoori-Pos6_ER: 3.

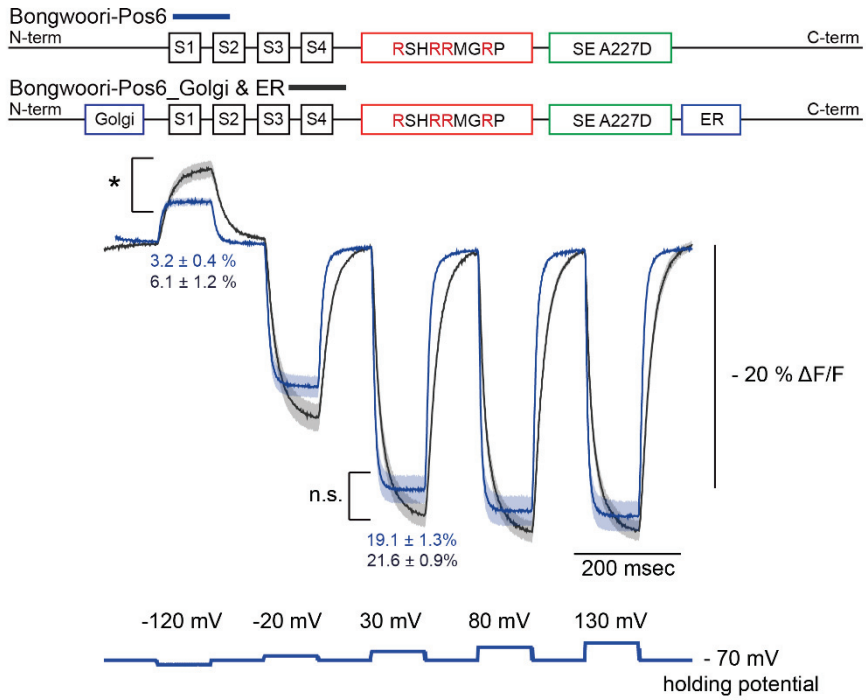

Figure 3. 2. Comparison of Bongwoori-Pos6_Golgi & ER and the original Bongwoori-Pos6.

The ΔF/F value of Bongwoori-Pos6_Golgi & ER for the hyperpolarized membrane potential (-50 mV from resting potential) was larger than Bongwoori-Pos6 (* p value < 0.05) but not for 100 mV depolarization (n.s. : not significant). The shaded area denotes standard error of the mean. The number of cells analzyed; Bongwoori-Pos6: 4 and Bongwoori-Pos6_Golgi & ER: 4.

Constructs	Δ F/F (%)	$V_{1/2}$ (mV)	Weighted T_{on} (msec)	Weighted T_{off} (msec)	Number of cells
Bongwoori-Pos6	19.1 ± 1.3	- 28 ± 3	6 ± 1	7 ± 1	4 cells
Bongwoori-Pos6_Golgi	15.7 ± 1.0	-	7 ± 2	10 ± 1	3 cells
Bongwoori-Pos6_ER	18.3 ± 0.6	-	23 ± 1	28 ± 1	3 cells
Bongwoori-Pos6_Golgi & ER	21.6 ± 0.9	- 43 ± 4	25 ± 4	23 ± 1	4 cells
Bongwoori-R3	20.0 ± 1.3	- 3 ± 1	11 ± 1	10 ± 2	5 cells
Bongwoori-R3_Golgi	19.1 ± 1.3	-	10 ± 1	7 ± 1	4 cells
Bongwoori-R3_ER	24.8 ± 2.1	-	34 ± 3	33 ± 7	3 cells
Bongwoori-R3_Golgi & ER	27.1 ± 1.0	- 20 ± 1	25 ± 2	20 ± 1	5 cells
Bongwoori-R3_Golgi & ER_ N-term tandem	16.2 ± 1.8	-	18 ± 2	14 ± 1	5 cells
Bongwoori-R3_Golgi & ER_ C-term tandem	18.3 ± 1.5	-	14 ± 1	12 ± 1	7 cells
Bongwoori-R3_Golgi & ER_ S2-S3	0.50 ± 0.4	-	n.a.	n.a.	3 cells
Bongwoori-R3_Golgi & ER_ Linker 1	14.1 ± 1.6	-	15 ± 3	18 ± 2	5 cells
Bongwoori-R3_Golgi & ER_ Linker 2	11.5 ± 1.0	-	18 ± 2	14 ± 2	5 cells
Bongwoori-R3_Golgi & ER_ LP stuffer	25.1 ± 1.6	-	28 ± 2	20 ± 1	7 cells
Bongwoori-R3_Golgi & ER_ 6aa stuffer	22.4 ± 1.8	- 19 ± 4	15 ± 1	16 ± 1	8 cells
Bongwoori-R3_Golgi & ER_ 12aa stuffer	24.5 ± 1.4	- 10 ± 2	12 ± 1	10 ± 1	6 cells
Bongwoori-R3_Golgi & ER_ 18aa stuffer	23.2 ± 1.1	- 5 ± 2	10 ± 1	8 ± 1	5 cells

Table 3. 2. Characteristics of the targeting motif variants.

All the values were shown as mean ± SEM. Time constants for Bongwoori-R3_Golgi & ER_S2-S3 version could not be determined due to the extremely small fluorescence response.

3.3.3 Bongwoori-R3 with Golgi TS and ER export motifs showed increased ΔF/F signal size for both hyperpolarization and depolarization

The effects of Golgi TS and ER export motifs on membrane trafficking efficiency were also tested in Bongwoori-R3. Similar to Bongwoori-Pos6_Golgi, the Golgi TS motif version of Bongwoori-R3 did not show any notable improvement (Table 3.2). On the other hand, Bongwoori-R3 with the ER export signal displayed quite a different fluorescence response than Bongwoori-R3 but similar to what Bongwoori-Pos6_ER showed (Figure 3.3). The combination of the two targeting motifs in Bongwoori-R3 resulted in a variant showed larger fluorescence response throughout the tested voltage range. Unlike Bongwoori-Pos6 with Golgi TS and ER export motifs, Bongwoori-R3_Golgi & ER showed significantly larger ΔF/F values at all voltage pulses tested except for the 200 mV pulse which was not physiologically relevant (Figure 3.4 and Table 3.2). The 200 mV signal was not statistically significant but still larger than Bongwoori-R3. The overall increase in ΔF/F could be interpreted as the result of improved membrane trafficking solely, independent of the shift of the responsive voltage range. However, the kinetics was notably slower, similar to the

Bongwoori-Pos6 version (Table 3.2).

A simultaneous voltage imaging and current clamp recording experiment was conducted on primary neurons for Bongwoori-R3_Golgi & ER. The slow response speed impeded the resolution of evoked action potentials (Figure 3.5 below) compared to that of Bongwoori-R3 (Figure 3.5 above).

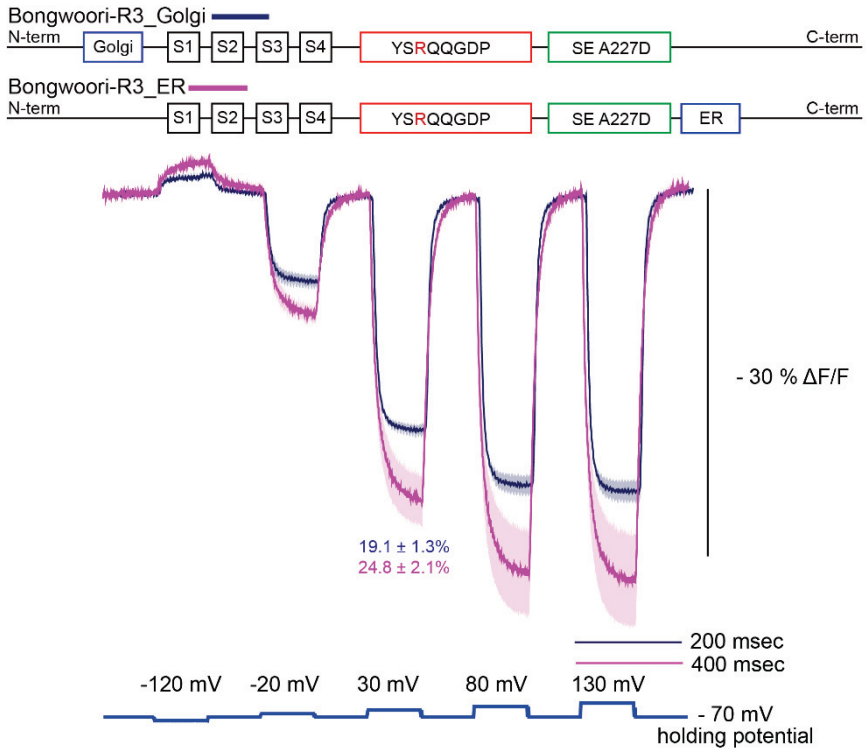

Figure 3. 3. Bongwoori-R3 variants with either the Golgi TS or ER export signal sequences.

The values indicated under the 100 mV membrane depolarization pulse are averaged ΔF/F. Note that 200 msec voltage pulse was used for Bongwoor-R3_ER. The shaded area denotes standard error of the mean. The number of cells analyzed; Bongwoori-R3_Golgi: 4, Bongwoori-R3_ER: 3.

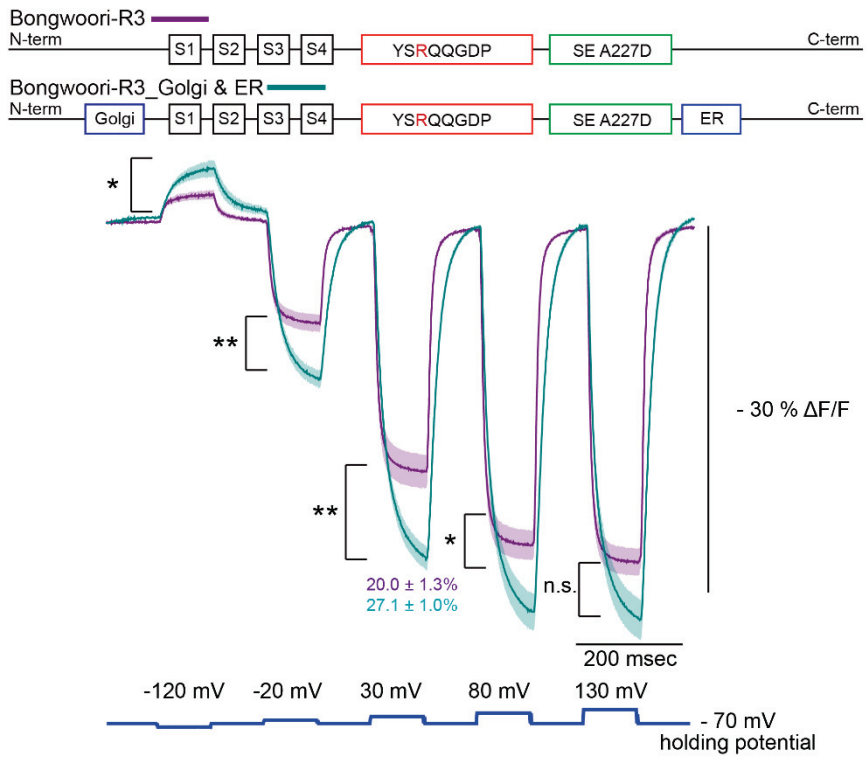

Figure 3. 4. Comparison of Bongwoori-R3_Golgi & ER and its original version, Bongwoori-R3.

All ΔF/F values of Bongwoori-R3_Golgi & ER were larger than those of Bongwoori-R3's except for the 200 mV membrnae depolarization pulse. The significance of means compared was indicated with following criteria; * p-value < 0.05, ** p-value < 0.01, and n.s.: not significant. The shaded area denotes standard error of the mean. The number of cells analzyed; Bongwoori-R3: 5 and Bongwoori-R3_Golgi & ER: 5.

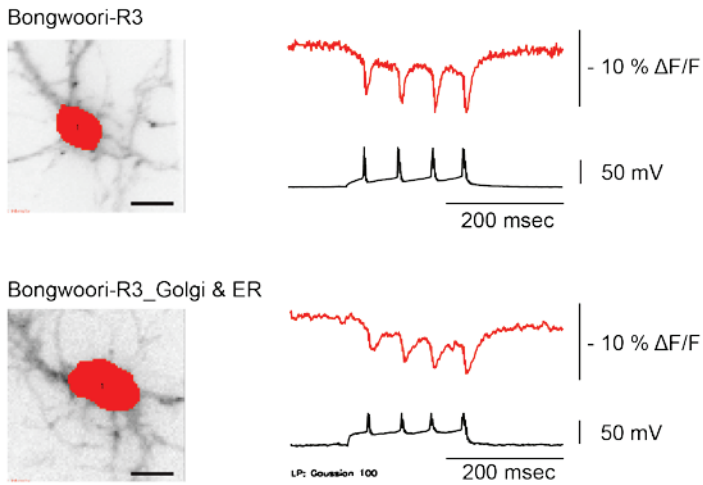

Figure 3. 5. Voltage imaging of evoked action potentials with Bongwoori-R3_Golgi & ER.

Fluorescence traces were averaged from pixels correspond to soma regions. The fluorescence trace from Bongwoori_R3-Golgi & ER was low-pass filtered.

3.3.4 Bongwoori-R3 variants with different ER export signal locations resulted in diminished ΔF/F signal size

Both Bongwoori-Pos6 and Bongwoori-R3 variants containing the ER motif showed slower response to voltage change. As the ER motif was located right after the FP, it might have disturbed the motion of SE A227D during the voltage change or its fluorescence mechanism. To address this issue, the ER motif location was varied in several different regions within the Bongwoori-R3_Golgi & ER construct. First, the ER motif was positioned at the 91st amino acid region substituting the 7 amino acids from 'DDGRMEI' into 'FCYENEV'. This variant which has both the Golgi TS and ER export signal motifs near its N-terminus was named Bongwoori-R3_Golgi & ER_N-term tandem. The next variant was designed to have both motifs in tandem at the C-terminus as reported in FRET – opsin type voltage sensors [83, 84]. The S2-S3 loop region of the VSD was also chosen as an ER motif location.

All three variants had diminished fluorescent response in comparison to the Bongwoori-R3_Golgi & ER construct (Figure 3.6). The newly tested ER locations not only failed to improve Bongwoori-R3_Golgi & ER's speed but also altered its voltage response back to a level slightly worse than Bongwoori-R3's. Specifically, the variant with the ER motif

at S2-S3 loop was almost insensitive to membrane potential change entirely. In this particular case, the expression pattern of the tested cell seemed to indicate improper expression (inset, Figure 3.6).

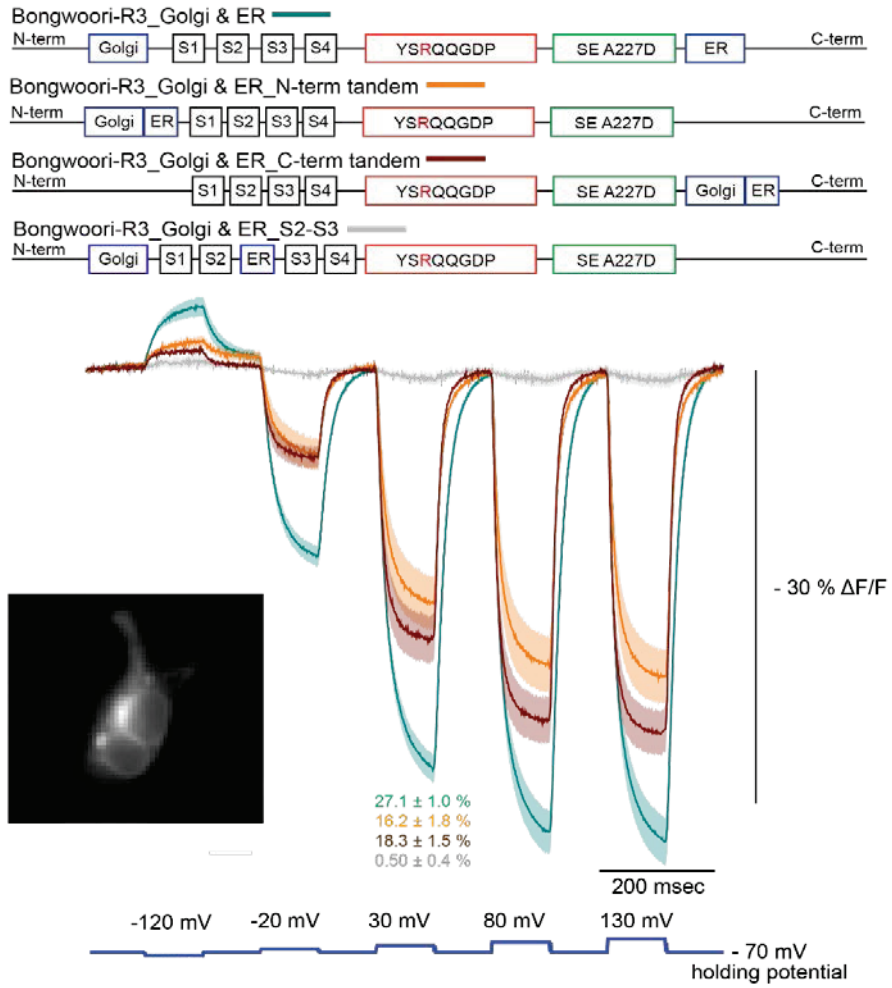

Figure 3. 6. Bongwoori-R3_Golgi & ER variants with relocated ER motif positions.

The inset shows a poorly expressed Bongwoori-R3_Golgi & ER_S2-S3 in an HEK 293 cell. The shaded area denotes standard error of the mean. The number of cell tested; Bongwoori-R3_Golgi & ER: 5, Bongwoori-R3_Golgi & ER_N-term tandem: 5, Bongwoori-R3_Golgi & ER_C-term tandem: 7, Bongwoori-R3_Golgi & ER_S2-S3: 3.

3.3.5 Placing the ER motif at the inter-domain linker region also decreased voltage induced fluorescence response

Previous efforts suggested that the 7 amino acids long ER motif can disrupt the voltage sensitivity of a voltage indicator if it is located at sensitive areas within the construct. Both VSD and FP regions had already been tested but failed to improve the kinetics of Bongwoori-R3_Golgi & ER. The linker area in between the VSD and FP was chosen as the next area to tackle. Two linker variants were generated either by simply adding the seven amino acid ER motif at the linker region (Bongwoori-R3_Golgi & ER_Linker 1) or by substituting the amino acid residues of the linker from 'YSRQQ' into 'FCYENEV' (Bongwoori-R3_Golgi & ER_Linker 2). Linker variant 1 maintained Bongwoori-R3_Golgi & ER's fluorescence signal size during membrane hyperpolarization but not membrane depolarization. Linker variant 2 showed decreased fluorescence response across the entire voltage range (Figure 3.7).

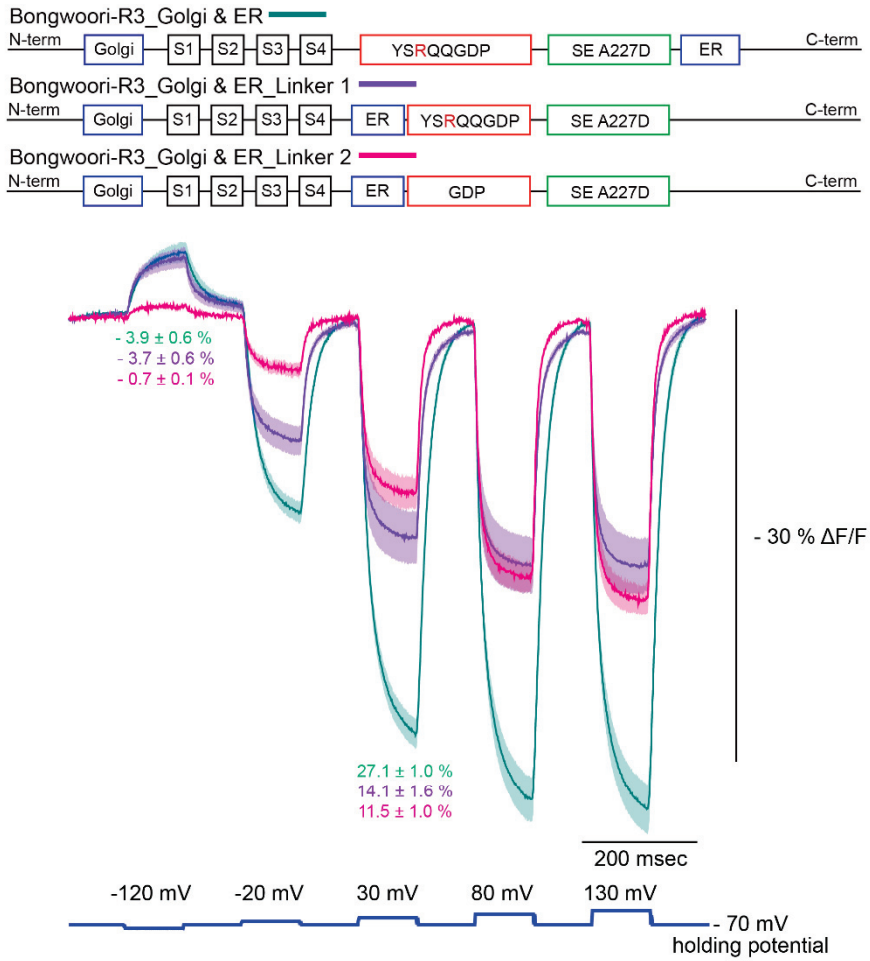

Figure 3. 7. Variants of Bongwoori-R3_Golgi & ER with ER motifs positions at linker regions.

The shaded area denotes standard error of the mean. The number of cell analyzed; Bongwoori-R3_Golgi & ER: 5, Bongwoori-R3_Golgi & ER_Linker 1: 5, Bongwoori-R3_Golgi & ER_Linker 2: 5.

3.3.6 Inserting a short 6 amino acid long spacer in between the FP and ER motif improved the kinetics

Relocating the ER motif throughout the construct did not improve the kinetics of Bongwoori-R3_Golgi & ER. An alternate way to resolve the kinetics issue while keeping the ER export motif at the current position would be to use a short spacer sequence to relieve any structural stress on the FP. Two different spacers were introduced in between the FP and the ER motif. Akerboom et al. [119] previously reported that they used leucine (L) and proline (P) in between a circularly permuted GFP (cpGFP) and calmodulin to improve the fluorescent dynamic range of GCaMP3. These residues were used continuously for GCaMP 5s, GCaMP 6s, and GCaMP 6f since then [17, 119]. Bongwoori-R3_Golgi & ER with the LP spacer showed voltage-dependent fluorescence response comparable to that of Bongwoori-R3_Golgi & ER (Figure 3.8). However, its on and off time constants at 100 mV depolarization did not show faster kinetics than the original version (Figure 3.8).

The second spacer variant of Bongwoori-R3_Golgi & ER adopted GGTGGS. The 6 amino acids long sequence has been popularly used in many optical probes [67, 104, 120] containing a cpGFP as it connects the N and C termini of the green fluorophore to enable circular permutation

[69]. Bongwoori-R3_Golgi & ER_6aa spacer (aa: amino acid) showed a slightly decreased fluorescence response to membrane depolarization than its original version but its signal size was still larger than 20 %. In addition to the fluorescence signal size, introducing the GGTGGS spacer made the probe faster. The time constant of the onset at 100 mV depolarization was calculated to be 15 ± 1 msec. This was statistically faster than Bongwoori-R3_Golgi & ER (Table 3.3).

Though the 6 amino acid long spacer showed important progress, the ΔF/F signal size was not significantly larger than the previously reported Bongwoori-R3 (p-value > 0.3) and its off-kinetics at 100 mV depolarization was not statistically different from that of Bongwoori-R3_Golgi & ER (p-value > 0.5). Nevertheless, considering the fact that all the variants with different ER motif locations showed less than 20 % ΔF/F values per 100 mV depolarization, the LP and GGTGGS spacer containing variants seemed promising.

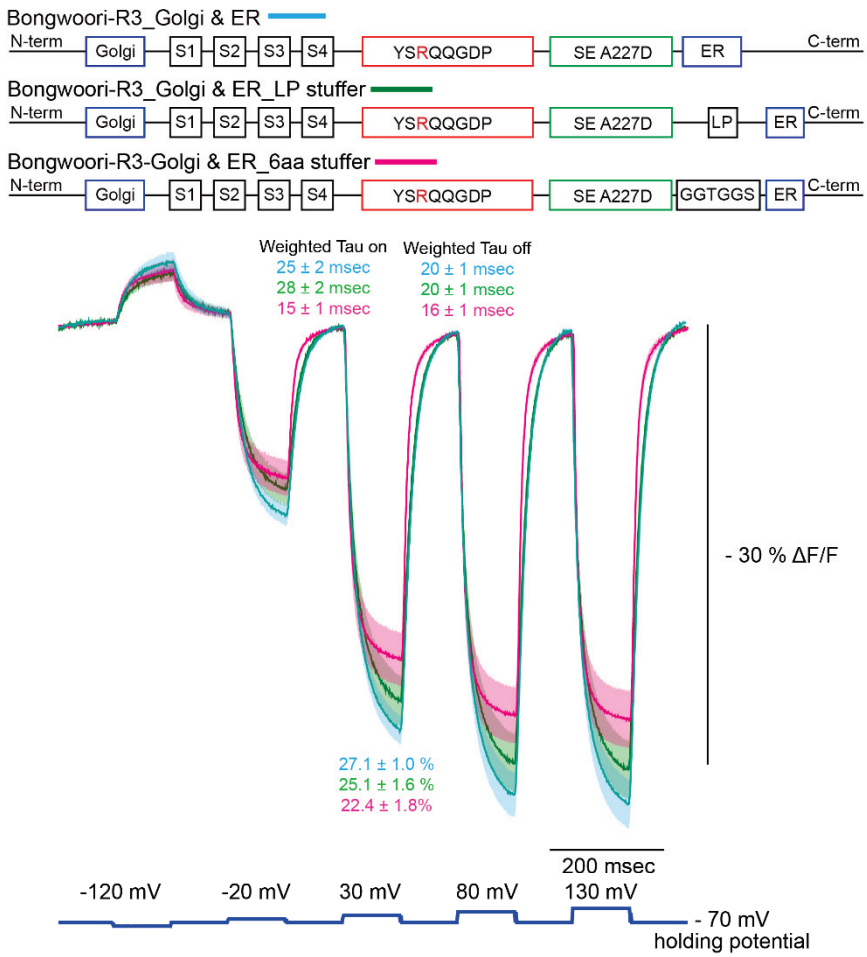

Figure 3. 8. Two Bongwoori-R3_Golgi & ER variants with inter-domain spacers inserted in between the FP and the ER motif.

The shaded area denotes standard error of the mean. The number of cell analyzed; Bongwoori-R3_Golgi & ER: 5, Bongwoori-R3_Golgi & ER_LP spacer: 7, Bongwoori-R3_Golgi & ER_6aa spacer: 8.

3.3.7 Bongwoori-R3_Golgi & ER with longer amino acids spacers recovered the kinetics while maintaining the large ΔF/F

The well-known flexibility of GGTGGS was verified but it was still unclear if 6 amino acids were an optimized length for the spacer. Therefore, 12 amino acid (GGTGGSGGTGGS) and 18 amino acid (GGTGGSGGTGGSGGTGGS) spacers were also tested (Figure 3.9). The 12 amino acid version showed increased ΔF/F per 100 mV depolarization that was comparable to the signal size of Bongwoori-R3_Golgi & ER. The 18 amino acid spacer also showed similar amplitude to a 100 mV voltage pulse but it was not larger than the 12 amino acid version. In terms of speed, the two longer spacer variants showed faster kinetics than Bongwoori-R3_Golgi & ER for both on and off time constants unlike the 6 amino acid version that was faster for the onset only (Figure 3.10 and Table 3.3). In conclusion, comparison of the two longer spacer variants to the original Bongwoori-R3's fluorescence response per 100 mV depolarization revealed that Bongwoori-R3_Golgi & ER_12aa spacer responded with larger ΔF/F while maintaining the fast speed (Figure 3.11).

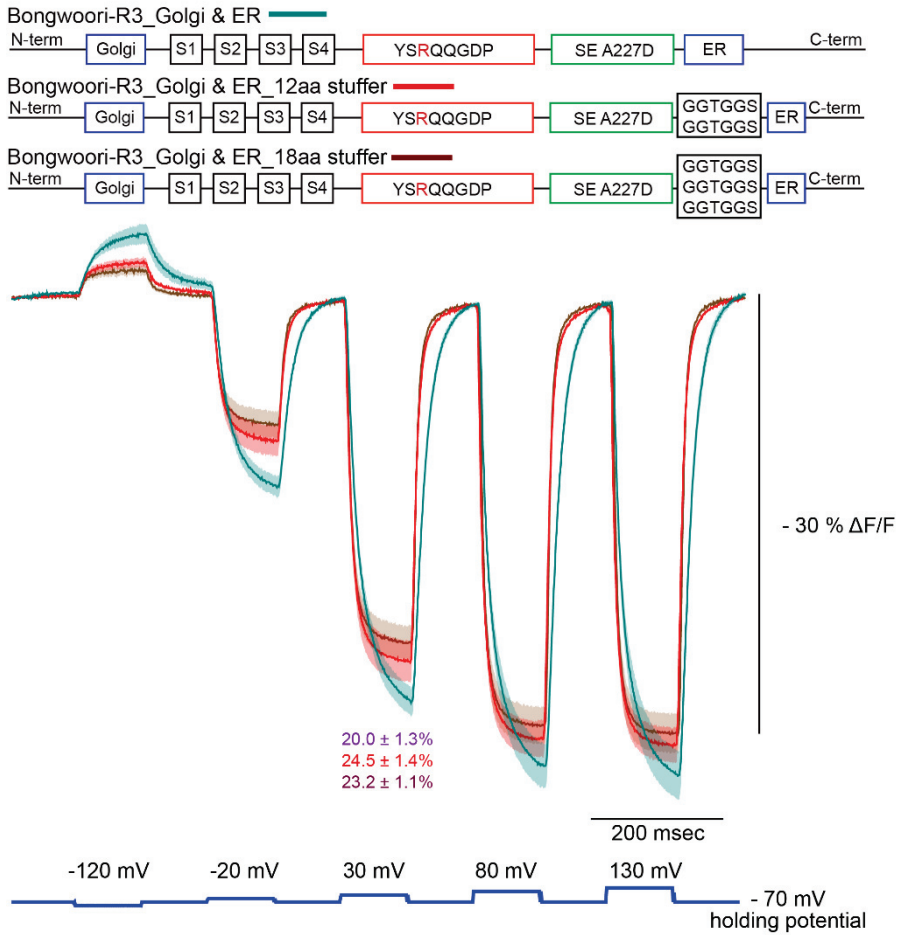

Figure 3. 9. The extended inter-domain spacer versions of Bongwoori-R3_Golgi & ER.

The shaded area denotes standard error of the mean. The number of cell analyzed; Bongwoori-R3_Golgi & ER: 5, Bongwoori-R3_Golgi & ER_12aa spacer: 6, Bongwoori-R3_Golgi & ER_18aa spacer: 5.

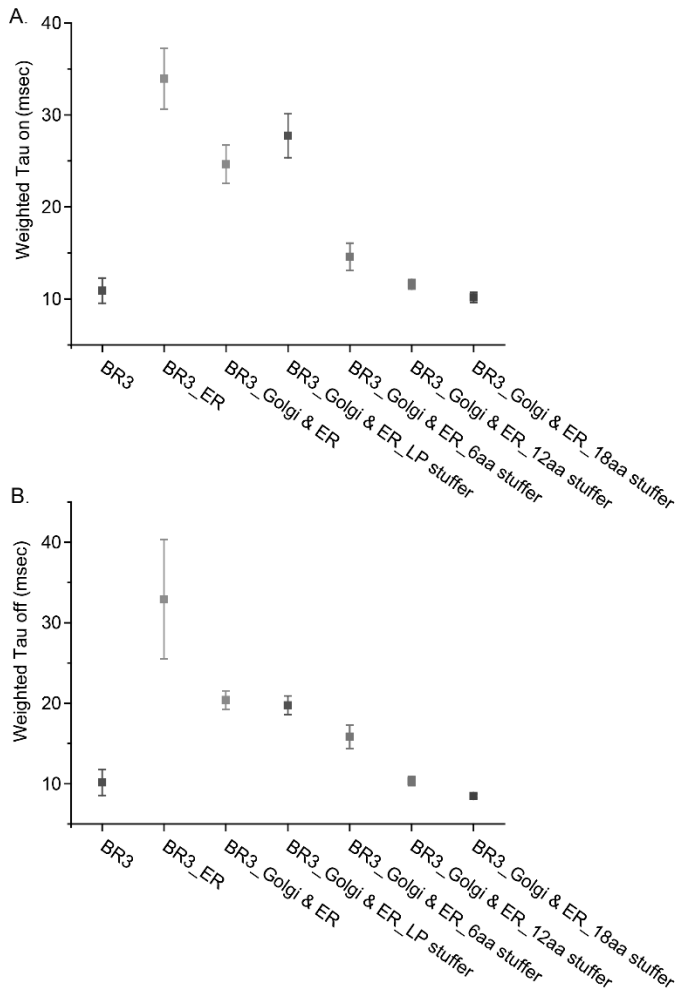

Figure 3. 10. Time constants for on (top) and off (bottom) kinetics responding to 100 mV membrane depolarization plotted for each GEVI.

Error bars are SEM. BR3: Bongwoori-R3. The number of cells analyzed: Bongwoori-R3: 5, Bongwoori-R3_ER: 3, Bongwoori-R3_Golgi & ER: 5, Bongwoori-R3_Golgi & ER_LP spacer: 7, Bongwoori-R3_Golgi & ER_6aa spacer: 8, Bongwoori-R3_Golgi & ER_12aa spacer: 6, Bongwoori-R3_Golgi & ER_18aa spacer: 5.

Faster variants	Slower variants	Significance	
		Ton	Toff
BR3_Golgi & ER_6aa stuffer	BR3_ER	***	***
	BR3_Golgi & ER	**	n.s.
	BR3_Golgi & ER_LP stuffer	***	n.s.
BR3_Golgi & ER_12aa stuffer	BR3_ER	***	***
	BR3_Golgi & ER	***	**
	BR3_Golgi & ER_LP stuffer	***	**
BR3_Golgi & ER_18aa stuffer	BR3_ER	***	***
	BR3_Golgi & ER	***	**
	BR3_Golgi & ER_LP stuffer	***	**

Table 3. 3. Significance level of the difference in averaged time constants between faster and slower Bongwoori-R3 membrane targeting motifs.

Individual values were acquired from each GEVI's optical response to a 100 mV membrane depolarization. Means were compared by using one-way ANOVA. The number of cell analyzed were; The number of cells analyzed: Bongwoori-R3: 5, Bongwoori-R3_ER: 3, Bongwoori-R3_Golgi & ER: 5, Bongwoori-R3_Golgi & ER_LP spacer: 7, Bongwoori-R3_Golgi & ER_6aa spacer: 8, Bongwoori-R3_Golgi & ER_12aa spacer: 6, Bongwoori-R3_Golgi & ER_18aa spacer: 5. Significance level was displayed by using following criteria; * $p < 0.05$, ** $p < 0.01$, *** $p < 0.001$, n.s.: not significant.

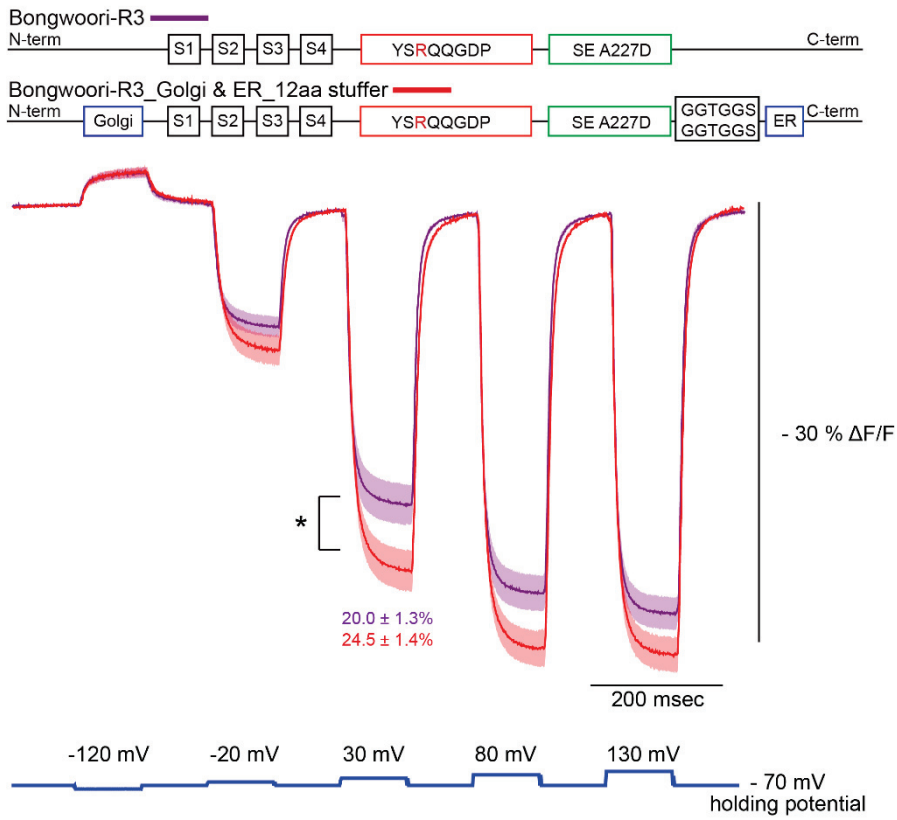

Figure 3. 11 Comparison of Bongwoori-R3 and Bongwoori-R3_Golgi & ER_12aa spacer.

The significance of means compared was indicated as; * p-value < 0.05. The shaded area denotes standard error of the mean. The number of cell analyzed; Bongwoori-R3: 5, Bongwoori-R3_Golgi & ER_12aa spacer: 6.

3.3.8 Inserting membrane targeting motifs affected $V_{1/2}$ value

Fitting the fluorescence traces of the five major targeting motif variants to the Boltzmann function revealed that Golgi TS & ER export signal sequences actually shifted voltage responsiveness (Figure 3.12 and Table 3.2). Both Bongwoori-Pos6 and Bongwoori-R3 with Golgi TS and ER export signal sequences showed negatively shifted $V_{1/2}$ values. This is particularly disadvantageous for Bongwoori-Pos6 as its original voltage range was already tuned at subthreshold activity. The responsive voltage range of Bongwoori-R3_Golgi & ER was also negatively shifted to near - 20 mV. This is quite interesting since the construct maintained enlarged signal amplitudes throughout the tested voltage range, which in turn suggests an improvement of voltage induced optical signal via optimized membrane trafficking. Also, the left-shifted voltage response suggests that the slower speed of this variant may be neglected if it is use to observe hyperpolarization or subthreshold neuronal activities.

Increasing the flexibility of the voltage probe by inserting a certain length of spacer cancelled out the voltage range shift. In particular, when the spacer length was increased from 6 amino acids to 18 amino acids, the shift in voltage range was reduced to close to the $V_{1/2}$ value of Bongwoori-R3. The 6 amino acid spacer variant's $V_{1/2}$ value was not

different from that of Bongwoori-R3_Golgi & ER. Nonetheless, the fact that it still improved the time constant upon the onset of the voltage pulse also implies its possible contribution to resolve the disturbed fluorescence mechanism.

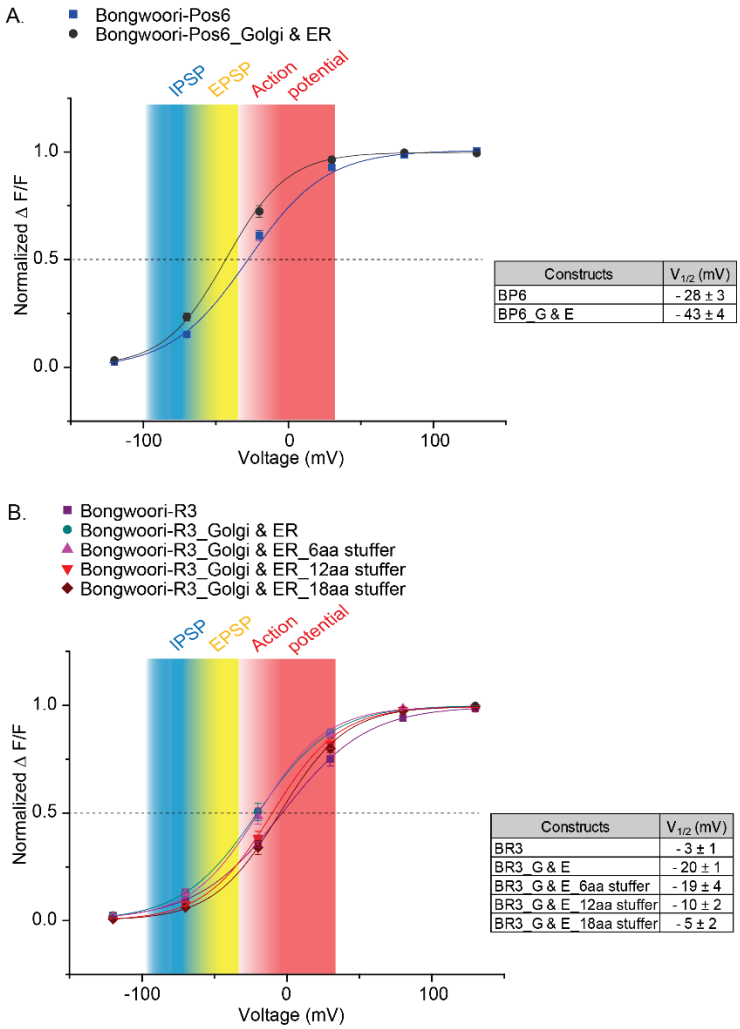

Figure 3. 12. The responsive voltage ranges of Bongwoori-R3 and targeting motif variants.

Normalized ΔF/F values were plotted and fitted to Boltzmann function. Error bars are SEM. The number of cells analyzed: Bongwoori-R3: 5, Bongwoori-R3_Golgi & ER: 5, Bongwoori-R3_Golgi & ER_6aa spacer: 8, Bongwoori-R3_Golgi & ER_12aa spacer: 6, Bongwoori-R3_Golgi & ER_18aa spacer: 5.

3.4 Conclusion

The effects of Golgi to membrane trafficking signal and ER export signal sequences in Bongwoori linker variants were demonstrated in this chapter. Since previous examples of incorporating the trafficking signals seemed heterogeneous to laboratory to laboratory or sensor to sensor, the targeting motifs' individual effect on the voltage imaging ability was first tested. While the ER export signal improved amplitudes of the fluorescence response of Bongwoori-Pos6 for membrane hyperpolarization only, it mainly improved membrane depolarization range of Bongwoori-R3. The improved optical signal size was thought to overcome the slower kinetics of Bongwoori-R3_Golgi & ER for resolving action potentials but it did not.

The ER export signal sequence that was inserted right after the SE A227D obviously caused slower response speed. It appeared that the ER export signal that helped recruit the protein to the cell membrane also interrupted the FP's fluorescence mechanism.

Relocating the ER export signal sequences to different regions in the construct did not draw positive results. Instead, introducing the flexible spacer composed of GGTGGS made the sensor faster. Increasing the length of the spacer in between the FP and the ER export signal sequence

resulted in Bongwoori-R3_Golgi & ER_12aa spacer that exhibited recovered kinetics that was comparable to the original Bongwoori-R3 but still showed a 20 % increase in ΔF/F signal size for a 100 mV depolarization.

In terms of the voltage range, Bongwoori-Pos6 and Bongwoori-R3 with the two membrane targeting motifs showed about 15 to 17 mV negatively shifted $V_{1/2}$ values. Extending the flexible spacer from 6 amino acids to 12 and 18 shifted the voltage range back to zero mV level. It was interesting that insertion of the flexible spacer both improved the kinetics and recovered the $V_{1/2}$ close to the original Bongwoori-R3. This suggests that changes in the two voltage-sensing properties might have been caused by the same restraint introduced by the ER export signal.

Chapter 4. Development of photoactivatable optical bio-sensors of physiological voltage and pH changes

4.1 Introduction

Genetically encoded fluorescent sensors often suffer from extensive background fluorescence when they are expressed in densely populated cells of tissues [14, 121, 122]. Confining their expression to certain cell types by using certain promoters can help but it is not always effective. Figure 2.16 showed that expression of Bongwoori-R3 in CaMK2α^{+} cells still displayed strong background fluorescence that hindered recognization of single neurons.

Optically highlighting fluorophores in a certain region of interest can help circumvent this issue. This can be realized by using the fluorescent protein (FP) that can emit fluorescence only when it was activated by a certain wavelength of light. As described in chapter 1, the wild-type GFP is photoactivatable. A variant with more pronounced photoactivatability was reported by Patterson and Lippincott-Schwartz in 2002 [96]. It was developed by introducing three rationally designed mutations to increase the contrast between 390 nm and 470 nm excitation peaks.

The photoactivatable genetically-encoded calcium indicators (PA-GCaMPs) reported in Berlin et al. [106] nicely demonstrated how the photoactivation can be useful in studying calcium dynamics of neuronal cells. As the observation of intracellular calcium transients is an indirect

measure of neuronal depolarization, having a photoactivatable GEVI (PA-GEVI) would facilitate probing a neuronal activity even more. There has been a report that the Archaerhodopsin version of GEVI was developed enabling two-photon photoactivatable voltage imaging but this manuscript was only shared as a preprint and not in a peer-reviewed journal yet (Link to the preprint: arXiv:1710.10080).

In this chapter, the design strategies and experimental results of the voltage indicators with photoactivatability are described. Based on the rationales used for the development of the original PAGFP and the photoactivatable GCaMP, four candidates of PA-GEVIs were designed and constructed. The increase in fluorescence intensities of the photoactivated versions was measured. One of the candidates, PA-Bongwoori-R3 demonstrated voltage-dependent fluorescence change after photoactivation but not before.

Meanwhile, it was learned that the optical bio-sensor field has not employed the photoactivation into the development of genetically encoded pH indicators (GEPIs) yet [91, 97, 123]. In the process of making the photoactivatable version of Bongwoori-R3, a voltage insensitive variant of pH-sensitive GFP, ecliptic pHluorin D227A was developed. The cytoplasmic version of photoactivatable pH indicator

was then generated and tested to image pH changes in HEK 293 cells.

4.2 Materials and methods

4.2.1 Gene constructs design and cloning

Photoactivatable Bongwoori-R3 (PA-Bongwoori-R3) was prepared by replacing Bongwoori-R3's [112] VSD with a mutated ecliptic pHluorin that was synthesized [114]. T203H and A227D mutations were introduced in the synthesized gene fragment to confer photoactivatable property and voltage-sensitivity, respectively. BamH1 and Xho1 restriction sites were used for a simple cut and paste cloning into Bongwoori-R3 construct. Then a voltage-sensitive but not photoactivatable version (PA-Bongwoori-R3-H203T) and a photoactivatable but not voltage-sensitive version (PA-Bongwoori-R3 D227A) were generated by PCR with SM105A and SM105B, and SM106A and SM106B primers respectively. A cytoplasmic version of photoactivatable GFP (pPAGFP-N1) was purchased from a nonprofit plasmid repository (#11909, Addgene, USA).

Two versions of photoactivatable ASAP-1 [67] were prepared. ASAP-1 with three photoactivatable mutations (ASAP1-PATM) was generated by two separate gene clonings. L163F and T164S mutations (correspond to L64F and T65S mutations in original PAGFP) were first introduced by PCR using SM067A and SM067B primers. Then T59H mutation that

corresponds to T203H mutation in the PAGFP construct was substituted by PCR using SM068A and SM068B primers. A PCR with SM070 and SM071Xho1 primers was conducted to cut and paste the whole ASAP1-PATM insert into pcDNA3.1(+) vector. Another type of photoactivatable ASAP-1 was generated by switching the OPT (optimum) variant of circularly permuted superfolder GFP (cpsfGFP-OPT) in ASAP-1 into a photoactivatable circularly permuted GFP from the short superfolder photoactivatable GCaMP6f (ssPA-GCaMP6f) developed by Berlin et al. [106]. The latter was designed to have Nhe1 and Xho1 restriction sites at both ends and synthesized commercially (Integrated DNA technologies, USA). Restriction digest was then carried out with the two enzymes to cut both ends of the synthesized fragment and it was ligated into a pcDNA3.1 backbone vector to acquire ASAP1-ssPA version.

A FRET version PA-GEVI was prepared by mutating Nabi2.242 developed by Sung et al. [124]. The original Nabi 2.242 has Clover and mRuby2 FPs as a FRET pair. To replace Clover into PAGFP, a 1279 base pairs long gene fragment that includes a Nhe1 site, PAGFP, and an Apa1 site was synthesized (Integrated DNA technologies, USA) and cloned into Nabi2.242 vector. Another set of PCR was conducted on resulting gene construct, PA-Nabi2.242, where SM100A and SM100B primers

were used to introduce PA-Nabi2.242 into pcDNA3.1(+) backbone vector.

A cytoplasmic version of photoactivatable ecliptic pHluorin was generated by a simple one-step PCR with SM103 and SM013 to acquire only the ecliptic pHluorin part from PA-Bongwoori-R3_D227A. The polymerized insert was ligated back into pcDNA3.1(+) backbone vector resulting photoactivatable ecliptic pHluorin D227A.

All primers are listed in Table 4.1. The sequences of newly generated gene constructs were commercially verified (Cosmogenetech, South Korea).

Primer	Sequence	Construct
SM103	AAGCTGGCTAGCATGAGTAAAGGAGAAGAACTTTTCACTGGAG	To make cytoplasmic PA-EA227D (from PA-Bongwoori-R3)
SM105A	AACCATTACCTGTTTacaACTTCTACTCTTTCGAAAGATCCCAACG	H203T for Photoactivatable _Bongwoori-R3
SM105B	CGAAAGAGTAGAAGTtgtAAACAGGTAATGGTTGTCTGGTAAAAGGAC	
SM106A	TTCTTGAGTTTGTAACAGCTgccGGGATTACACATGGCATGGATGAAC	D227A for Photoactivatable _Bongwoori-R3
SM106B	ATGCCATGTGTAATCCCggcAGCTGTTACAAACTCAAGAAGGACCATG	
SM107	ttaatgcgccgctacagggcgcgtgggg	Reverse primer for cloning of T203 and A227 positions
SM070	CCACTGAGATCTGCATGAGCTAGCCGCCACCATGG	5' forward primer for ASAP1
SM071	CCACCACACTGGACTAGTGGATCCGAGCTCGGTACCAAGC	3' reverse primer for ASAP1
SM072R1	GAG TTC CCA TGT ACG GAT TGC CTT CTC C	Two sequencing primers (reverse) for Nabi2 construct
SM072R2	CCT CAT TTT ATT AGG AAA GGA CAG TG	
SM100A	GGAGACCCAAGCTGGCTAGCGTTTatggaggg	Nhe1 site including primer to PCR pUB-pa-Nabi2.242_v02 and paste it into pcDNA3.1+
SM100B	aaaactcgagTCGAGGGCGCGCCTaTTActtgtacagctcg	Xho1 site including primer to PCR pUB-pa-Nabi2.242_v02 and paste it into pcDNA3.1+
SM071XHO1	TAGACTCGAGTTCTAGATCATTAGGTTACCACTTCAAGTTGTTTC	to insert the PCR product of ASAP1-PATM into pcDNA3.1

Table 4. 1. List of primers used for the gene construction of photoactivatable variants of genetically encoded optical bio-sensors.

4.2.2 Cell culture and transfection

HEK 293 cells and primary neurons were cultured and transfected following the method described in Lee et al. [112] and section 2.2.2. of this thesis paper.

4.2.3 Photoactivation, voltage and pH imaging

A 385 nm light-emitting diode (bandwidth: 10 nm) placed in a 4-wavelength LED housing (LED4D242, Thorlabs, USA) was used for photoactivation of all photoactivatable variants. To find a photoactivatable optical sensor expressing cell and for photoactivation with the 385 nm LED, a filter cube consisting of a 385 nm / 23 excitation filter (FF01-386/23-25, Semrock, USA), a 495 nm dichroic mirror (FF495-Di03, Semrock, USA) and a 520 nm / 35 emission filter (FF01-520/35, Semrock, USA) was used. After photoactivation, a 470 nm LED (bandwidth: 25 nm) delivered excitation light to green fluorophores in the specimen. A 4 - channel LED driver and its software (DC4100, Thorlabs, USA) were used to control the LEDs. Protocols for simultaneous voltage imaging and electrophysiology experiments were as described in Lee et al. [112] and section 2.2.2. The high-speed CCD camera (Neuro CCD, RedShirtImaging, USA) and the camera software

(Neuroplex, RedShirtImaging, USA) were used to acquire images and send triggers to the electrophysiology amplifier (EPC 10, HEKA, UK) and the LED driver. For photoactivation at 385 nm and epifluorescence imaging at 470 nm, the LEDs were modulated at their full intensities. The intensities of 385 nm and 470 nm at their full currents were measured to be 2.7 mW / mm^2 and 5.3 mW / mm^2, respectively. Before the photoactivation, the 390 nm LED was used at its 10 % intensity to locate a transfected cell while preventing unintended photoactivation.

To locate a cell expressing the FRET version photoactivatable voltage indicator (PA-Nabi 2. 242), a 565 nm LED (bandwidth: 104 nm), a 561 nm / 14 excitation filter (FF01-561/14, Semrock, USA), a 561 nm dichroic mirror (Di02-R561, Semrock, USA) and a 609 nm / 54 emission filter (FF01-609/54, Semrock, USA) were used. For the imaging of a FRET pair, an image splitter (Optosplit 2, Cairn, UK) was placed in between the high-speed CCD camera and the c-mount port of the microscope to divide the CCD sensor into two halves for a simultaneous imaging of green (ET 520/40, Chroma, USA) and red (ET 645/75, Chroma, USA) fluorescence. For the FRET imaging, the 470 nm LED light was filtered by a 475nm / 23 excitation filter (FF01-475/23-25, Semrock, USA).

For pH imaging experiment of PA - ecliptic pHluorin D227A, gramicidin D (Sigma-Aldrich) was applied to transfected cells to perforate their cell membranes for 20 min at a concentration of 25 μM at 34 ºC. The gramicidin was prepared and stored as described in Kang and Baker [113]. After the photoactivation, each bath solution with different pH value filled the patching chamber at least 20 min to induce pH-dependent fluorescence change of the photoactivatable probe.

4.2.4 Analyses

As described earlier in section 2.2.8, fluorescence traces from selected pixels were derived from Neuroplex software (RedShirtImaging, USA). Calculation of averaged ΔF/F values and statistics of means for comparison was all conducted in Origin 9.0 (OriginLab, USA).

4.3 Results

4.3.1 Schematics of designing photoactivatable voltage indicator

The photoactivatable GFP (PAGFP) reported by Patterson and Lippincott-Schwartz [96] had 4 unique mutations compared to eGFP . L64F and T65S mutations recovered the 390 nm absorbance peak that initially existed in the wild-type GFP. The T203H mutation maximized the contrast in the two absorption bands so the FP could stay darker during 470 nm excitation until activated by 390 nm light. V163 was mutated to alanine to improve protein folding at 37 ºC as an alternative to F64L mutation in eGFP.

Four photoactivatable voltage indicator candidates were designed based on the rationale described above (Figures 4.1 and 4.2). Firstly, a photoactivatable version of ASAP-1 was prepared by introducing the triple photoactivatable mutations, F64L, S65T and T203H into the GEVI's FP (ASAP1-PATM). The V163A mutation is present originally ASAP-1. Another photoactivatable variant of ASAP1 was prepared by using a photoactivatable circularly permuted GFP (PA - cpGFP) developed by Berlin et al. [106]. The circularly permuted GFP in ASAP-1 was simply replaced by the PA – cpGFP (ASAP1-ssPA). Thirdly, a photoactivatable GEVI utilizing FRET was also generated. Nabi 2.242

is a FRET-type GEVI [124] that consisting Clover and mRuby2 as the FRET donor and acceptor. As Clover had excitation and emission spectra similar to the photoactivated PAGFP, it was replaced by the photoactivatable FP. Lastly, a photoactivatable version of Bongwoori-R3 was prepared. Since the super ecliptic pHluorin in Bongwoori-R3 is basically an eGFP version of ecliptic pHluorin, the older version that shows wild-type GFP's photophysical properties was cloned into the GEVI. Subsequently, A227D and T203H mutations were introduced to the ecliptic pHluorin to confer voltage sensitivity and photoactivatability.

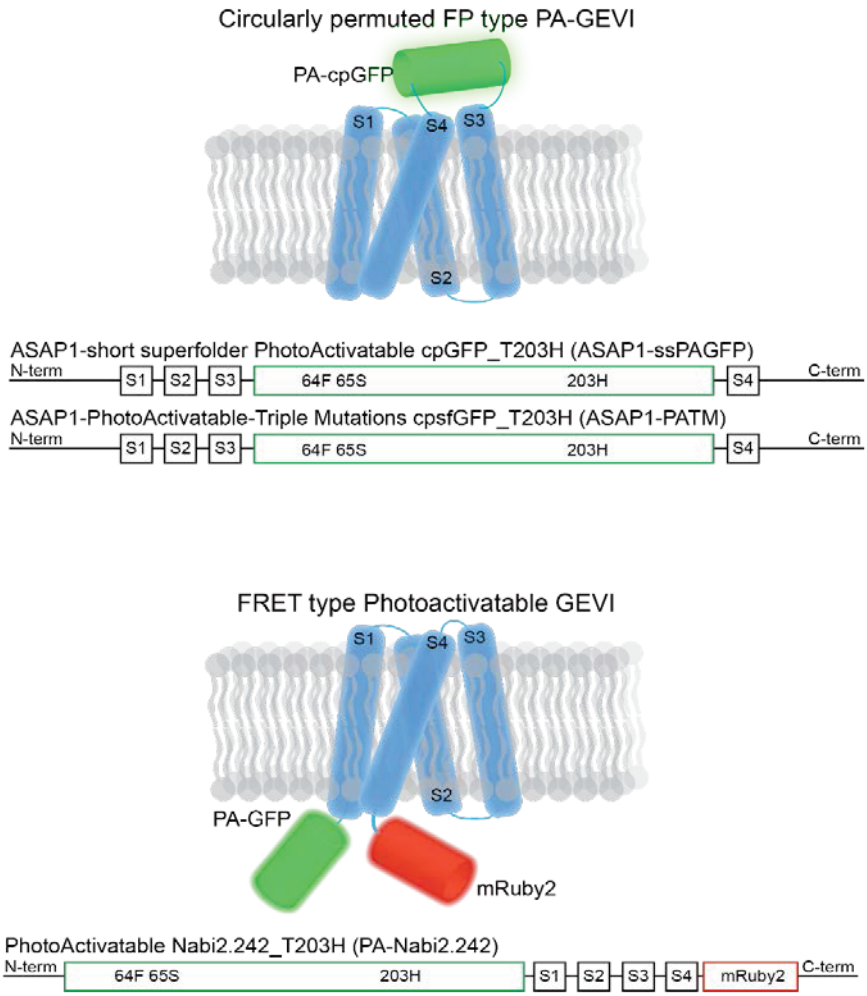

Figure 4. 1. Schematics of two types of photoactivatable GEVIs.

(Top) A circularly permuted FP type photoactivatable GEVI design and suggested gene constructs of ASAP-1 variants. (Bottom) A FRET type photoactivatable GEVI design and suggested gene construct design including the PAGFP as a FRET donor. The amino acid mutations indicated in the FP regions followed the numbering system of eGFP.

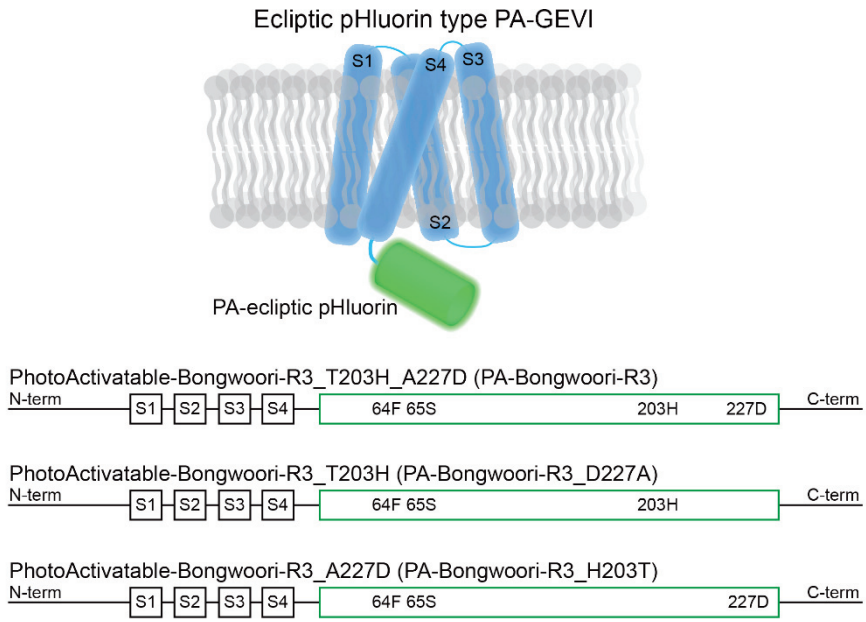

Figure 4. 2. A schematic design of the photoactivatable versions of the ecliptic pHluorin.

The amino acid mutations indicated in the FP regions followed the numbering system of eGFP.

4.3.2 ASAP1-ssPA did not express well and ASAP1-PATM was bright already before photoactivation

ASAP1-ssPA transfected HEK 293 cells were imaged with both 385 nm and 470 nm excitation light but there was no fluorescence observed due to poor expression of the probe.

The ASAP-1 with triple photoactivatable mutations did express and showed an increase in fluorescence after photoactivation. However, the FP was bright enough even before photoactivation to a level where voltage imaging experiment could be performed. (Figure 4.3). This is undesirable as one of the most important goals of using a photoactivatable FP is to minimize the background fluorescence from cells not in the region or plane of interest. This could indicate the triple mutation introduced to the cpGFP of ASAP-1 may not have reduced the absorption at 470 nm effectively.

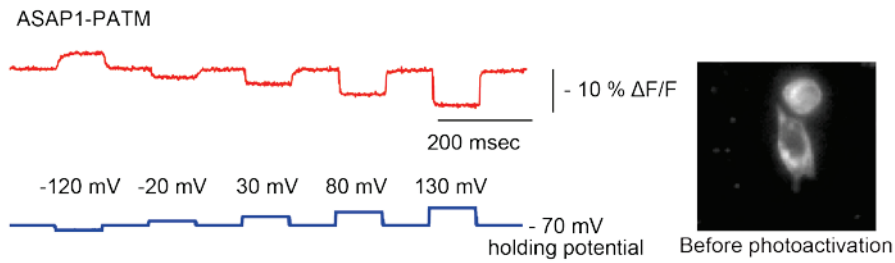

Figure 4. 3. The voltage imaging result of a ASAP1-PATM expressing HEK 293 cell before photoactivation.

The image on the right shows the cell exhibiting the voltage dependent fluorescence change.

4.3.3 The photoactivatable FRET donor in PA-Nabi 2.242 was photoactivated for more than 2 - fold but the FRET acceptor showed a mild increase its fluorescence

To verify expression of the FRET photoactivatable voltage indicator, excitation light from a 565 nm LED illuminated the transfected cells to verify mRuby2 fluorescence while keeping the photoactivatable FRET donor inactive. Red fluorescence was observed from membrane region (Figure 4.4.A). From a subsequent FRET imaging with a 470 nm LED, weak green and red fluorescence could be seen from each half of the CCD sensor. After photoactivation, the green fluorescence from PAGFP increased more than 2 - fold. Whereas the FRET acceptor's fluorescence increased by only 10 % (Figure 4.4.B).

The small increase of the red fluorescence might have been caused by either poor FRET efficiency, or insufficient energy transferred from the donor, or both factors. Several properties affect FRET efficiency. For example, the distance between the chromophores of donor and acceptor, the spectral overlap between the donor's emission and the acceptor's excitation bands, and the relative orientation of the donor and acceptor dipoles [47, 125]. Both PAGFP and Clover are variants of eGFP and the construction of PA-Nabi 2.242 was a simple substitution of Clover to

PAGFP (Figure 4.1 bottom). The emission maxima of the two FPs are 517 nm and 515 nm, respectively. A comparison of emission spectra of PAGFP (after photoactivation) and Clover in Figure 4.5 suggests the overlap with the mRuby2's excitation spectrum was not altered significantly. The quantum yields of PAGFP and Clover are 0.79 and 0.76, respectively [97, 126]. The extinction coefficients for PAGFP and Clover were measured to be 17,400 and 111,000 M^{-1} cm^{-1} [96, 126]. As intrinsic brightness of a fluorophore is determined by extinction coefficient multiplied by quantum yield, Clover is far brighter than PAGFP. The brightness of photoactivated PAGFP was measured to be 0.42 - fold of eGFP [97]. Clover is about 2.5 - fold brighter than eGFP [126]. A rough extrapolation of the two values would suggest that PAGFP is about 5 to 6 - fold dimmer than Clover. This was also verified in Nabi 2.242 and PA-Nabi 2.242. An advantage of having a FRET pair in a protein molecule is to determine an FP's brightness by comparing it against the paired FP's brightness. pair against the other. Since there was no photoactivatable Clover available for a comparison under the same condition, the donor / acceptor fluorescence ratios of Nabi 2.242 (Clover / mRuby2) and PA-Nabi 2.242 (photoactivated PAGFP / mRuby2) were compared to each other (Figure 4.4.C). In accordance with the

extrapolated value above, the Clover was calculated to be 5.58 - fold brighter relative to the PAGFP.

Although it was dimmer than the original donor, the FRET phenomenon was still verified and needs to be further developed.

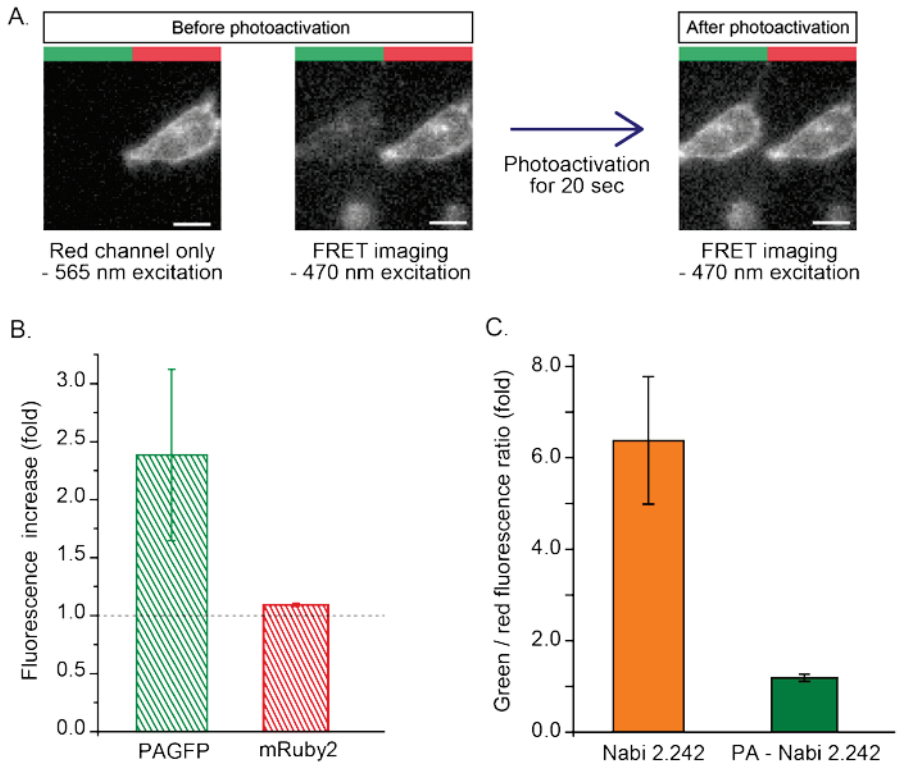

Figure 4. 4 Photoactivatability of PA-Nabi 2.242 was determined.

A. A PA-Nabi 2.242 expressing HEK 293 cell before and after photoactivation. The image was obtained by using an image splitter. The left half of the image represents green fluorescence and the right half represents red fluorescence. **B.** The increase in fluorescence intensity after photoactivataion for the FRET donor (PAGFP) and the FRET acceptor (mRuby2). C. Green (donor) / red (acceptor) fluorescence ratio calculated for both Nabi 2.242 and the photoactivatable Nabi 2.242 to compare the brightness of Clover and PAGFP in relative to the mRuby2 fluorescence. The number of cells tested; Nabi 2.242: 4, PA-Nabi 2.242: 3 cells. The photoactivation time for PA-Nabi 2.242 cells varied for 30 sec (cell1), 10 sec (cell2), and 20 sec (cell3).

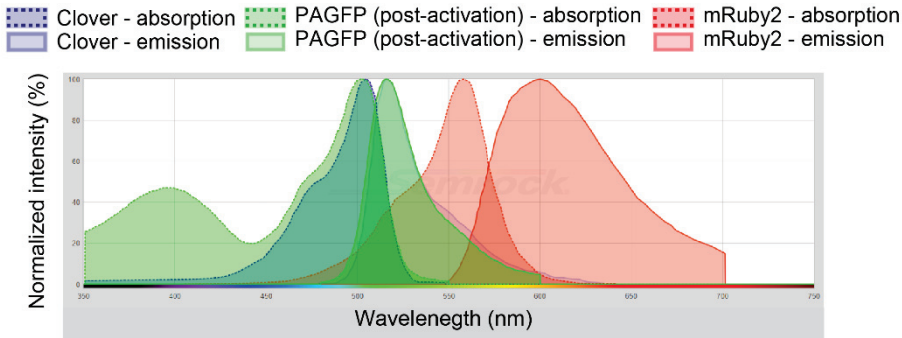

Figure 4. 5 Absorption and emission spectra of Clover, PAGFP and mRuby2.

The spectra were obtained from “https://searchlight.semrock.com/”. The reuse permission acquired.

4.3.4 Photoactivatable-Bongwoori-R3 was well expressed in membrane region and photoactivated by 385 nm LED

Bongwoori-R3 with ecliptic pHluorin with A227D and T203H mutations expressed well in HEK 293 cells. A 30 second photoactivation at 385 nm wavelength increased the green fluorescence imaged with 470 nm excitation light about 1.5 - fold (Figure 4.6). To examine its voltage-sensitivity, a 100 mV voltage change was induced before and after the photoactivation while imaging at a frame rate of 1000 Hz. With the optical setup used for this experiment, the fluorescence level before the photoactivation was inadequate to resolve the 100 mV voltage pulse. After the photoactivation, 2 % Δ F/F was observed from the same cells.

To verify if the mutations introduced in the ecliptic pHluorin contributed to the observed voltage sensitivity and photoactivatability of PA-Bongwoori-R3, two variants with either H203T or D227A were tested. PA-Bongwoori-R3_H203T showed decreased fluorescence level after photoactivation with 385 nm light (Figure 4.7). Moreover, this variant responded to voltage pulses with larger Δ F/F signal size than PA-Bongwoori-R3. Next, PA-Bongwoori-R3 without D227 was tested (Figure 4.8). As expected, this version did not show notable fluorescence change upon a voltage pulse even after reaching the photoactivated state.

The expression of PA-Bongwoori-R3 in primary neuron cultures was also verified (Figure 4.9). A hippocampal neuron expressing the probe underwent more than a 1.5 - fold increase in fluorescence at the soma.

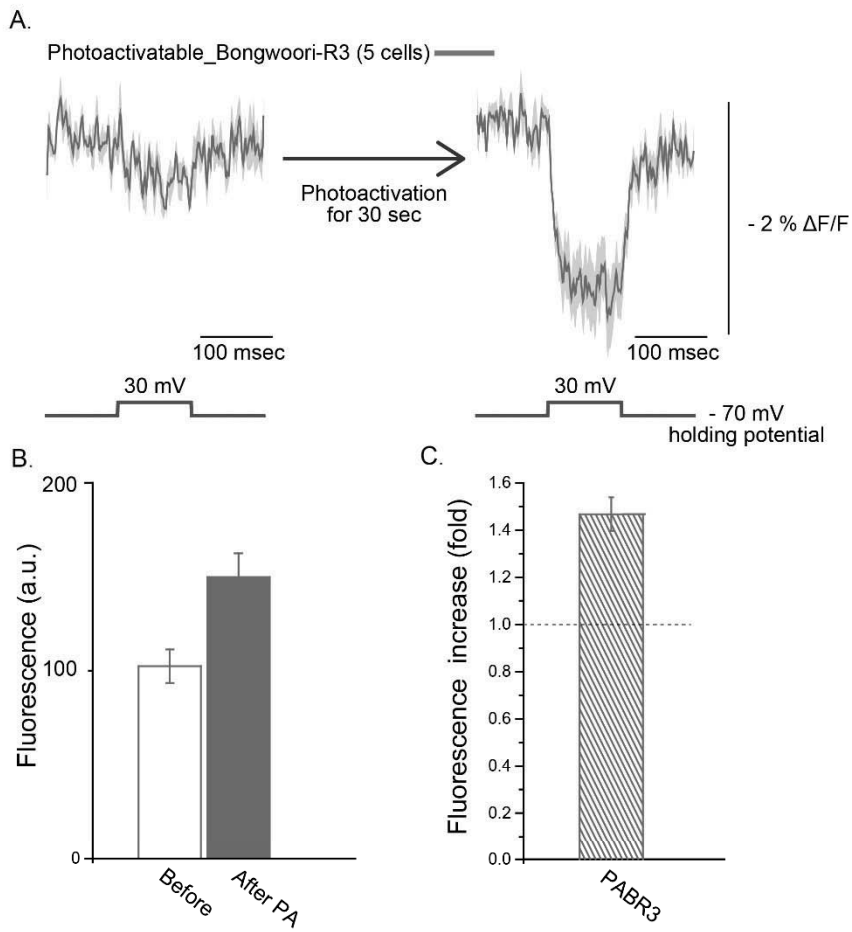

Figure 4. 6 Photoactivatable version of Bongwoori-R3 tested in HEK 293 cells.

A. PA-Bongwoori-R3 responding to a 100 mV membrane depolarization. **B.** The fluorescence intensities before and after photoactivation. C. The increase ratio of fluorescence intensity after photoactivation. Five PA-Bongwoori-R3 expressing cells were analyzed. The shaded area denotes standard error of the mean.

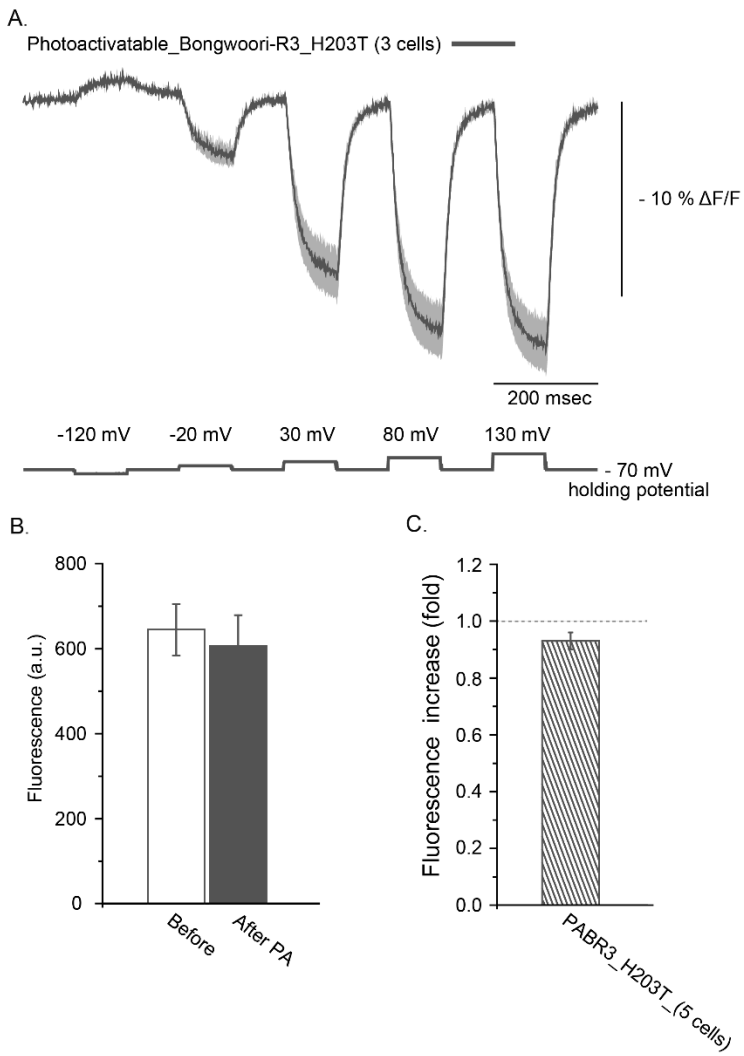

Figure 4. 7 None photoactivatable version of PA-Bongwoori-R3.

A. Photoactivatable Bongwoori-R3 with the H203T mutation responded to induced voltage pulses before photoactivataion. **B.** The fluorescence intensities (in a.u.) before and after photoactivatiaon. **C.** Fluorescence increase after photoactivation. Five cells were analyzed. The shaded area denotes standard error of the mean.

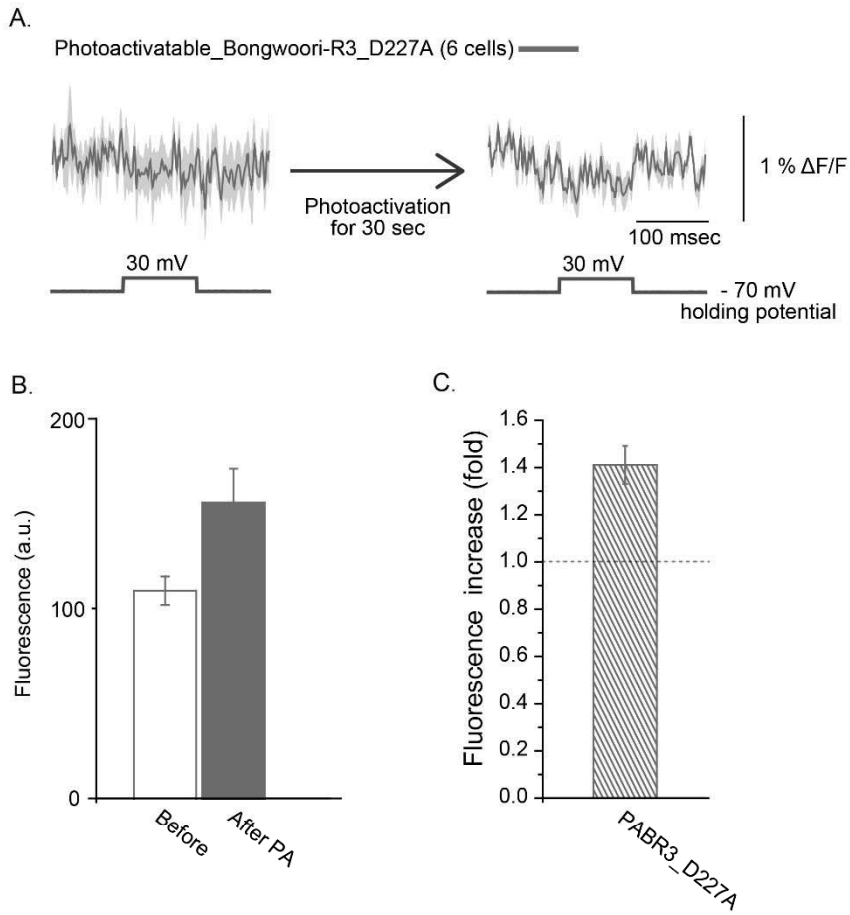

Figure 4. 8 Photoactivatable but voltage insensitive version of PA-Bongwoori-R3.

A. Voltage imaging results showing the voltage insensitivity of PA-Bongwoori-R3 with the D227A mutaton. **B.** The raw fluorescence intensities before and after photoactivation. **C.** The increase ratio after photoactivation. Six cells were analyzed. The shaded area denotes standard error of the mean.

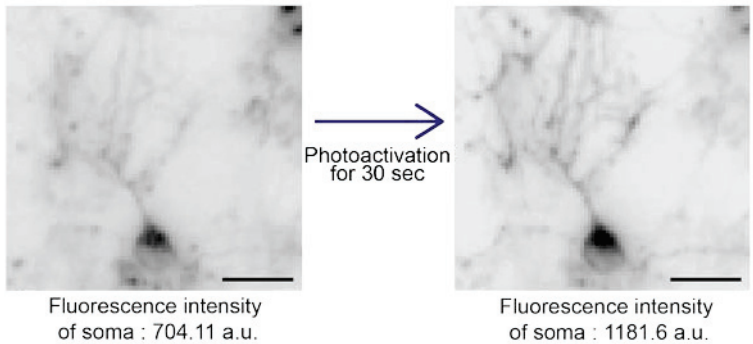

Figure 4. 9 PA-Bongwoori-R3 expressed in a primary neuron showing increased fluorescence after photoactivation.

The intensities indicated below the images were averaged from pixels corresponding to the soma region. The neuron was imaged at 40 frames per second speed with 3x camera amplifier gain for the optical signal. Scale bar = 20 μm.

4.3.5 Photoactivatable ecliptic pHluorin with T203H mutation

Since the photoactivatable version of Bongwoori-R3 used a pH-sensitive GFP, ecliptic pHluorin, it was logical to conduct photoactivatable pH imaging of the FP as well. As it was unnecessary for the probe to sense voltage change, the VSD and D227 mutation in the FP were removed. The cytoplasmic version of ecliptic pHluorin D227A was expressed in HEK 293 cells. When this pH indicator was photoactivated, it exhibited more than 2 - fold increase in fluorescence (Figure 4.10). Interestingly, a brief incubation of the transfected cell with bath solutions prepared at different pH levels did not affect the fluorescence level. To ensure a proper change of intracellular hydrogen ion concentration, an ionophore (Gramacidin, Sigma-Aldrich, USA) was used to perforate cell membranes. After the cell membranes became porous to external hydrogen ions in the bath solution, photoactivation was conducted at pH 6.4 (Figure 4.11). As expected, the photoactivation increased the cell's fluorescence intensity about 2 - fold (1.84 - fold). Then the bath solutions prepared at pH 7.4 and 8.4 filled the patching chamber for at least 20 min for each solution to make sure the cytoplasm area had homogeneous proton concentration. As a result, the photoactivated cytoplasmic ecliptic pHluorin became brighter at a basic pH level. From pH 6.4 to pH 7.4, the

increase in fluorescence was calculated to be about 1.8 - fold and from pH 7.4 to pH 8.4, it also showed 1.8 - fold brighter emission.

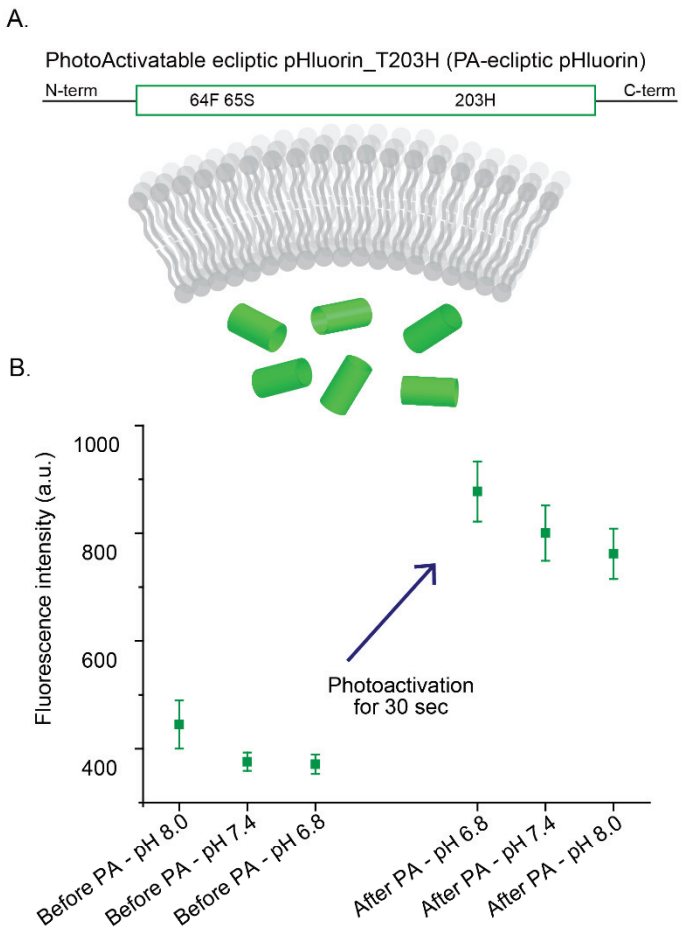

Figure 4. 10 Schematics of a cytoplasmic photoactivatable optical sensor and pH imaging results with the PA - ecliptic pHluorin D227A.

A. The voltage insensitive but photoactivatable version of ecliptic pHluorin was designed to express in cytoplasm of a mammalian cell. **B.** A preliminary photoactivatable pH imaging experiment with the PA-ecliptic pHluorin. Error bars are SEM. Total five cells were tested and analyzed.

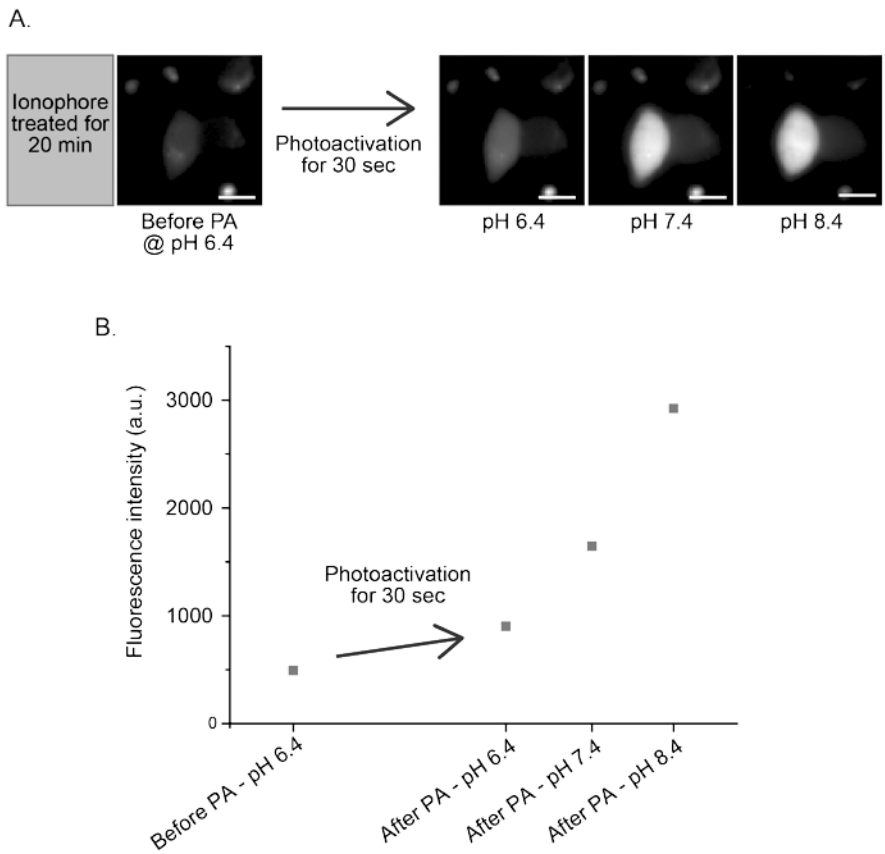

Figure 4. 11 Photoactivatable pH imaging of the ionophore treated HEK 293 cells.

A. Images of the Gramicidin treated cell expressing PA-ecliptic pHluorin D227A before and after photoactivation at differing pH values. Gramicidin was treated for 20 min at 25 μM **B.** Fluorescence intensities of the cell in A. at different conditions.

4.4 Conclusion

Four photoactivatable GEVIs candidates and one photoactivatable GEPI were rationally designed and generated in this work. Except for ASAP1-ssPA, all the other candidates expressed in HEK 293 cells and showed increase in fluorescence level upon photoactivation. The ASAP1-PATM was bright enough to resolve the induced voltage pulses even before photoactivation. However, it can be useful if the increase in fluorescence level after photoactivation is large enough to make the activated cell easily distinguishable. The 385 nm LED light used to photoactivate all the photoactivatable variants in this work was measured to be 2.7 mW / mm^2. As this light intensity was both mild and a little bit off centered from the typical 400 - 405 nm light used for illuminating a photoactivatable FP, the increase after photoactivation may increase more once a stronger 400 - 405 nm light source is used in the future.

The FRET version GEVI, PA-Nabi 2.242 needs to be tested to see if this variant is capable of resolving voltage pulses at its photoactivated state even though its FRET donor signal from PAGFP is about 6 – fold dimmer than the original Nabi 2.242. If it failed to show an impressive voltage imaging result, another photoactivatable donor FP will be needed as a replacement.

Photoactivatable Bongwoori-R3 and its derivatives nicely demonstrated functions of the voltage sensitive mutation (A227D) and the photoactivatable mutation (T203H). Combining the two distinct mutations successfully accomplished a photoactivatable GEVI. However, the intensity of PA-BR3 in its photoactivated state showed less than 2 - fold increase. This was about 50 - fold weaker than PAGFP that was reported to increase about 100 - fold [96]. Though the 100 - fold increase from the original work was measured from purified proteins embedded in a polyacrylamide gel, PA-BR3's photoactivation was mild. This may suggest that the mutations in the photoactivatable ecliptic pHluorin A227D hindered proper photoactivation. Another possibility could again be the weak 385 nm LED light used to photoactivation.

The GEPI candidate was simply prepared by removing the Ci-VSD and the arginine containing linker from PA-Bongwoori-R3 (D227A). The Ci-VSD and D227 were removed since voltage sensitivity is no longer needed to study cytoplasmic pH level. The photoactivation and pH change into the basic level successfully increased the brightness of the cytoplasmic photoactivatable pH-sensitive FP.

Chapter 5. Conclusion

The development and application of optogenetic recording tools have been very successful in the last 13 years. Electrophysiology has been the most important method to study neuronal activity and it will still be in the future. However, the limitations of electrophysiology that comes from its fundamental disadvantages such as tissue invasiveness, difficulties to simultaneous recording and limited spatial resolution will necessitate alternative ways to complement the conventional methodology.

This dissertation introduced some endeavors to achieve that goal. Voltage imaging has been the brightest future expected to replace electrophysiology since its first appearance in the 1970s. The recent progress in the development of GEVIs seems to be promising. Bongwoori-R3 and Bongwoori-Pos6 could be one of the promising GEVIs. The single pixel imaging of action potentials shown by Bongwoori-R3 was achieved by only one amino acid difference in its interdomain linker compared to its parent, Bongwoori. Further applications of Bongwoori-R3 in various biological tissues such as the retina, cerebellum, or other areas of hippocampus should demonstrate the GEVI's ability better.

The membrane trafficking motif work in chapter 3 nicely displayed the empirical nature of introducing such signaling sequences to different optical sensor molecules. As it was expected from previous results from other researchers, the effects caused by the targeting motifs were quite unpredictable. Nevertheless, the variant with 12 amino acid spacer in between the FP and the ER export signal sequence showed another promising result. Utilization of the new membrane trafficking optimized version in various *ex vivo* or *in vivo* experiments is expected to be fruitful.

The last chapter described a very interesting property of the wild-type GFP. The photoconversion of the FP due to a shift in its absorption spectrum almost sounds like a magic trick in nanometer scale. There are no photoactivatable GEVIs or GEPIs available in the optical indicator field yet, not in a peer-reviewed journal at least. Although the results from the photoactivatable candidates introduced in this dissertation may appear insufficient, further developments should improve their applicability.

References

1. Scanziani, M. and M. Hausser, Electrophysiology in the age of light. *Nature*, 2009. **461**(7266):930-939.
2. Hodgkin, A.L. and A.F. Huxley, A quantitative description of membrane current and its application to conduction and excitation in nerve. *J Physiol*, 1952. **117**(4):500-544.
3. Hodgkin, A.L. and A.F. Huxley, Action Potentials Recorded from Inside a Nerve Fibre. *Nature*, 1939. **144**:710-711.
4. Molleman, A., *Patch clamping : an introductory guide to patch clamp electrophysiology*. 2003, New York: J. Wiley. x, 175 pages.
5. Neher, E. and B. Sakmann, Single-channel currents recorded from membrane of denervated frog muscle fibres. *Nature*, 1976. **260**(5554):799-802.
6. Carter, M. and J.C. Shieh, *Guide to research techniques in neuroscience*. Second edition. ed. 2015, Amsterdam: Elsevier/AP, Academic Press is an imprint of Elsevier. xxviii, 388 pages.
7. Spira, M.E. and A. Hai, Multi-electrode array technologies for neuroscience and cardiology. *Nat Nanotechnol*, 2013. **8**(2):83-94.
8. Buzsaki, G., C.A. Anastassiou, and C. Koch, The origin of extracellular fields and currents--EEG, ECoG, LFP and spikes. *Nat Rev Neurosci*, 2012. **13**(6):407-420.
9. Lee, J., et al., Transparent intracortical microprobe array for simultaneous spatiotemporal optical stimulation and multichannel electrical recording. *Nat Methods*, 2015. **12**(12):1157-1162.
10. Royer, S., et al., Control of timing, rate and bursts of hippocampal place cells by dendritic and somatic inhibition. *Nat Neurosci*, 2012. **15**(5):769-775.
11. Geiller, T., et al., Place cells are more strongly tied to landmarks in deep than in superficial CA1. *Nat Commun*, 2017. **8**: No.14531.

12. Marshall, J.D., et al., Cell-Type-Specific Optical Recording of Membrane Voltage Dynamics in Freely Moving Mice. *Cell*, 2016. **167**(6):1650-1662, e15.
13. Lee, D., B.J. Lin, and A.K. Lee, Hippocampal Place Fields Emerge upon Single-Cell Manipulation of Excitability During Behavior. *Science*, 2012. **337**(6096):849-853.
14. Lin, M.Z. and M.J. Schnitzer, Genetically encoded indicators of neuronal activity. *Nat Neurosci*, 2016. **19**(9):1142-1153.
15. Xu, Y., P. Zou, and A.E. Cohen, Voltage imaging with genetically encoded indicators. *Curr Opin Chem Biol*, 2017. **39**:1-10.
16. Kim, C.K., et al., Simultaneous fast measurement of circuit dynamics at multiple sites across the mammalian brain. *Nat Methods*, 2016. **13**(4):325-328.
17. Chen, T.W., et al., Ultrasensitive fluorescent proteins for imaging neuronal activity. *Nature*, 2013. **499**(7458):295-300.
18. Packer, A.M., et al., Simultaneous all-optical manipulation and recording of neural circuit activity with cellular resolution in vivo. *Nat Methods*, 2015. **12**(2):140-146.
19. Wang, H., M. Jing, and Y. Li, Lighting up the brain: genetically encoded fluorescent sensors for imaging neurotransmitters and neuromodulators. *Curr Opin Neurobiol*, 2018. **50**:171-178.
20. Mutoh, H. and T. Knopfel, Probing neuronal activities with genetically encoded optical indicators: from a historical to a forward-looking perspective. *Pflugers Arch*, 2013. **465**(3):361-371.
21. Mutoh, H., W. Akemann, and T. Knopfel, Genetically engineered fluorescent voltage reporters. *ACS Chem Neurosci*, 2012. **3**(8):585-592.
22. Miesenbock, G., The optogenetic catechism. *Science*, 2009. **326**(5951):395-399.
23. Storace, D.A., et al., Monitoring brain activity with protein voltage

and calcium sensors. *Sci Rep*, 2015. **5**:No.10212.
24. Tang, J., et al., Nanowire arrays restore vision in blind mice. *Nat Commun*, 2018. **9**(1):No.786.
25. Drinnenberg, A., et al., How Diverse Retinal Functions Arise from Feedback at the First Visual Synapse. *Neuron*, 2018. **99**(1):117-134.
26. Raimondo, J.V., et al., Genetically encoded proton sensors reveal activity-dependent pH changes in neurons. *Front Mol Neurosci*, 2012. **5**:No.68.
27. Raimondo, J.V., et al., A genetically-encoded chloride and pH sensor for dissociating ion dynamics in the nervous system. *Front Cell Neurosci*, 2013. **7**:No.202.
28. Raimondo, J.V., et al., Tight Coupling of Astrocyte pH Dynamics to Epileptiform Activity Revealed by Genetically Encoded pH Sensors. *J Neurosci*, 2016. **36**(26):7002-7013.
29. Sankaranarayanan, S., et al., The use of pHluorins for optical measurements of presynaptic activity. *Biophys J*, 2000. **79**(4):2199-2208.
30. Li, Y. and R.W. Tsien, pHTomato, a red, genetically encoded indicator that enables multiplex interrogation of synaptic activity. *Nat Neurosci*, 2012. **15**(7):1047-1053.
31. Patriarchi, T., et al., Ultrafast neuronal imaging of dopamine dynamics with designed genetically encoded sensors. *Science*, 2018. **360**(6396) *(Page numbers not final at time of first release).
32. Oh, Y., et al., Tracking tonic dopamine levels in vivo using multiple cyclic square wave voltammetry. *Biosens Bioelectron*, 2018. **121**:174-182.
33. Park, C., et al., Fast Cyclic Square-Wave Voltammetry To Enhance Neurotransmitter Selectivity and Sensitivity. *Anal Chem*, 2018. **90**(22):13348-13355.
34. Gan, J.O., M.E. Walton, and P.E. Phillips, Dissociable cost and

benefit encoding of future rewards by mesolimbic dopamine. *Nat Neurosci*, 2010. **13**(1):25-27.
35. Popovic, M.A., et al., Cortical dendritic spine heads are not electrically isolated by the spine neck from membrane potential signals in parent dendrites. *Cereb Cortex*, 2014. **24**(2):385-395.
36. Popovic, M.A., et al., Electrical behaviour of dendritic spines as revealed by voltage imaging. *Nat Commun*, 2015. **6**:No.8436.
37. Mace, E., et al., Functional ultrasound imaging of the brain. *Nat Methods*, 2011. **8**(8):662-664.
38. Deffieux, T., et al., Functional ultrasound neuroimaging: a review of the preclinical and clinical state of the art. *Curr Opin Neurobiol*, 2018. **50**:128-135.
39. Buxton, R.B., *Introduction to functional magnetic resonance imaging : principles and techniques*. 2nd ed. 2009, Cambridge ; New York: Cambridge University Press. 457 pages.
40. Akemann, W., S.J. Middleton, and T. Knopfel, Optical imaging as a link between cellular neurophysiology and circuit modeling. *Front Cell Neurosci*, 2009. **3**:No.5.
41. Ross, W.N., et al., A large change in dye absorption during the action potential. *Biophys J*, 1974. **14**(12):983-986.
42. Cohen, L.B., R.D. Keynes, and B. Hille, Light scattering and birefringence changes during nerve activity. *Nature*, 1968. **218**(5140):438-441.
43. Badreddine, A.H., T. Jordan, and I.J. Bigio, Real-time imaging of action potentials in nerves using changes in birefringence. *Biomed Opt Express*, 2016. **7**(5):1966-1973.
44. Shimomura, O., F.H. Johnson, and Y. Saiga, Extraction, purification and properties of aequorin, a bioluminescent protein from the luminous hydromedusan, Aequorea. *J Cell Comp Physiol*, 1962. **59**:223-239.

45. Morise, H., et al., Intermolecular energy transfer in the bioluminescent system of Aequorea. *Biochemistry*, 1974. **13**(12):2656-2662.
46. Ormo, M., et al., Crystal structure of the Aequorea victoria green fluorescent protein. *Science*, 1996. **273**(5280):1392-1395.
47. Tsien, R.Y., The green fluorescent protein. *Annu Rev Biochem*, 1998. **67**:509-544.
48. Shaner, N.C., P.A. Steinbach, and R.Y. Tsien, A guide to choosing fluorescent proteins. *Nat Methods*, 2005. **2**(12):905-909.
49. Prasher, D.C., et al., Primary structure of the Aequorea victoria green-fluorescent protein. *Gene*, 1992. **111**(2):229-233.
50. Rost, B.R., et al., Optogenetic Tools for Subcellular Applications in Neuroscience. *Neuron*, 2017. **96**(3):572-603.
51. Kwon, T., et al., Attenuation of Synaptic Potentials in Dendritic Spines. *Cell Rep*, 2017. **20**(5):1100-1110.
52. Piatkevich, K.D., et al., A robotic multidimensional directed evolution approach applied to fluorescent voltage reporters. *Nat Chem Biol*, 2018. **14**(4):352-360.
53. Cao, G., et al., Genetically targeted optical electrophysiology in intact neural circuits. *Cell*, 2013. **154**(4):904-913.
54. Storace, D.A. and L.B. Cohen, Measuring the olfactory bulb input-output transformation reveals a contribution to the perception of odorant concentration invariance. *Nat Commun*, 2017. **8**(1):No.81.
55. Lee, S., et al., Imaging Membrane Potential with Two Types of Genetically Encoded Fluorescent Voltage Sensors. *J Vis Exp*, 2016(108):e53566.
56. Siegel, M.S. and E.Y. Isacoff, A genetically encoded optical probe of membrane voltage. *Neuron*, 1997. **19**(4):735-741.
57. Guerrero, G., et al., Tuning FlaSh: redesign of the dynamics, voltage range, and color of the genetically encoded optical sensor of

membrane potential. *Biophys J*, 2002. **83**(6):3607-3618.
58. Sakai, R., et al., Design and characterization of a DNA-encoded, voltage-sensitive fluorescent protein. *Eur J Neurosci*, 2001. **13**(12):2314-2318.
59. Ataka, K. and V.A. Pieribone, A genetically targetable fluorescent probe of channel gating with rapid kinetics. *Biophys J*, 2002. **82**(1 Pt 1):509-516.
60. Baker, B.J., et al., Three fluorescent protein voltage sensors exhibit low plasma membrane expression in mammalian cells. *J Neurosci Methods*, 2007. **161**(1):32-38.
61. Knopfel, T., J. Diez-Garcia, and W. Akemann, Optical probing of neuronal circuit dynamics: genetically encoded versus classical fluorescent sensors. *Trends Neurosci*, 2006. **29**(3):160-166.
62. Murata, Y., et al., Phosphoinositide phosphatase activity coupled to an intrinsic voltage sensor. *Nature*, 2005. **435**(7046):1239-1243.
63. Akemann, W., et al., Imaging brain electric signals with genetically targeted voltage-sensitive fluorescent proteins. *Nat Methods*, 2010. **7**(8):643-649.
64. Jin, L., et al., Single action potentials and subthreshold electrical events imaged in neurons with a fluorescent protein voltage probe. *Neuron*, 2012. **75**(5):779-785.
65. Piao, H.H., et al., Combinatorial mutagenesis of the voltage-sensing domain enables the optical resolution of action potentials firing at 60 Hz by a genetically encoded fluorescent sensor of membrane potential. *J Neurosci*, 2015. **35**(1):372-385.
66. Storace, D., et al., Toward Better Genetically Encoded Sensors of Membrane Potential. *Trends Neurosci*, 2016. **39**(5):277-289.
67. St-Pierre, F., et al., High-fidelity optical reporting of neuronal electrical activity with an ultrafast fluorescent voltage sensor. *Nat Neurosci*, 2014. **17**(6):884-889.

68. Pedelacq, J.D., et al., Engineering and characterization of a superfolder green fluorescent protein. *Nat Biotechnol*, 2006. **24**(1):79-88.
69. Baird, G.S., D.A. Zacharias, and R.Y. Tsien, Circular permutation and receptor insertion within green fluorescent proteins. *Proc Natl Acad Sci U S A*, 1999. **96**(20):11241-11246.
70. Abdelfattah, A.S., et al., A Bright and Fast Red Fluorescent Protein Voltage Indicator That Reports Neuronal Activity in Organotypic Brain Slices. *J Neurosci*, 2016. **36**(8):2458-2472.
71. Boyden, E.S., et al., Millisecond-timescale, genetically targeted optical control of neural activity. *Nat Neurosci*, 2005. **8**(9):1263-1268.
72. Zhang, F., et al., Multimodal fast optical interrogation of neural circuitry. *Nature*, 2007. **446**(7136):633-639.
73. Zhang, F., et al., Circuit-breakers: optical technologies for probing neural signals and systems. *Nat Rev Neurosci*, 2007. **8**(8):577-581.
74. Gradinaru, V., K.R. Thompson, and K. Deisseroth, eNpHR: a Natronomonas halorhodopsin enhanced for optogenetic applications. *Brain Cell Biol*, 2008. **36**(1-4):129-139.
75. Gradinaru, V., et al., Molecular and cellular approaches for diversifying and extending optogenetics. *Cell*, 2010. **141**(1):154-165.
76. Fenno, L., O. Yizhar, and K. Deisseroth, The development and application of optogenetics. *Annu Rev Neurosci*, 2011. **34**:389-412.
77. Zhang, F., et al., The microbial opsin family of optogenetic tools. *Cell*, 2011. **147**(7):1446-57.
78. Kato, H.E., et al., Crystal structure of the channelrhodopsin light-gated cation channel. *Nature*, 2012. **482**(7385):369-374.
79. Kralj, J.M., et al., Optical recording of action potentials in mammalian neurons using a microbial rhodopsin. *Nat Methods*, 2011. **9**(1):90-95.

80. Kralj, J.M., et al., Electrical spiking in Escherichia coli probed with a fluorescent voltage-indicating protein. *Science*, 2011. **333**(6040):345-348.
81. Hochbaum, D.R., et al., All-optical electrophysiology in mammalian neurons using engineered microbial rhodopsins. *Nat Methods*, 2014. **11**(8):825-833.
82. Zou, P., et al., Bright and fast multicoloured voltage reporters via electrochromic FRET. *Nat Commun*, 2014. **5**:No.4625.
83. Gong, Y., et al., Imaging neural spiking in brain tissue using FRET-opsin protein voltage sensors. *Nat Commun*, 2014. **5**:No.3674.
84. Gong, Y., et al., High-speed recording of neural spikes in awake mice and flies with a fluorescent voltage sensor. *Science*, 2015. **350**(6266):1361-1366.
85. Gong, Y., J.Z. Li, and M.J. Schnitzer, Enhanced Archaerhodopsin Fluorescent Protein Voltage Indicators. *PLoS One*, 2013. **8**(6):e66959.
86. Ramirez, O.A. and A. Couve, The endoplasmic reticulum and protein trafficking in dendrites and axons. *Trends Cell Biol*, 2011. **21**(4):219-227.
87. Peterka, D.S., H. Takahashi, and R. Yuste, Imaging voltage in neurons. *Neuron*, 2011. **69**(1):9-21.
88. Hofherr, A., B. Fakler, and N. Klocker, Selective Golgi export of Kir2.1 controls the stoichiometry of functional Kir2.x channel heteromers. *J Cell Sci*, 2005. **118**(Pt 9):1935-1943.
89. Stockklausner, C. and N. Klocker, Surface expression of inward rectifier potassium channels is controlled by selective Golgi export. *J Biol Chem*, 2003. **278**(19):17000-17005.
90. Akemann, W., et al., Imaging neural circuit dynamics with a voltage-sensitive fluorescent protein. *J Neurophysiol*, 2012. **108**(8):2323-2337.

91. Lippincott-Schwartz, J. and G.H. Patterson, Photoactivatable fluorescent proteins for diffraction-limited and super-resolution imaging. *Trends Cell Biol*, 2009. **19**(11):555-565.
92. Betzig, E., et al., Imaging intracellular fluorescent proteins at nanometer resolution. *Science*, 2006. **313**(5793):1642-1645.
93. Shroff, H., et al., Live-cell photoactivated localization microscopy of nanoscale adhesion dynamics. *Nat Methods*, 2008. **5**(5):417-423.
94. Hess, S.T., T.P. Girirajan, and M.D. Mason, Ultra-high resolution imaging by fluorescence photoactivation localization microscopy. *Biophys J*, 2006. **91**(11):4258-4272.
95. Ha, T. and P. Tinnefeld, Photophysics of fluorescent probes for single-molecule biophysics and super-resolution imaging. *Annu Rev Phys Chem*, 2012. **63**:595-617.
96. Patterson, G.H. and J. Lippincott-Schwartz, A photoactivatable GFP for selective photolabeling of proteins and cells. *Science*, 2002. **297**(5588):1873-1877.
97. Lukyanov, K.A., et al., Innovation: Photoactivatable fluorescent proteins. *Nat Rev Mol Cell Biol*, 2005. **6**(11):885-891.
98. Ando, R., et al., An optical marker based on the UV-induced green-to-red photoconversion of a fluorescent protein. *Proc Natl Acad Sci U S A*, 2002. **99**(20):12651-12656.
99. Wiedenmann, J., et al., EosFP, a fluorescent marker protein with UV-inducible green-to-red fluorescence conversion. *Proc Natl Acad Sci U S A*, 2004. **101**(45):15905-15910.
100. Tsutsui, H., et al., Semi-rational engineering of a coral fluorescent protein into an efficient highlighter. *EMBO Rep*, 2005. **6**(3):233-238.
101. Chudakov, D.M., et al., Photoswitchable cyan fluorescent protein for protein tracking. *Nat Biotechnol*, 2004. **22**(11):1435-1439.
102. Souslova, E.A. and D.M. Chudakov, Photoswitchable cyan

fluorescent protein as a FRET donor. *Microsc Res Tech*, 2006. **69**(3):207-209.

103. Habuchi, S., et al., mKikGR, a monomeric photoswitchable fluorescent protein. *PLoS One*, 2008. **3**(12):e3944.

104. Nakai, J., M. Ohkura, and K. Imoto, A high signal-to-noise Ca^{2+} probe composed of a single green fluorescent protein. *Nat Biotechnol*, 2001. **19**(2):137-141.

105. Ahrens, M.B., et al., Whole-brain functional imaging at cellular resolution using light-sheet microscopy. *Nat Methods*, 2013. **10**(5):413-420.

106. Berlin, S., et al., Photoactivatable genetically encoded calcium indicators for targeted neuronal imaging. *Nat Methods*, 2015. **12**(9):852-858.

107. Baker, B.J., et al., Genetically encoded fluorescent voltage sensors using the voltage-sensing domain of Nematostella and Danio phosphatases exhibit fast kinetics. *J Neurosci Methods*, 2012. **208**(2):190-196.

108. Han, Z., et al., Fluorescent protein voltage probes derived from ArcLight that respond to membrane voltage changes with fast kinetics. *PLoS One*, 2013. **8**(11):e81295.

109. Platisa, J., et al., Directed Evolution of Key Residues in Fluorescent Protein Inverses the Polarity of Voltage Sensitivity in the Genetically Encoded Indicator ArcLight. *ACS Chem Neurosci*, 2017. **8**(3):513-523.

110. Jung, A., et al., Linker length and fusion site composition improve the optical signal of genetically encoded fluorescent voltage sensors. *Neurophotonics*, 2015. **2**(2):No.021012.

111. Barnett, L., et al., A fluorescent, genetically-encoded voltage probe capable of resolving action potentials. *PLoS One*, 2012. **7**(9):e43454.

112. Lee, S., et al., Improving a genetically encoded voltage indicator by modifying the cytoplasmic charge composition. *Sci Rep*, 2017. **7**(1):No.8286.
113. Kang, B.E. and B.J. Baker, Pado, a fluorescent protein with proton channel activity can optically monitor membrane potential, intracellular pH, and map gap junctions. *Sci Rep*, 2016. **6**:No.23865.
114. Miesenbock, G., D.A. De Angelis, and J.E. Rothman, Visualizing secretion and synaptic transmission with pH-sensitive green fluorescent proteins. *Nature*, 1998. **394**(6689):192-195.
115. Chesler, M., Regulation and modulation of pH in the brain. *Physiol Rev*, 2003. **83**(4):1183-1221.
116. Mathis, D.M., J.L. Furman, and C.M. Norris, Preparation of acute hippocampal slices from rats and transgenic mice for the study of synaptic alterations during aging and amyloid pathology. *J Vis Exp*, 2011(49):e2330.
117. Xu, N.L., et al., Nonlinear dendritic integration of sensory and motor input during an active sensing task. *Nature*, 2012. **492**(7428):247-251.
118. Nakajima, R., et al., Optogenetic Monitoring of Synaptic Activity with Genetically Encoded Voltage Indicators. *Front Synaptic Neurosci*, 2016. **8**:No.22.
119. Akerboom, J., et al., Optimization of a GCaMP calcium indicator for neural activity imaging. *J Neurosci*, 2012. **32**(40):13819-13840.
120. Tian, L., et al., Imaging neural activity in worms, flies and mice with improved GCaMP calcium indicators. *Nat Methods*, 2009. **6**(12):875-881.
121. Song, C., et al., Transgenic Strategies for Sparse but Strong Expression of Genetically Encoded Voltage and Calcium Indicators. *Int J Mol Sci*, 2017. **18**(7):No.1461.
122. Bayguinov, P.O., et al., Imaging Voltage in Genetically Defined

Neuronal Subpopulations with a Cre Recombinase-Targeted Hybrid Voltage Sensor. *J Neurosci*, 2017. **37**(38):9305-9319.

123. Chudakov, D.M., et al., Fluorescent proteins and their applications in imaging living cells and tissues. *Physiol Rev*, 2010. **90**(3):1103-1163.

124. Sung, U., et al., Developing Fast Fluorescent Protein Voltage Sensors by Optimizing FRET Interactions. *PLoS One*, 2015. **10**(11):e0141585.

125. Campbell, R.E., Fluorescent-protein-based biosensors: modulation of energy transfer as a design principle. *Anal Chem*, 2009. **81**(15):5972-5979.

126. Lam, A.J., et al., Improving FRET dynamic range with bright green and red fluorescent proteins. *Nat Methods*, 2012. **9**(10):1005-1012.

국 문 초 록

광학 센서들의 눈부신 발전으로 인해 세포신경생리학 연구에 있어 전기생리학적으로는 밝혀내기 어려운 정보의 습득에도 이러한 광센서들이 사용되고 있다. 예를 들면, 신경 세포 dendritic spine의 전기적인 신호 변화나 혹은 한 지역에 있으나 전기적으로는 구별해 내기 힘든 서로 다른 세포들을 구분해 내어 광학적으로 그 활성을 측정하는데 활용되고 있다. 이러한 광학 센서의 성공은 생명공학 기술의 발전, 생물 실험에 최적화된 광학 장비 그리고 향상된 수준의 형광 센서 개발에 기인한다. 특히, 유전적으로 부호화된 형광 바이오센서들의 출현은 조사하려는 세포 자체의 단백질 생산 메커니즘을 사용함으로써 광학 센서의 세포 유형별 표적화를 가능하게 하였다.

본 학위 논문은 유전자 부호화 전압 표시장치를 개발하고, 센서 분자의 세포막 발현을 최적화하며, 또한 형광 단백질의 광활성화를 가능케 하는 방법을 다루고 있다.

신경세포의 전압변화를 측정하는 것은 곧 신경 활동을 직접 측정한다는 것을 의미한다. 유전자 부호화된 전압 표시장치는 1997년에 처음 보고되었는데, 특히 지난 7년간 눈부신 발전을 이뤄왔다. 이 학위 논문의 첫 번째 부분에서는 유전자 부호화된 전압 표

시장치의 기본 개념과 그간의 개발 이력을 간략히 소개함과 동시에 이번 연구에서 새롭게 개발한 전압 표시장치를 소개하고 있다.

유전적으로 암호화된 광학 센서의 주요 장점 중 하나는 해당 단백질을 특정 지역, 더 나아가 세포 소기관으로 보내는 표적 능력이다. 따라서, 센서 단백질을 특정한 위치에 더 잘 발현 시키기 위한 수단들을 경험적으로 연구하였고, 이 또한 이 논문의 두 번째 부분에서 논의될 것이다.

마지막으로, 센서 단백질을 광학적으로 활성화하기 위해 설계된 논리적 돌연변이 전략을 소개한다. 이 부분에서는 2002년에 처음 보고된 광활성이 가능한 녹색 형광 단백질의 개발에 사용된 전략을 적극적으로 활용하였다. 이를 통하여 광활성화가 가능한 유전자 부호화된 전압 표시장치 및 산성도 표시장치를 개발한 과정과 결과를 소개한다.

학 번: 2012-22449